Precambrian Research 302 (2017) 221–254

Contents lists available at ScienceDirect

Precambrian Research

journal homepage: www.elsevier.com/locate/precamres

Tectonic evolution of the Juvenile Tonian Serra da Prata magmatic arc in the Ribeira belt, SE Brazil: Implications for early west Gondwana amalgamation

Caroline de Araujo Peixoto[a,*], Monica Heilbron[a], Diana Ragatky[a], Richard Armstrong[c], Elton Dantas[d], Claudio de Morisson Valeriano[a,b], Antonio Simonetti[e]

[a] TEKTOS Research Group, Geology Institute, Rio de Janeiro State University, Rua São Francisco Xavier 524/4030-A, Maracanã, Rio Janeiro 20550-900, Brazil
[b] LAGIR Geochronology and Radiogenic Isotope Laboratory, Geology Institute, Rio de Janeiro State University, Rua São Francisco Xavier 524/4043-F, Maracanã, Rio Janeiro 20550-900, Brazil
[c] Geochronology Laboratory, School of Earth Sciences, Australian National University, College of Physical & Mathematical Sciences, Building 142 Mills Road, Acton, ACT 2601, Australia
[d] Geochronology Laboratory, Geosciences Institute, Brasília University-UNB, Campus Universitário Darcy Ribeiro ICC – Ala Central 70.910-900, Brasília, DF 70919-970, Brazil
[e] Dept. Civil & Environmental Engineering & Earth Sciences, 156 Fitzpatrick Hall, University of Notre Dame, Notre Dame, IN 46556, USA

ABSTRACT

The evolution of the Ribeira belt resulted from the progressive amalgamation of several terranes against the eastern margin of the São Francisco Craton between ca. 620 and 580 Ma. This work brings new field, U-Pb geochronology, geochemistry and isotopic (Sm-Nd and Sr) data on the evolution primitive rocks from the Serra da Prata magmatic arc and their relationships with the previously described Rio Negro arc. The new U-Pb data allow the distinction of two episodes of arc generation: the Serra da Prata Arc (856–838 Ma) and the Rio Negro Arc (790–620 Ma). Rocks from the oldest stage are composed of metaluminous calc-alkaline diorites, tonalites and granodiorites, and geochemical signatures compatible with magmatic arc scenarios. Their rocks are associated to a metamorphosed volcano-sedimentary of intra or back-arc basin setting platform carbonates, amphibolites (basaltic lavas) and psammitic rocks of the Italva group. Whole-rock Nd and Sr isotope data indicate more primitive contribution than earliest stage: initial $\varepsilon Nd = -3.7$ to $+5.2$, TDM = 1.68–0.92 Ga and $^{87}Sr/^{86}Sr$ initial ratios between 0.7061 and 0.7113. The second stage – Rio Negro arc – yielded more mature arc signatures: initial $\varepsilon Nd = -8.4$ to -2.5, TDM = 1.93–1.33 Ga and $^{87}Sr/^{86}Sr$ initial ratios between 0.7098 and 0.7211. The new data have been interpreted as an evolution of a Tonian primitive intra-oceanic stage of the magmatic arc generation, followed by more continental or transitional arcs during the Rio Negro stage. The data from both arc stages contrast with the younger Serra da Bolívia and Rio Doce continental arcs (570–590 Ma) developed in a proximal location. The data are similar to other Tonian-Ediacaran magmatic arcs: the Goiás arc in the Brasília Belt (ca. 862–630 Ma) and the São Gabriel arc (ca. 840–690 Ma), located respectively along the western margin of the São Francisco and Rio de La Plata cratons. In a Western Gondwana scenario, the juvenile signature indicates intra-oceanic tectonic settings. The combination of the older Tonian arcs with the more evolved Cryogenian to Ediacaran arcs within the Neoproterozoic belts, suggests more than 200 m.y. of subduction around the older cratonic blocks that made up Western Gondwana.

1. Introduction

The identification of magmatic arcs and related basins, ophiolitic sutures and high-pressure metamorphic rocks, together with paleomagnetic data are key to better understanding of the paleogeography before Gondwana amalgamation during Neoproterozoic to Cambrian times. Most of the belts that made up the Western Gondwana are presently deeply eroded, and the study of those magmatic arcs allows inference about the vergence and duration of the subduction process that took place before the final amalgamation of the supercontinent.

To address to these questions, our natural laboratory is the Ribeira belt, located in southeastern Brazil (Cordani et al., 2000; Brito Neves, 2003). The belt integrates a complex network of Neoproterozoic belts that led to Western Gondwana amalgamation. The evolution of the Ribeira belt resulted from the progressive accretion of several terranes against the eastern margin of the São Francisco Craton (Heilbron et al.,

* Corresponding author.
E-mail address: carolineapeixoto@hotmail.com (C. de Araujo Peixoto).

http://dx.doi.org/10.1016/j.precamres.2017.09.017
Received 10 April 2017; Received in revised form 16 August 2017; Accepted 18 September 2017
Available online 23 September 2017
0301-9268/

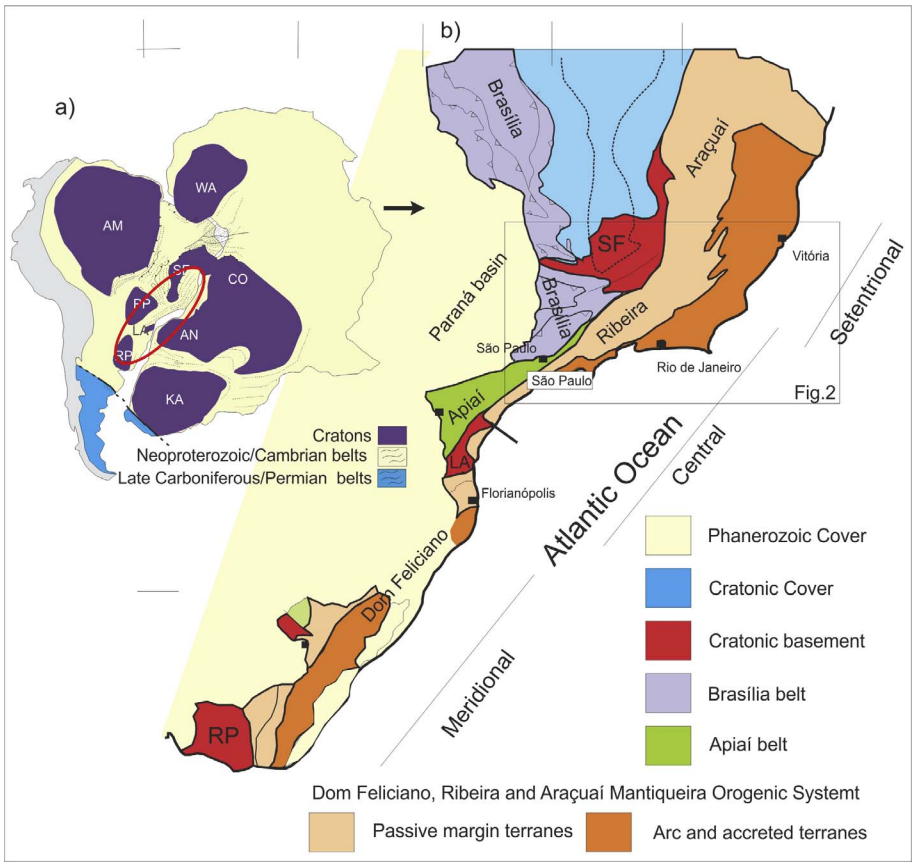

Fig. 1. a) Location of the Mantiqueira Orogenic System of the Western Gondwana compiled from Heilbron et al. (2000); b) Subdivision of the Mantiqueira Orogenic System Heilbron et al. (2004a,b).

2000, 2004a,b, 2008; Trouw et al., 2000). Among these terranes, the Paraíba do Sul/Embú and the Oriental Terrane encompass the Neoproterozoic magmatic arcs of the belt that accreted against the São Francisco Craton between ca. 620 and 580 Ma (Machado et al., 1996; Tupinambá & Heilbron, 2002; Heilbron and Machado, 2003; Tupinambá et al., 2012; Heilbron et al., 2013).

A subject of debate concerning the Neoproterozoic evolution of the belts in southeastern Brazil and western Africa (Araçuaí, Ribeira, Dom Feliciano and Kaoko) is the width of the Adamastor Ocean located between the São-Francisco-Congo, Angola, Rio de La Plata and Kalahari paleoplates (Kröner and Cordani, 2003; D'Agrella Filho et al., 2016; Pisarevsky et al., 2003, 2008; Meert and Torsvik, 2003; Cordani et al., 2013; Heilbron et al., 2008; Tupinambá et al., 2012; Pedrosa Soares et al., 2008; Gray et al., 2009). Reported long intervals of subduction highlight the large time span of magmatic arc production (ca. 790–595 Ma) and favors the hypothesis of consumption of a large oceanic plate during the Neoproterozoic (Tupinambá et al., 2011; Heilbron et al., 2010, Heilbron et al., 2008, 2013).

Recently, two magmatic arcs have been described in detail in the Ribeira belt: the inner cordilleran Serra da Bolívia Arc (Heilbron et al., 2013) and correlatives in the Araçuaí belt to the north (Degler et al., 2017; Tedeschi et al., 2016; Nalini-Junior et al., 2000, 2005), and the more primitive Rio Negro Arc (Tupinambá et al., 2011; Heilbron and Machado, 2003), exposed in the mountain ranges of Rio de Janeiro State (Figs. 1 and 2).

Previous data has displayed one single Tonian age in a local publication that is the Explanatory Note for 1: 100,000 sheet we produced for the Brazilian Geological Survey. Now, detailed geological has reinforce the occurrence of older (ca. 860 Ma) and even more primitive tonalitic gneisses of the Serra da Prata complex (Peixoto, 2010; Peixoto and Heilbron, 2010; Heilbron et al., 2013, 2012), see Figs. 1 and 2. In this work, we present updated detailed geology of the region of the occurrence of the Serra da Prata arc to compare and show its field relationships with the previously described Rio Negro Arc rocks by Tupinambá et al. (2011). New geochemical, U-Pb geochronology and isotopic (Nd and Sr) data of the Serra da Prata arc-related rocks are presented. Data related to the coeval and associated meta-volcano-sedimentary rocks of the Italva group are presented to draw the complete picture of the convergence processes around São Francisco-Congo cratons in the Adamastor Ocean.

The obtained data suggest a more complex evolution in two stages (older Serra da Prata and younger Rio Negro) and corroborates with the consumption of a large oceanic space between the continental blocks that made up the central portion of Western Gondwana. Finally, a comparison with other Tonian to Cryogenian arcs of Gondwana is addressed.

2. Tectonic organization of Ribeira belt

The Ribeira belt is one of the belts of the Mantiqueira Province (or orogenic system) that extends for almost 1400 km along the Atlantic coast of Brazil (Almeida, 1977; Almeida et al., 1981; Heilbron et al., 2000, 2004a,b). Ribeira belt composed of several tectonostratigraphic terranes (Fig. 1) imbricated toward the WNW and includes the São Francisco Craton, Occidental Terrane, Paraíba do Sul and Embú terranes and Oriental Terrane, which encompasses the more juvenile Neoproterozoic magmatic arcs, and the Cabo Frio Terrane. To the south, the Socorro and Apiaí terranes (Campos Neto, 2000; Janasi and Ulbrich, 1991; Janasi et al., 2001) complete the major tectonic units of the belt (Fig. 2).

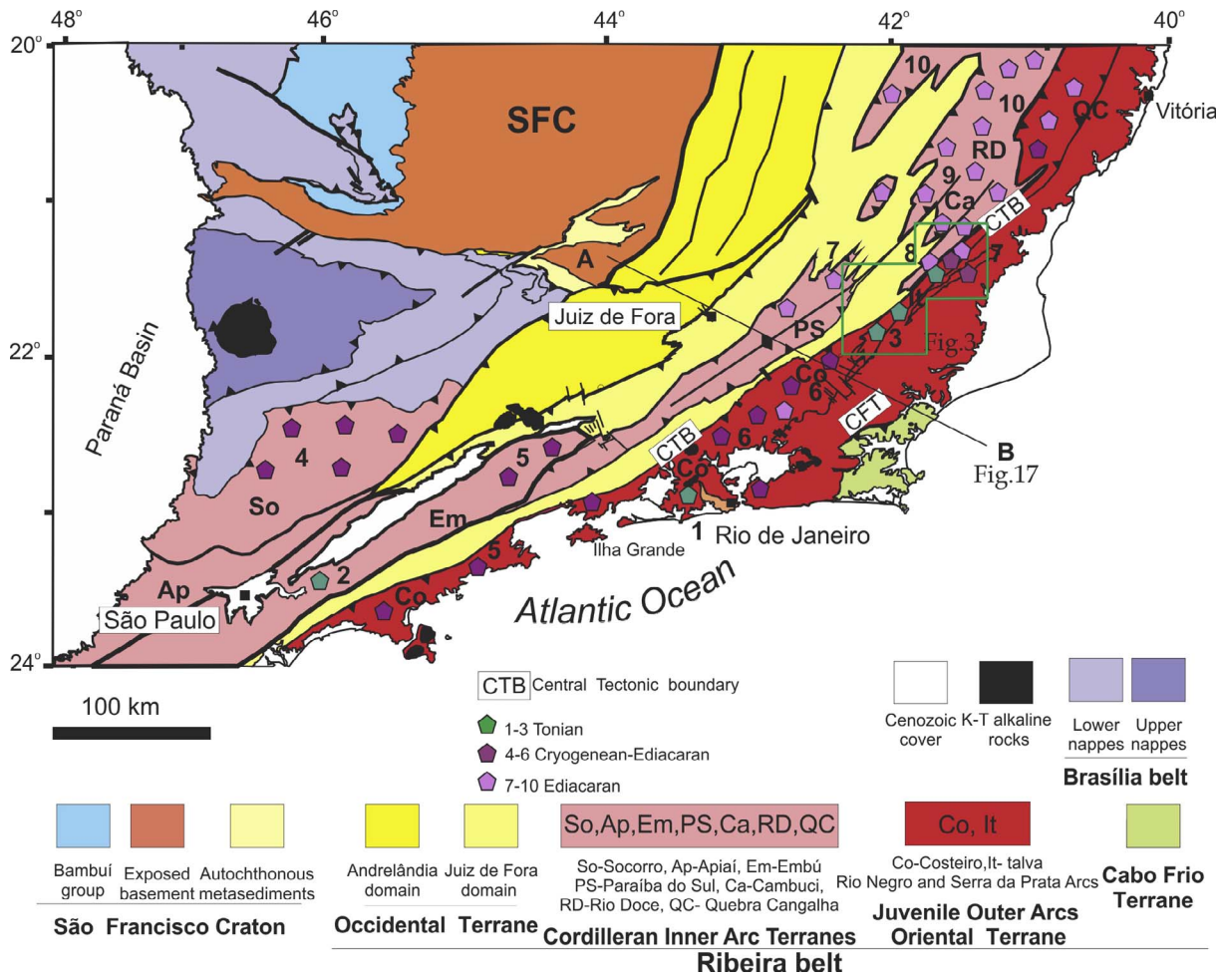

Fig. 2. Ribeira belt tectonic organization (modified from Heilbron et al., 2000, 2008, 2013; Campos Neto, 2000; Trouw et al., 2000).

Accretion of most of these terranes onto the São Francisco cratonic margin was diachronous between ca. 620–565 Ma and oblique resulting in the partition of the deformation between thrust and dextral transpressive shear zones (Machado et al., 1996; Heilbron et al., 2000, 2004b). The Cabo Frio terrane docked later, during Cambrian times (Schmitt et al., 2004).

3. The Oriental Terrane

The Oriental Terrane includes the Neoproterozoic arc-related associations (Fig. 3) that occur within three structural domains imbricated northwestern wards (Rosier, 1957; Menezes, 1973; Oliveira et al., 1978; Sad and Donadello, 1978; Sad et al., 1980; Machado Filho et al., 1983; Sad and Dutra, 1988; Machado et al., 1996; Tupinambá and Heilbron, 2002; Heilbron and Machado, 2003; Moraes, 2006; Peixoto, 2008; Peixoto and Heilbron, 2010; Tupinambá et al., 2012; Heilbron et al., 2013):

(a) The terrane consists of Serra da Bolívia Arc (Heilbron et al., 2013) which developed between ca. 650 and 590 Ma as a cordilleran magmatic arc that continues northward into the Rio Doce arc of the Araçuaí belt (G1 granitoids, Nalini-Junior et al., 2000, 2005; Pedrosa-Soares et al., 2008; Heilbron et al., 2013; Tedeschi et al., 2016), and southward into the Socorro arc (Hackspacher et al., 2003; Campos Neto, 2000; Janasi et al., 2001). This association is now considered to be associated to the Paraíba do Sul-Embú terrane because of the above mentioned geological correlation (Fig. 2).

(b) The Rio Negro Complex (Tupinambá et al., 2012; Heilbron and Machado, 2003) extends for more than 500 km in the mountains of the Rio de Janeiro and southern Espírito Santo states (Fig. 2), and consists of 790–620 Ma intra-oceanic to cordilleran tectonic settings and consistent juvenile signature (Heilbron and Machado, 2003; Tupinambá et al., 2012).

(c) The Serra da Prata Complex (Peixoto and Heilbron, 2010) the focus of this work, crops out in the uppermost thrust sheet of the Oriental Terrane, (Fig. 3) and consists of foliated orthogneisses represented by diorites, tonalities, and granodiorites intruded by granitic leucogneisses. A single age of ca. 860 Ma for a hornblende-rich tonalitic orthogneiss has been publish by Heilbron et al. (2012). The arc-related rocks occur associated with marbles and amphibolites of the Italva group, and yielded a crystallization age of ca. 848 Ma (Heilbron and Machado, 2003).

4. Geologic context

In the studied area, (Figs. 3 and 4) rocks of the Costeiro domain are tectonically overlaying by the associations of the Italva Domain, with represents the uppermost thrust sheet of the Oriental Terrane. This

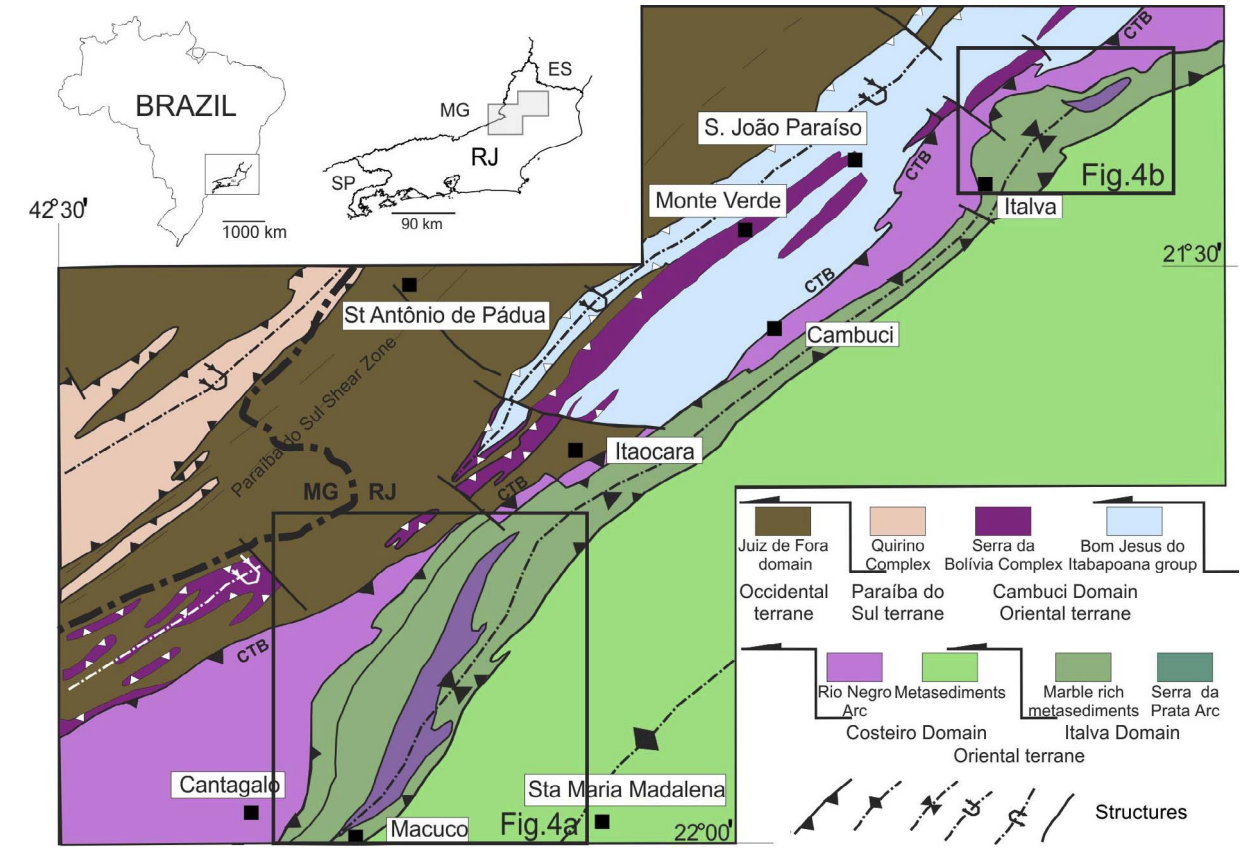

Fig. 3. Geological map from the northern region of Rio de Janeiro State, nearby the Espírito Santo and Minas Gerais borders, compiled from Heilbron et al. (2013).

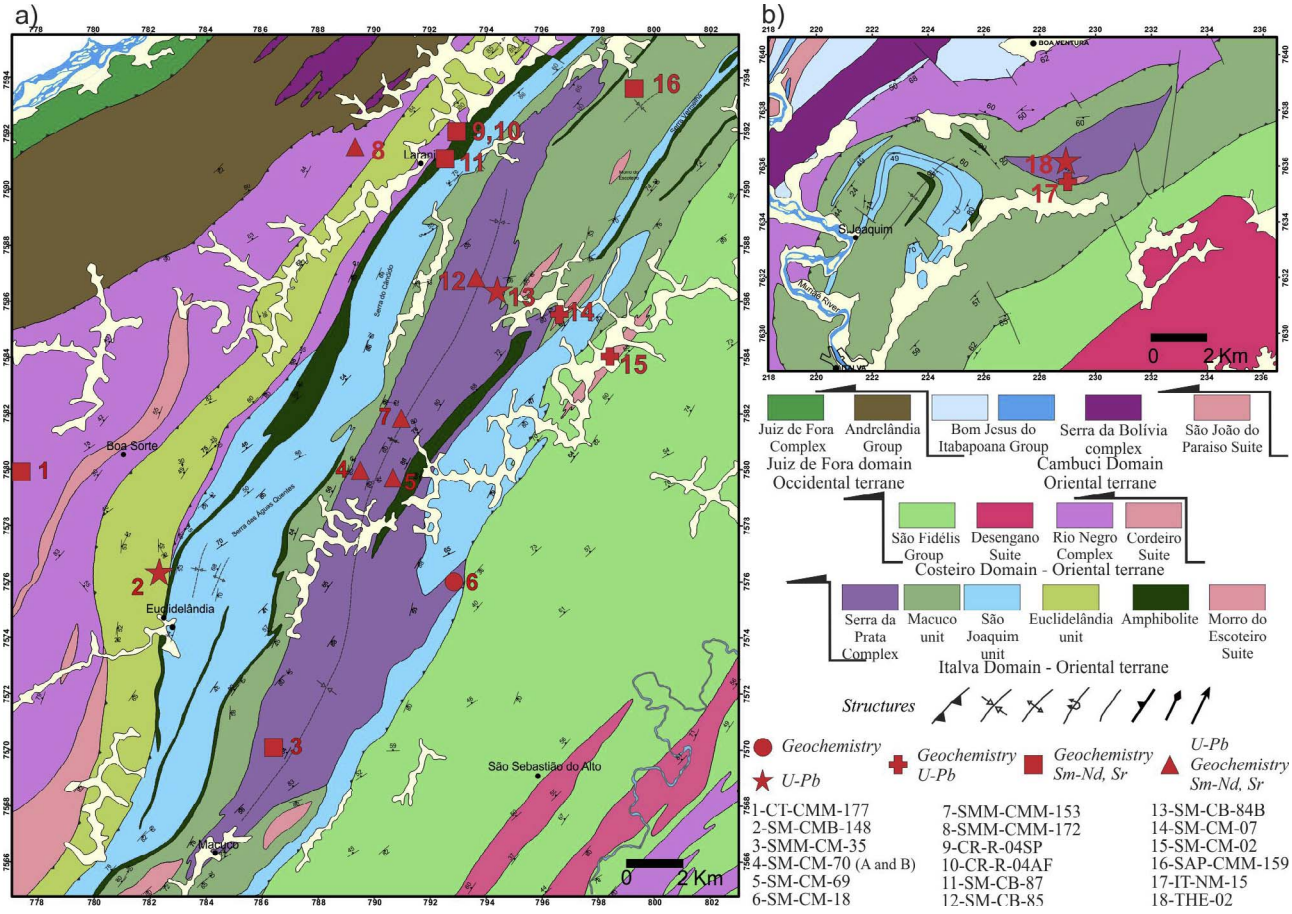

Fig. 4. Geological map of the target area with the location of the analyzed samples.

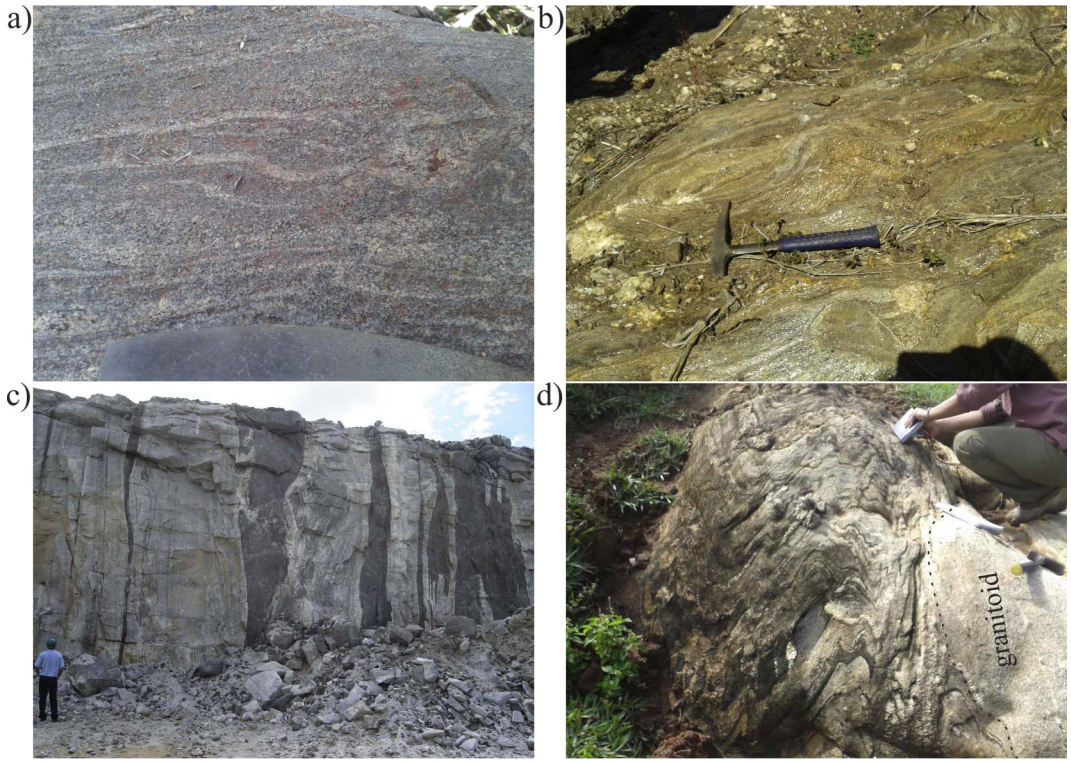

Fig. 5. Photos from Italva Group: Migmatitic biotite gneiss (a) and foliated muscovite gneiss (b) of Euclidelândia Unit; c) layers and boudins of amphibolites intercalated with marble of São Joaquim Unit; d) Garnet-biotite gneiss with amphibolite boudins from Macuco unit, besides an intrusive granitoid.

tectonic unit was thrust (as a duplex structure) over the Costeiro Domain and refolded in a synformal structure (Peixoto, 2008; Peixoto and Heilbron, 2010).

The Costeiro domain encompasses the granulite facies metasedimentary rocks of the São Fidelis group and the arc-related orthogneisses of the Rio Negro complex (Tupinambá et al., 2012). The Italva Domain consists of metasedimentary rocks of the Italva group and orthogneisses of the Serra da Prata Complex, besides amphibolites and leucogranites. Metamorphism reached upper amphibolite facies with incipient anatexis that resulted in migmatitic textures. The orthogneisses of both the Rio Negro and Serra da Prata Complex, the metasedimentary units and amphibolites of the Italva Domain, the focus of our investigation, are described bellows.

4.1. The Italva group

The Italva group consists of three lithostratigraphic units mapped in detail in the southern segment of the Italva Domain (Fig. 4), named from bottom to top as Euclidelândia, São Joaquim, and Macuco units.

4.1.1. The Euclidelândia unit

Located in the western portion of the studied area (Fig. 4), this unit consists of coarse to fine-grained, foliated biotite-muscovite gneiss, composed of quartz, microcline, plagioclase, biotite and muscovite (Fig. 5a, b). Tourmaline, magnetite, garnet and sillimanite, zircon and apatite, are common accessory minerals.

Conspicuous centimetric banding and migmatitic structures melanosomes are common. The protoliths are supposed to psammo-pelitic composition with some proportion of volcanic or volcaniclastic contribution.

Pegmatite intrusions are very common and are composed of quartz, feldspar and black tourmaline

The contact between the Euclidelândia unit and the orthogneisses of the Costeiro Terrane was not observed. The boundary with the São Joaquim unit is marked by an abrupt tectonic contact, with repetitions of both units (Fig. 4).

4.1.2. São Joaquim Unit

The unit is composed to foliated and banded calcitic marbles with intercalated amphibolites, biotite gneisses (metapelites), centimetre-scale quartzite layers and calcsilicate rocks (Fig. 4). The marbles vary in color from white, yellow, and gray to blue. Carbonate-rich layers are usually coarser grained than layers with white mica and tremolite.

In addition, graphite flakes and disseminated sulfides are common and are distributed in thin layers, suggesting preservation of primary sedimentary compositions. Some layers may include quartz, diopside, and prismatic pale green tremolite. Centimetre to metre-scale layers of gneisses, layers and boudins of amphibolites and quartz-rich centimetric levels are common (Fig. 5c).

The gneissic and the quartz-rich layers are interpreted as pelitic and psammitic intercalations that were deposited in a carbonate plataform.

In the west part of the area, the contacts between this marble-rich unit and the lowermost Euclidelândia unit is highly deformed, characterized by the presence of mylonitic rocks and tectonic repetitions of both units (Figs. 3 and 4). In the east part, the boundary with the paragneisses of the Costeiro Domain was not observed, but a clear metamorphic discontinuity is detected, as the amphibolite facies rocks of the Italva group contrast with the granulite facies of those paragneisses.

4.1.3. Macuco Unit

The uppermost Macuco Unit occupies the central region in the Italva Domain (Fig. 4). This unit consists of coarse to fine-grained, banded and foliated garnet-biotite gneisses composed of biotite, garnet, quartz, K-

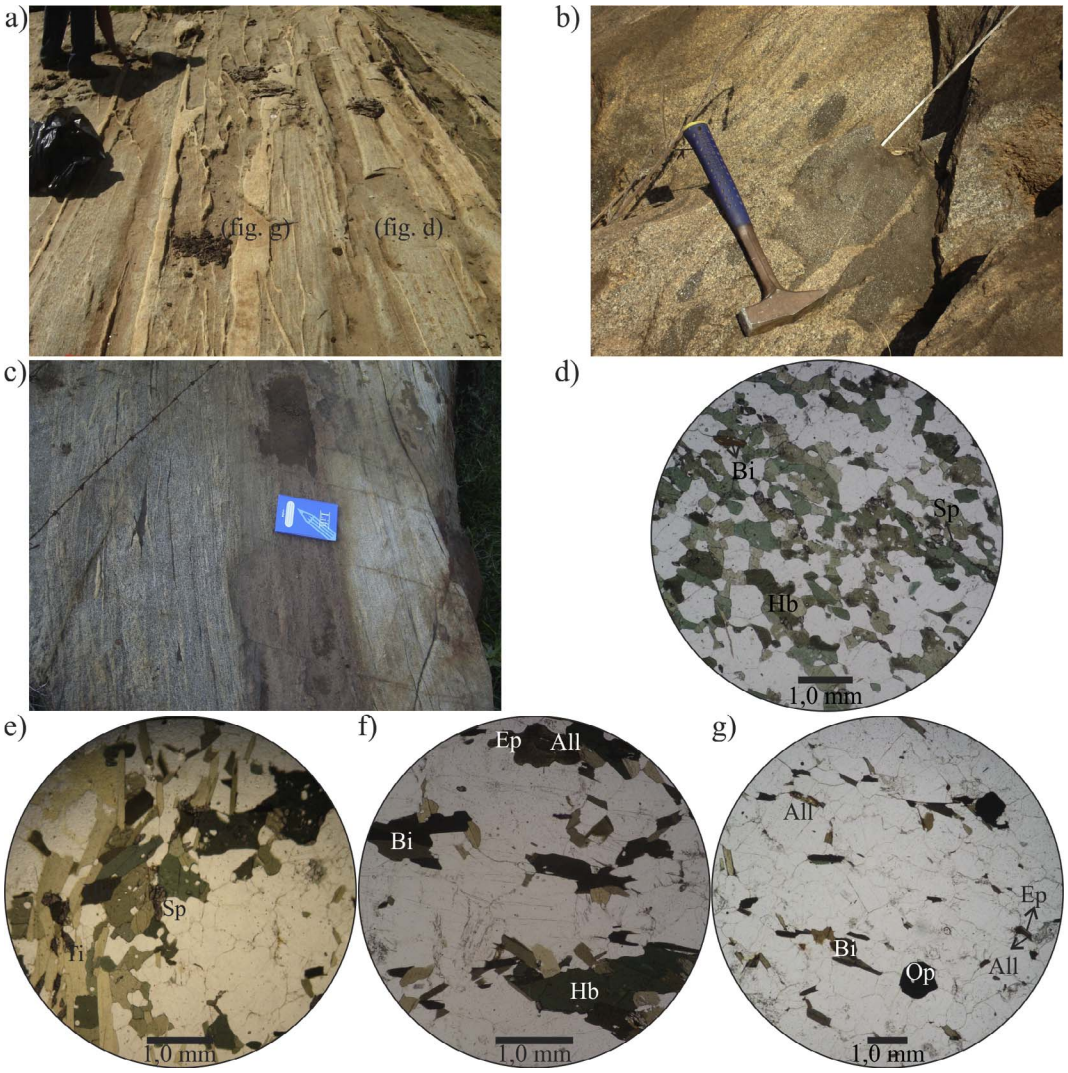

Fig. 6. Plutonic rocks from the Serra da Prata Complex: a) Intercalation of tonalitic hornblende biotite orthogneiss (fig. d) and granitic biotite orthogneiss (fig. g); b) Amphibolites enclave within hornblende biotite orthogneiss; c) Hornblende biotite orthogneiss transitioning into the biotite orthogneiss; d–f) Photomicrographs illustrating the tonalitic to granitic varieties; d) Dioritic hornblende orthogneiss with sphene; e) Tonalitic hornblende biotite orthogneiss with sphene; f) Granodiorite hornblende biotite orthogneiss; g) Granitic biotite orthogneiss with allanite, epidote, and opaque mineral. Allanite (All); Biotite (Bi); Epidote (Ep); (Hb) Hornblende; Opaque mineral (Op); Sphene (Sp).

feldspar (microcline) and plagioclase, locally with sillimanite and sulfide minerals. Again, despite the amphibolite facies and lack of preserved primary structures, we supposed that this unit is made up of psammitic rocks, but some volcanic or volcaniclastic contribution could not be discarded once amphibolite lenses and boudins are common (Fig. 5d).

Locally, strongly migmatitic rocks characterize the boundary between the Macuco unit and paragneisses of the Costeiro Domain. The paragneiss consist of sillimanite garnet-biotite gneiss with centimetre to metre-scale intercalated sillimanita-feldspar-muscovite bearing quartzite and calcsilicate rocks. Leucosomes contain garnet and cordierite. The leucosomes commonly intrude granitoids of the Morro do Escoteiro Suite (Fig. 5d).

4.2. Orthogneisses, Granitoids, and amphibolites

4.2.1. Serra da Prata Complex

This complex crops out in the central portion of the synform structure and overlies all units of the Italva Domain (Figs. 3 and 4). It consists of mesocratic gray hornblende biotite orthogneisses, pale gray biotite orthogneisses and leucocratic biotite orthogneisses. The composition of the hornblende and biotite orthogneisses varies from diorites, tonalities, granodiorites, while the leucogneisses are mostly granitic (Fig. 6a–c).

The dioritic to granodiorite orthogneisses (Fig. 6d –f) are composed of hornblende, biotite, quartz, plagioclase, K-feldspar, locally with diopside. Primary porphyritic texture and local migmatitic structures are observed. Accessory minerals include magnetite, allanite, epidote, sphene, zircon and garnet. The complex commonly contains lenses of foliated coarse-grained amphibolite (quartz diorite rocks) of variable size.

Field and petrographic observations indicate that modal hornblende are inversely proportional to the modal concentration of biotite. The contact between the dioritic/tonalitic hornblende biotite orthogneiss and the granodiorite biotite orthogneiss is gradational, suggesting an original magmatic layering (Fig. 6c).

Layers of white-colored and coarse-grained biotite orthogneiss with granitic composition also occur (Fig. 6a, g). They are composed of biotite, quartz, plagioclase, K-feldspar and rare garnet, hornblende, and diopside. Accessory opaque minerals, allanite, epidote, sphene, and

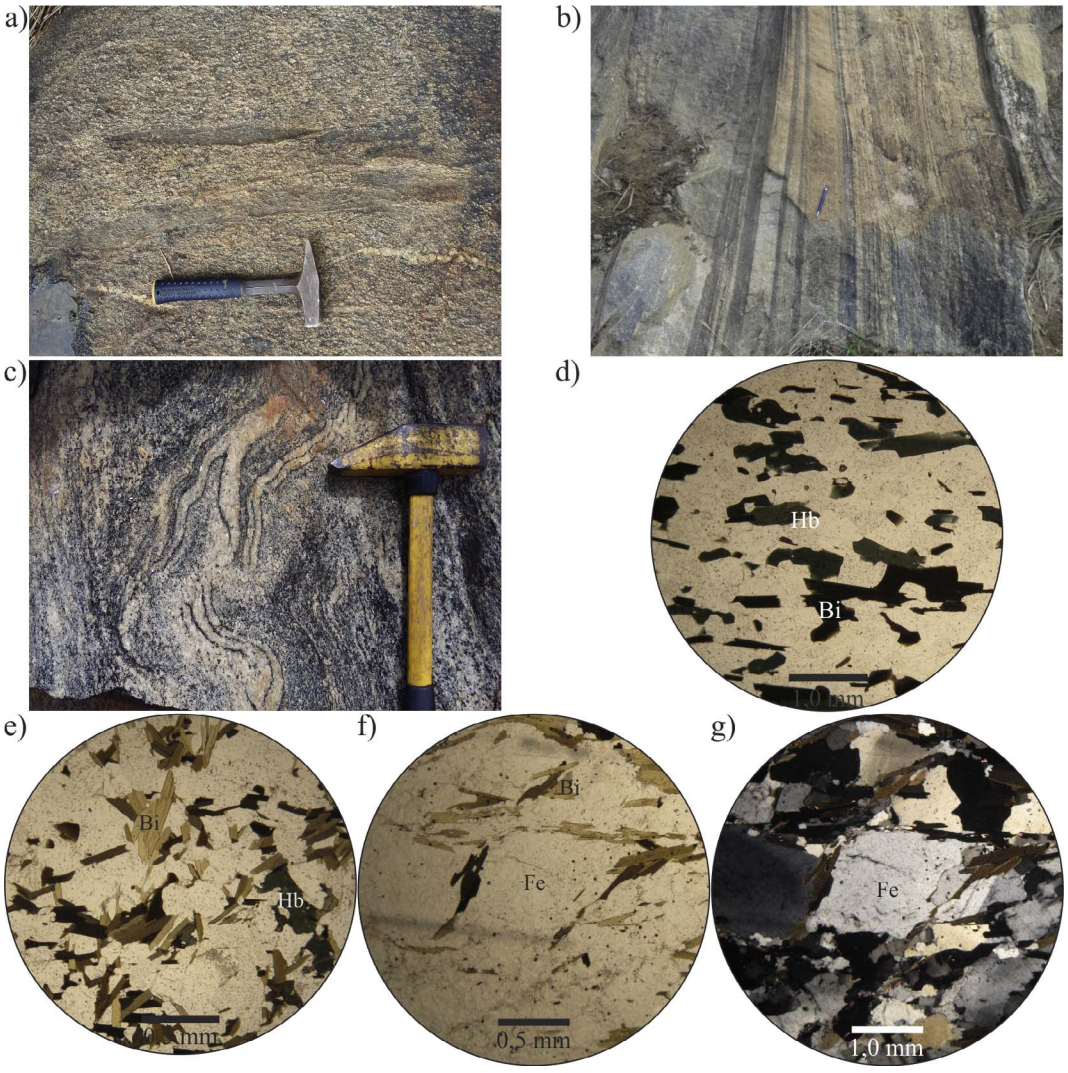

Fig. 7. Plutonic rocks from the Rio Negro Complex: a) coarse-grained hornblende biotite orthogneiss with gneissic foliation and mafic enclave; b) Mylonitic banding showing porphyroclastic feldspars; c) Migmatitic and folded biotite orthogneiss; d-f) Photomicrographs illustrating compositional and texture varieties for orthogneiss; d) Tonalitic hornblende biotite orthogneiss with gneissic foliation; e) Granodiorite hornblende biotite orthogneiss with weak foliation; f and g) Mylonitic texture showing porphyroclastic feldspar with recrystallized rims and surrounded by biotite. Biotite (Bi); (Hb) Hornblende; (Fe) Feldspar.

zircon are observed. Locally, large plagioclase crystals, interpreted as relict phenocrysts, have been observed.

4.2.2. Amphibolites

The amphibolites are associated with both the metasedimentary rocks of the Italva group (Fig. 5c, d) and the orthogneisses of the Serra da Prata Complex (Fig. 6b). They occur as thin lenses and *boudins* of outcrop scale, and also as large-decametric map scale lenses (Fig. 4). Based on this very homogeneous and mafic composition, we interpret the amphibolites as metamorphosed mafic igneous rocks.

In most outcrops, the amphibolite layers display a strong foliation, but coarse-grained granoblastic textures are also observed. These rocks comprise hornblende as the major constituent (55–95%) indicating mafic to ultramafic compositions, besides plagioclase, sphene, apatite, zircon, garnet and pyrite.

4.2.3. Morro do Escoteiro Suite Granitoids

The Morro do Escoteiro Suite crops out as discontinuous lenses that intrude Italva group rocks. The suite comprises garnet-biotite-muscovite granitoid rocks foliated, with coarse-grained and non-foliated to poors textures. Porphyritic varieties with tabular K-feldspar phenocrysts were observed.

The granitoid is composed of quartz, microcline, and minor plagioclase, with rare muscovite, biotite, and garnet. Microcline and plagioclase make up the largest crystals, probably representing relicts of primary phenocrysts.

4.2.4. Rio Negro Complex

The orthogneisses of the Rio Negro complex occur structurally below the rocks of the Italva domain (Fig. 3). Near this contact (Fig. 4a), the orthogneisses are more foliated and tectonically intercalated with rocks of the Italva group. Heilbron and Machado (2003) dated one of those lenses, which yielded a U-Pb concordant age of 635 ± 5 Ma.

Lenses of the orthogneisses of the Serra da Prata Complex enclosed within the rocks of the Rio Negro Complex were observed in one outcrop. In the northern segment of the Italva domain, bodies of coarse-grained to porphyritic orthogneisses within the marbles of the Italva Group. The field relationships suggest that these rocks represent

Table 1
Chemical analyses of major (%), and trace elements (ppm) for samples of the orthogneisses (Serra da Prata and Rio Negro Complexes), granitoids (Morro do Escoteiro Suite) and amphibolites. EU – Euclidelândia Unit; MES – Morro do Escoteiro Suite; SPC – Serra da Prata Complex; RNC – Rio Negro Complex; Amp – amphibolites.

Sample	Unit	Coordinates	SiO2	Al2O3	FeOt	MnO	MgO	CaO	Na2O	K2O	TiO2
SM-CM-07	MES	797205/7585648	73.02	14.38	1.45	0.02	0.31	1.24	2.75	4.68	0.22
SM-CM-02		799453/7584650	70.94	15.69	2.27	0.01	0.83	3.54	3.52	2.34	0.47
IT-NM-15		228871/7635640	73.24	13.60	2.58	0.06	0.22	2.06	3.79	3.21	0.22
SM-CB-85	SPC	795256/7587490	57.09	18.01	7.18	0.13	3.26	7.27	4.40	1.13	0.81
SM-CM-70A		789945/7580337	63.79	15.43	5.81	0.10	2.25	5.07	3.94	1.93	0.78
SM-CM-70B		789945/7580337	72.02	14.84	1.73	0.03	0.75	3.12	3.67	2.58	0.21
CR-R-04SP		793943/7592450	58.29	16.75	7.14	0.14	3.02	6.74	3.48	1.35	0.76
SM-CM-69		791839/7580485	71.55	14.11	2.65	0.04	0.75	2.86	3.48	3.54	0.43
SMM-CM-35		786663/7570186	55.76	17.05	8.50	0.16	4.14	7.39	2.86	1.53	1.08
SMM-CMM-153		791819/7582016	59.32	17.10	7.29	0.19	2.96	5.66	3.72	2.01	0.70
SMM-CMM-172	RNC	789649/7591762	64.79	16.12	4.88	0.08	1.51	4.27	3.10	2.96	0.91
CT-CMM-177A		775587/7581034	71.79	13.67	2.53	0.05	1.09	3.66	3.60	1.16	0.28
CT-CMM-177B		775587/7581034	66.95	15.91	3.60	0.08	1.81	4.23	3.84	1.35	0.58
CA-NM-22		773058/7570588	71.86	14.57	1.63	0.02	0.40	1.95	2.94	4.63	0.29
SAP-SMM-179A		804376/7600531	63.40	15.89	5.29	0.10	1.98	5.01	2.93	2.89	0.70
SAP-SMM-179B		804376/7600531	66.26	15.71	4.18	0.06	1.41	4.13	2.93	3.01	0.71
SAP-SMM-179C		804376/7600531	67.97	15.33	3.30	0.05	1.12	3.93	2.84	3.37	0.62
SMM-CB-87	Amp	793605/7591123	50.74	13.51	12.66	0.22	7.10	10.20	2.88	0.24	1.26
CAM-CMM-184B		197657/7608536	48.87	16.74	8.61	0.18	6.11	11.91	2.91	0.54	1.18
CR-R-04AF		793943/7592450	55.62	16.34	8.72	0.17	3.07	7.36	3.24	1.13	1.21
SAP-CMM-159		799308/7593420	49.61	13.92	11.58	0.36	4.22	12.25	3.09	0.79	1.76
SM-CM-18		793171/7576227	51.29	18.23	10.16	0.18	4.50	9.68	1.92	1.49	0.95

Sample	P2O5	LOI	Total	Y	Sc	Ba	Sr	Zr	Be	V	Cr
SM-CM-07	0.07	1.48	99.62	24	3	1152	228	117	2	10	20
SM-CM-02	0.11	0.76	100.50	4	4	871	418	139	1	29	20
IT-NM-15	0.06	0.25	99.14	13	6	2205	263	161	1	14	25
SM-CB-85	0.16	1.07	100.50	19	19	389	486	140	1	147	20
SM-CM-70A	0.19	1.09	100.40	21	14	763	298	228	1	110	20
SM-CM-70B	0.05	0.94	99.93	2	4	1079	339	65	1	32	20
CR-R-04SP	0.20	0.69	99.33	20	18	606	416	125	1	143	50
SM-CM-69	0.12	1.17	100.70	17	1	1382	416	221	1	51	20
SMM-CM-35	0.30	0.84	100.60	20	22	676	330	298	< 1	142	70
SMM-CMM-153	0.22	0.68	100.70	27	26	537	422	128	2	137	50
SMM-CMM-172	0.21	0.60	99.97	25	10	732	287	283	2	93	70
CT-CMM-177A	0.07	0.72	98.90	5	5	384	362	71	3	55	30
CT-CMM-177B	0.14	1.69	100.60	11	6	590	448	119	2	71	40
CA-NM-22	0.09	0.85	99.39	8	3	1539	316	185	1	12	20
SAP-SMM-179A	0.12	0.92	99.82	24	22	757	289	141	2	92	100
SAP-SMM-179B	0.20	0.70	99.77	12	6	872	308	273	2	69	80
SAP-SMM-179C	0.15	0.56	99.60	18	6	1057	316	282	2	58	60
SMM-CB-87	0.11	0.45	100.80	33	48	39	91	76	< 1	366	160
CAM-CMM-184B	0.15	0.85	99.00	22	29	179	474	97	< 1	248	190
CR-R-04AF	0.26	0.47	98.55	22	24	636	422	160	1	173	50
SAP-CMM-159	0.17	0.60	99.65	32	41	331	235	105	< 1	339	90
SM-CM-18	0.17	1.12	99.70	23	32	307	259	116	1	242	20

Sample	Unit	Coordinates	Co	Rb	Ni	Cu	Zn	Ga	Ge	As	Nb	Mo	Ag
SM-CM-07	MES	797205/7585648	38	116	20	10	50	19	1	5	10	2	1
SM-CM-02		799453/7584650	25	58	20	10	50	19	1	5	8	2	1
IT-NM-15		228871/7635640	10	73	20	10	54	15	2	5	5	2	1
SM-CB-85	SPC	795256/7587490	32	26	20	10	70	18	1	5	6	2	1
SM-CM-70A		789945/7580337	28	53	20	20	50	16	1	5	8	2	1
SM-CM-70B		789945/7580337	32	55	20	10	30	13	1	5	4	2	1
CR-R-04SP		793943/7592450	26	38	< 20	20	80	18	1	< 5	7	< 2	< 0.5
SM-CM-69		791839/7580485	31	57	20	10	30	13	1	5	8	2	1
SMM-CM-35		786663/7570186	27	45	< 20	20	100	19	1	< 5	5	< 2	1
SMM-CMM-153		791819/7582016	20	69	< 20	40	100	19	2	< 5	10	< 2	< 0.5
SMM-CMM-172	RNC	789649/7591762	11	128	< 20	< 10	110	23	1	< 5	16	< 2	1
CT-CMM-177A		775587/7581034	16	70	< 20	110	40	18	2	< 5	4	< 2	< 0.5
CT-CMM-177B		775587/7581034	20	68	20	< 10	50	18	1	< 5	5	< 2	< 0.5
CA-NM-22		773058/7570588	9	105	20	10	38	19	1	5	6	2	1
SAP-SMM-179A		804376/7600531	13	101	< 20	< 10	90	21	2	< 5	11	< 2	< 0.5
SAP-SMM-179B		804376/7600531	8	123	< 20	< 10	80	20	1	< 5	9	< 2	1
SAP-SMM-179C		804376/7600531	9	113	< 20	< 10	60	19	1	< 5	12	< 2	1
SMM-CB-87	Amp	793605/7591123	45	5	60	20	100	16	2	< 5	2	< 2	< 0.5
CAM-CMM-184B		197657/7608536	49	5	140	30	60	15	1	< 5	3	< 2	< 0.5
CR-R-04AF		793943/7592450	24	28	< 20	20	120	21	1	< 5	7	< 2	< 0.5
SAP-CMM-159		799308/7593420	43	4	80	60	90	19	2	< 5	7	< 2	< 0.5
SM-CM-18		793171/7576227	41	38	20	30	90	19	1	5	8	2	1

(*continued on next page*)

Table 1 (*continued*)

Sample	In	Sn	Sb	Cs	Hf	W	Ta	Tl	Pb	Bi	Th	U
SM-CM-07	0	1	1	1.5	3.7	489.0	0.7	0.4	26.0	0.4	13.1	2.0
SM-CM-02	0	1	1	1.0	3.9	392.0	0.4	0.1	16.0	0.4	4.7	0.4
IT-NM-15	0	1	0	1.3	4.1	87.2	0.3	0.4	13.2	0.1	5.1	0.7
SM-CB-85	0	1	1	1.2	3.5	160.0	0.3	0.1	9.0	0.4	0.7	0.5
SM-CM-70A	0	1	1	1.5	5.8	199.0	0.5	0.2	11.0	0.4	5.9	0.9
SM-CM-70B	0	1	1	1.5	2.0	503.0	0.3	0.1	15.0	0.4	6.1	0.3
CR-R-04SP	< 0.2	< 1	< 0.5	1.7	3.0	54.0	0.4	0.1	7.0	< 0.4	1.1	0.5
SM-CM-69	0	1	1	1.4	6.0	413.0	1.4	0.1	17.0	0.4	9.7	1.0
SMM-CM-35	< 0.2	< 1	< 0.5	0.9	5.7	36.0	0.3	0.2	6.0	< 0.4	0.8	0.5
SMM-CMM-153	< 0.2	2	< 0.5	2.2	3.3	28.0	0.5	0.3	11.0	< 0.4	8.2	0.5
SMM-CMM-172	< 0.2	< 1	< 0.5	1.8	6.8	37.0	0.9	0.5	14.0	< 0.4	9.7	0.9
CT-CMM-177A	< 0.2	2	< 0.5	1.1	1.8	94.0	0.6	0.2	10.0	< 0.4	1.8	1.5
CT-CMM-177B	< 0.2	2	< 0.5	0.7	2.8	109.0	0.5	0.3	7.0	< 0.4	1.1	1.2
CA-NM-22	0	1	0	1.3	5.0	86.1	0.5	0.4	10.1	0.1	14.7	0.9
SAP-SMM-179A	< 0.2	3	< 0.5	2.2	3.5	57.0	1.0	0.4	15.0	< 0.4	7.5	1.1
SAP-SMM-179B	< 0.2	1	< 0.5	2.8	6.7	22.0	0.9	0.5	16.0	< 0.4	17.2	1.5
SAP-SMM-179C	< 0.2	2	< 0.5	2.2	7.0	44.0	1.7	0.5	18.0	< 0.4	10.9	1.8
SMM-CB-87	< 0.2	< 1	< 0.5	< 0.5	2.1	14.0	0.1	< 0.1	< 5	< 0.4	0.4	0.1
CAM-CMM-184B	< 0.2	< 1	< 0.5	< 0.5	2.1	30.0	0.2	< 0.1	< 5	< 0.4	0.4	0.5
CR-R-04AF	< 0.2	1	< 0.5	1.1	4.0	27.0	0.4	< 0.1	13.0	< 0.4	2.9	0.7
SAP-CMM-159	< 0.2	< 1	< 0.5	< 0.5	2.6	27.0	0.5	< 0.1	6.0	< 0.4	0.9	0.4
SM-CM-18	0	1	1	0.9	3.2	286.0	0.4	0.1	6.0	0.4	1.2	0.6

different evolutionary stages of a single magmatic arc, instead of two juxtaposed magmatic arcs, as previously thought by Heilbron et al. (2013). This supposition is confirmed by the new U-Pb data.

In the studied area, the Rio Negro Complex is typically foliated hornblende biotite orthogneisses which a composition varies between granodiorites and granites not rarely with mafic enclaves (Fig. 7a, d, e). The rocks are coarse grained, either magmatic structure or weakly foliated to mylonitic (Fig. 7b, c). The mineralogy is dominated by, orthoclase, quartz, plagioclase with biotite as the major mafic component. Porphyritic texture is common with feldspars as phenocrysts or porphyroclasts with rims made of fine-grained crystals (Fig. 7f, g). Hornblende, garnet, apatite and zircon are the most common accessory minerals.

Large bodies of leucogneisses with the granitic composition are common, near its contact with other units. Besides microcline, plagioclase, and quartz, minor biotite, muscovite and garnet occur. Zircon, apatite, and monazite are accessory minerals. Heilbron and Machado (2003) dated one of these decametric lenses and yielded crystallization ages of ca. 580 Ma.

5. Geochemical analyses

5.1. Geochemical analyses

The selected least weathered samples from the Italva Domain and Rio Negro arc were crushed and milled at the "*Laboratório Geológico de Processamento de* Amostras" (LGPA) of the Rio de Janeiro State University (UERJ). Whole rock chemical analyses were carried out in the Activation Laboratories Ltd (Act-Labs), Ancaster, Canada.

The analytical techniques used were Lithium Metaborate/Tetraborate Fusion – Inductively Coupled Plasma (ICP) for major and part of trace elements and Mass Spectrometry (MS) for trace elements including rare earth elements. The analytical procedures follow the detailed description found in http://www.actlabs.com/page.aspx?page=516&app=226&cat1=549&tp=12&lk=no&menu=64&print=yes.

5.2. Results

Twenty-two samples were analyzed for major and trace elements

Table 2
Chemical analyses of REE (ppm) for samples of the orthogneisses (Serra da Prata and Rio Negro Complexes), granitoids (Morro do Escoteiro Suite) and amphibolites. EU – Euclidelândia Unit; MES – Morro do Escoteiro Suite; SPC – Serra da Prata Complex; RNC – Rio Negro Complex; Amp – amphibolite.

Sample	Unit	Coordinates	La	Ce	Pr	Nd	Sm	Eu	Gd	Tb	Dy	Ho	Er	Tm	Yb	Lu
SM-CM-07	MES	797205/7585648	56.6	86.0	11.5	42.2	7.7	2.3	5.8	0.8	4.5	0.8	2.3	0.3	2.2	0.3
SM-CM-02		799453/7584650	31.3	59.4	6.6	24.3	4.2	1.3	2.9	0.3	1.3	0.2	0.4	0.1	0.3	0.0
IT-NM-15		228871/7635640	33.9	60.6	6.4	22.9	3.7	1.4	3.3	0.5	2.4	0.5	1.3	0.2	1.4	0.2
SM-CB-85	SPC	795256/7587490	7.9	18.8	2.7	12.5	3.4	1.2	3.8	0.6	3.8	0.7	2.2	0.3	2.1	0.3
SM-CM-70A		789945/7580337	21.7	42.1	4.7	18.4	4.1	1.2	4.0	0.7	4.0	0.8	2.3	0.4	2.4	0.4
SM-CM-70B		789945/7580337	15.2	27.3	2.7	8.8	1.3	0.4	0.9	0.1	0.4	0.1	0.2	0.1	0.2	0.0
CR-R-04SP		793943/7592450	14.3	31.9	3.7	15.7	3.8	1.2	3.8	0.6	3.7	0.8	2.3	0.3	2.2	0.4
SM-CM-69		791839/7580485	37.9	75.3	8.4	30.7	5.7	1.0	4.6	0.7	3.6	0.7	1.9	0.3	1.7	0.3
SMM-CM-35		786663/7570186	13.9	33.1	4.4	19.4	4.3	1.5	4.1	0.6	3.9	0.8	2.4	0.4	2.4	0.4
SMM-CMM-153		791819/7582016	26.3	46.2	5.5	22.6	5.7	1.2	5.4	0.9	5.5	1.0	3.0	0.4	2.9	0.5
SMM-CMM-172	RNC	789649/7591762	35.6	76.1	9.1	35.2	8.1	1.5	7.2	1.0	5.8	1.0	2.6	0.3	1.7	0.3
CT-CMM-177A		775587/7581034	4.0	9.7	1.1	4.4	1.0	0.4	0.9	0.2	1.0	0.2	0.6	0.1	0.5	0.1
CT-CMM-177B		775587/7581034	11.5	24.4	2.9	11.9	2.4	0.8	2.0	0.3	1.9	0.4	1.1	0.2	1.2	0.2
CA-NM-22		773058/7570588	57.9	103.8	12.5	46.8	7.7	1.6	5.3	0.5	1.9	0.3	0.7	0.1	0.6	0.1
SAP-CMM-179A		804376/7600531	28.9	61.1	7.0	26.9	6.0	1.4	5.6	0.9	5.0	0.9	2.4	0.4	2.2	0.3
SAP-CMM-179B		804376/7600531	61.6	124.0	14.0	51.7	8.8	1.6	5.8	0.7	3.2	0.5	1.3	0.2	1.0	0.2
SAP-CMM-179C		804376/7600531	36.0	74.0	8.6	33.7	7.1	1.6	5.7	0.8	4.4	0.7	1.8	0.2	1.4	0.2
SMM-CB-87	Amp	793605/7591123	4.4	11.5	1.8	9.0	3.1	1.2	4.6	0.9	6.1	1.3	3.8	0.6	3.8	0.6
CAM-CMM-184B		197657/7608536	7.1	16.3	2.5	11.9	3.3	1.3	4.1	0.7	4.3	0.9	2.5	0.3	2.4	0.4
CR-R-04AF		793943/7592450	25.7	56.6	7.0	27.7	6.0	2.0	5.4	0.9	5.3	1.0	2.9	0.4	2.7	0.4
SAP-CMM-159		799308/7593420	10.2	21.4	3.2	15.2	4.4	1.7	5.6	1.0	6.4	1.3	3.7	0.6	3.4	0.6
SM-CM-18		793171/7576227	13.2	32.2	4.4	18.7	4.5	1.3	4.7	0.8	4.5	0.9	2.6	0.4	2.5	0.4

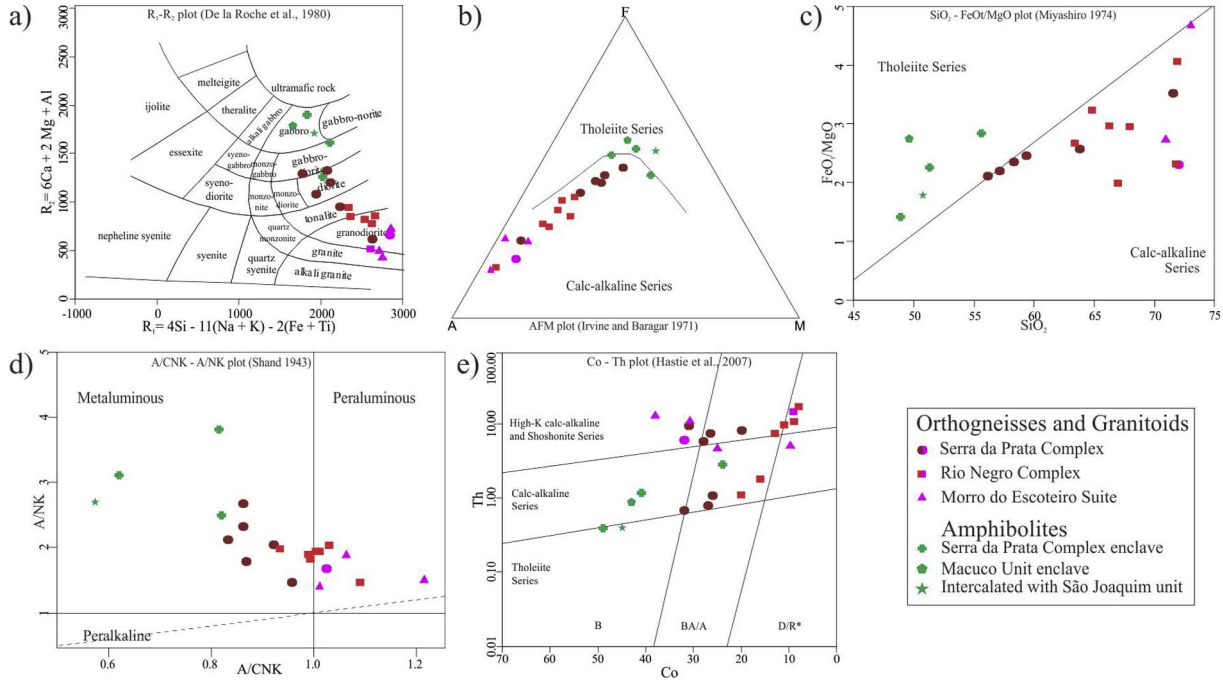

Fig. 8. Geochemistry diagrams from Serra da Prata Complex, Rio Negro Complex, granitoids of Morro do Escoteiro Suite and amphibolites: a) Classification diagram (R1–R2) of De la Roche et al. (1980); b) AFM Ternary Diagrams of Irvine and Baragar, 1971; c) Series diagram (FeO/MgO_3 vs. SiO_2) of Miyashiro (1974); d) Discrimination diagram A/CNK – A/NK of Shand (1943); e) Series diagram (Co – Th) of Hastie et al. (2007).

(Table 1) including rare earth elements (REE – Table 2): seven orthogneiss samples from the Serra da Prata Complex and seven from Rio Negro Complex; three granitoids samples from the Morro do Escoteiro Suite. Five amphibolite samples: three from enclaves within the Serra da Prata Complex (CAM-CMM-184B, CR-R-04AF, SM-CM-18), one within the Macuco unit (SAP-CMM-159) and one sample from amphibolite intercalated with marbles from São Joaquim Unit (SMM-CB-87).

5.3. Orthogneisses and granitoid rocks

Both the Serra da Prata and Rio Negro orthogneisses include rocks of dioritic, tonalitic and granodioritic chemical compositions (Fig. 8a). Foliated sub-alkaline granitoids of the Morro do Escoteiro Suite show calc-alkaline affinity, as visualized in the plots AFM and MgO + FeO_t *versus* SiO_2 diagrams (Fig. 8b, c).

From the Shand diagram (Fig. 8d), it is clear that the Serra da Prata Complex orthogneisses and most samples from the Rio Negro Complex are metaluminous. The leucogranites of the Morro do Escoteiro suite is

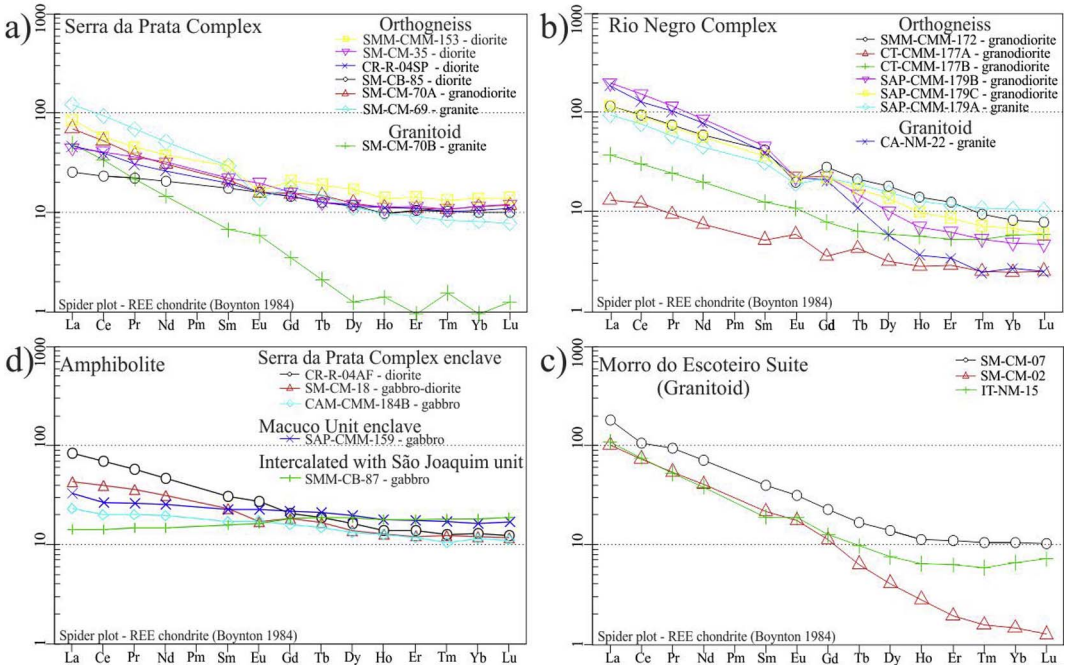

Fig. 9. Chondrite normalized REE diagrams (Boynton, 1984) for the (a) orthogneisses – Serra da Prata Complex – (b) granitoids – Morro do Escoteiro Suite – (c) amphibolites of the Italva Domain and (d) orthogneisses – Rio Negro Complex – of the Costeiro Domain.

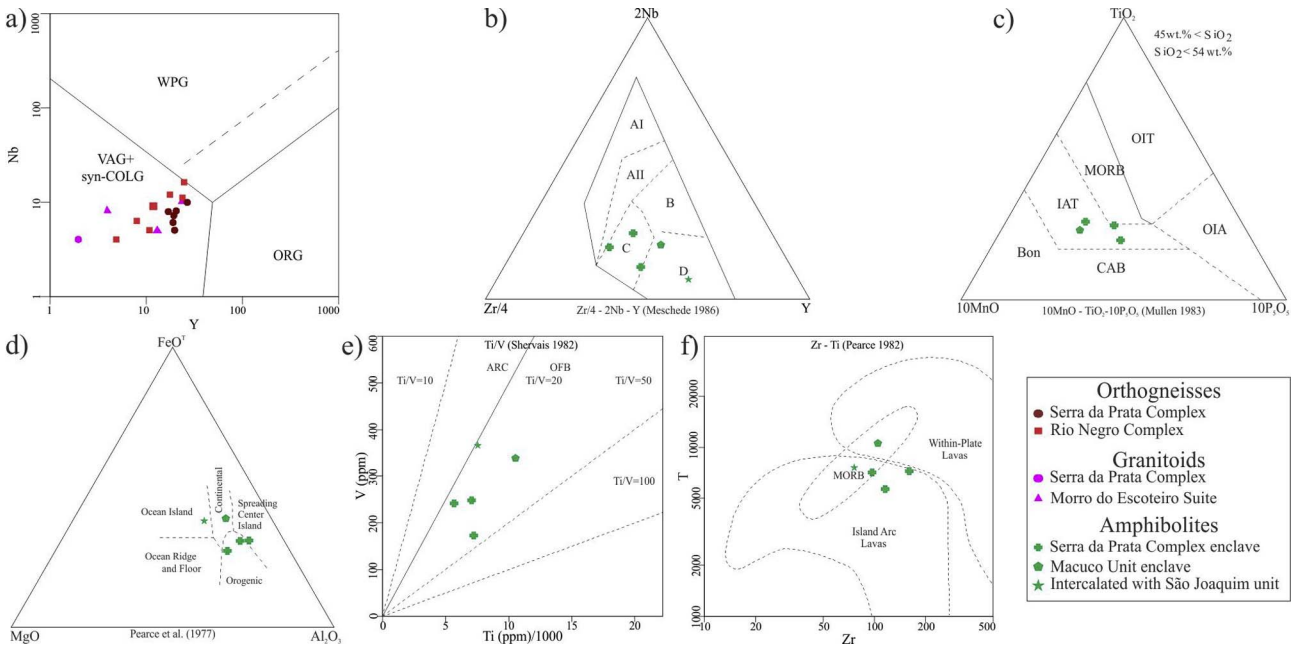

Fig. 10. Tectonic diagram for the orthogneisses, granitoids (a) and amphibolites (b–f) from Italva and Costeiro Domain.

slightly peraluminous. Both orthogneisses and granitoids define medium-K and high-K series (Fig. 8e).

The REE chondrite-normalized diagrams (Boynton, 1984) presented in Fig. 9a for the orthogneisses of the Serra da Prata Complex indicate enrichment in light rare earth elements (LREE), weak negative Eu anomalies and flat heavy rare earth elements (HREE) patterns. The La/Lu ratios increase with differentiation of the orthogneisses and granitoids. The few samples of the Rio Negro complex display more fractionated patterns, and variable Eu anomalies (Fig. 9b) related to the presence of different modal abundances of feldspar phenocrysts.

REE patterns of the peraluminous granitoids from the Morro do Escoteiro Suite (Fig. 9c) suggest homogeneous protoliths. The distribution of the HREE suggests the importance of garnet in the source rocks.

Tectonic discrimination diagrams (Fig. 10a) such as the NbxY (Pearce et al., 1984) corroborate a subduction environment suggesting arc environments for both the Serra da Prata and Rio Negro Complexes. Presumably, the Morro do Escoteiro Suite represents syn-collisional granites.

5.4. Amphibolites

Published geochemical data (Ragatky et al., 2007; Tupinambá and Heilbron, 2002; and Sad and Dutra, 1988) for the amphibolites of the Italva Domain indicate a predominance of tholeiitic rocks with Normal Mid-Oceanic Ridge Basalts (N-MORB) to Enriched-MORB to Back-Arc Basin Basalts (BABB) signature and more rarely, tholeiitic island arc basalts (IAB) signatures suggesting a back arc tectonic environment.

Five amphibolites samples were analyzed: three from Serra da Prata Complex enclaves, one Macuco Unit enclave and one sample intercalated with São Joaquim unit. The new data corroborates that the amphibolites include rocks of diorite, gabbro-diorite and gabbro chemical composition (Fig. 8a). These rocks belong to the sub-alkaline series with tholeiitic signature, as represented in the diagrams of Fig. 8b, c.

According to chondrite-normalized REE diagrams presented in Fig. 9d, the amphibolites from Serra da Prata Complex display flat patterns with slight enrichment in LREE suggesting island arc tholeiitic series (IAT) affinity. In contrast, two amphibolite samples from Macuco and São Joaquim units show a horizontal profile suggesting MORB affinities.

Table 3
Laboratories and methods used to yielder U-Pb geochronological data from Oriental Terrane.

Sample	Unit	Method U-Pb in zircon	Laboratory
SM-CB-84B SM-CM-07 SM-CM-02 SM-CM-69 SM-CM-70A SM-CM-70B SM-CB-85 SM-CMB-148	Amp MES MES SPC SPC SPC SPC EU	LA-MC-ICPMS	"Laboratório de Estudos Geocronológicos, Geodinâmicos e Ambientais" Geosciences Institute of the University of Brasília, Brazil
SMM-CMM-172 SMM-CMM-153	RNC SPC	LA-MC-ICPMS	Laboratório Multi usuário de Meio Ambiente e Materiais University of Rio de Janeiro State, Brasil (http://multilab-uerj.com.br/upb)
THE-02	RNC	SHRIMP	Laboratory of the Australian National University, Canberra, Australia. (http://shrimp.anu.edu.au/shrimp.php)
IT-NM-15	MES	SHRIMP	Radiogenic Isotope Facility of the Department of Earth and Atmospheric Sciences, University of Alberta, Edmonton, Canada. (Simonetti et al., 2006)

The tectonic discrimination diagrams of Fig. 10d–f (Pearce and Gale, 1977; Shervais, 1982; Pearce, 1982) also indicate signatures from MORB to IAT suggesting an immature arc tectonic setting, as previously considered by other authors (Sad and Dutra, 1988; Heilbron and Machado, 2003; Ragatky et al., 2007; Heilbron et al., 2008).

6. U-Pb Geochronological data

6.1. U-Pb geochronological analyses

The samples procedures for geochronological analyses were performed at the "*Laboratório Geológico de Processamento de* Amostras" of the Rio de Janeiro State University. First samples were crushed and milled, and heavy mineral concentrates were obtained by hand panning from disaggregated material. The heavy minerals were further separated with the Frantz magnetic separator into magnetic and diamagnetic fractions. Selection of zircons crystals, from the diamagnetic (preferably) and less magnetic fractions, was followed by the preparation of polished mounds.

The cathodoluminescence images (CL) were obtained at the "Laboratório de Microscopia Eletrônica de Varredura" (MEV) of the Geosciences Institute of the University of São Paulo (USP) and at the "Laboratório Multi usuário de Meio Ambiente e Materiais" (MuiltiLab) of the Rio de Janeiro State University (UERJ).

The U-Pb analyses of twelve samples were carried out in three different places depending on availability of each laboratory. The laboratories and methods used to analyze the samples are shown in Table 3.

Two international zircon standards were used for laser ablation: the UQ-Z1 (Machado and Gauthier, 1996) and the GJ-1 (Jackson et al., 2004). Laser frequency of 6 to 10 Hz was used with spot diameters of 20–30 μm.

The isotopic data was visualized by the Evaluation Neptune Software and transferred to Excel software for data reduction. The data was reduced and processed using UnB specific software developed by Bühn et al. (2009). The construction of the concordia diagrams was done using the Isoplot (version 3.00) statistical software of Ludwig (2003).

6.2. Results

Twelve samples were selected for geochronological investigation, and their location is presented in Fig. 4: one amphibolite sample; five orthogneisses from the Serra da Prata Complex; three leucogranite samples from the Morro do Escoteiro Suite; two orthogneisses from the Rio Negro Complex; and one metasedimentary sample from Euclidelândia Unit.

The following criteria were established to exclude analyses from age calculations: analyses from fractured zircons, analyses with more than 6% of discordance, high isotope ratio errors and when de laser analyzed either part of cores or rims yielding ages without geological meaning. The data are given in Tables 4–15 and the excluded data (*) are identified.

6.3. Amphibolite

The amphibolite sample (SM-CB-84B – Table 4) was collected from a decametric layer within hornblende biotite gneiss of the Serra da Prata Complex. Two zircon populations were identified, both translucent with white and yellow colors and with a size between 60 μm and 250 μm.

The first zircon population consists of prismatic grains more than 200 μm long and with width-to-length ratios of 2:1. The internal structure as observed in CL images shows typical igneous zoning with different phases of metamorphic overgrowth surrounding cores with oscillatory zoning (Fig. 11a, b).

Table 4
U-Pb isotopic data (LA-ICP-MS) from sample SM-CB-84B – Amphibolite. *Spots excluded from the calculation. Disc.: do not provide age.

SM-CB-84B	U ppm	Isotope Ratios						Ages (Ma)						Disc. %	f 206	Age (Ma)		$^{232}Th/^{238}U$	
		$^{207}Pb^*/^{235}U$	±	$^{206}Pb^*/^{238}U$	±	Rho 1	$^{207}Pb^*/^{206}Pb^*$	±	$^{206}Pb/^{238}U$	±	$^{207}Pb/^{235}U$	±	$^{207}Pb/^{206}Pb$	±					
First population																			
Z1	192.0	1.29276	4.83	0.13947	3.19	0.66	0.06722	3.62	842	27	843	41	845	31	0	0.0010	842	48	0.06
Z2*	559.8	0.82176	4.04	0.09910	2.40	0.59	0.06014	3.25	609	15	609	25	609	20	0	0.0003	609	27	0.53
Z3*	306.2	1.26191	5.29	0.13185	3.74	0.71	0.06941	3.74	798	30	829	44	911	34	12	0.0006	809	54	1.59
Z4B	443.8	0.74651	3.97	0.09157	2.22	0.56	0.05913	3.29	565	13	566	22	572	19	1	0.0005	565	24	0.32
Z4N	18.0	1.33965	10.81	0.14352	6.89	0.64	0.06770	8.33	865	60	863	93	859	72	-1	0.0029	864	110	0.23
Z5	27.5	1.25417	9.66	0.13773	6.87	0.71	0.06604	6.79	832	57	825	80	808	55	-3	0.0020	829	100	0.38
Z5B	49.0	1.40742	5.74	0.14776	4.22	0.73	0.06908	3.89	888	37	892	51	901	35	1	0.0019	890	64	0.23
Z6	55.6	1.35817	6.34	0.14499	4.63	0.73	0.06794	4.34	873	40	871	55	867	38	-1	0.0009	872	70	1
Z7*	-0.3	1.67483	18.51	0.16847	16.22	0.88	0.07210	8.93	1004	163	999	185	989	88	-1	0.0463	998	230	-3.51
Z8*	12.5	1.15995	7.29	0.13133	4.70	0.64	0.06406	5.58	795	37	782	57	743	41	-7	0.0054	791	67	0.28
Second population																			
0Z9	140.7	0.78041	5.55	0.09507	3.03	0.55	0.05953	4.65	585	18	586	32	587	27	0	0.0005	589	33	0.12
Z10	18.2	0.77572	5.40	0.09428	3.05	0.57	0.05968	4.45	581	18	583	31	592	26	2	0.0048	581	33	0.63
Z11*	39.5	0.96793	9.74	0.11256	6.52	0.67	0.06237	7.24	688	45	687	67	687	50	0	0.0020	688	82	0.40
Z12*	58.4	0.92588	7.60	0.10830	6.60	0.87	0.06200	3.78	663	44	665	51	674	26	2	0.0013	665	74	0.29
Z13*	47.0	1.15400	5.85	0.10030	4.04	0.69	0.08345	4.23	616	25	779	46	1280	54	Disc.	0.0036	–	–	0.45
Z14*	61.2	0.88886	8.39	0.10172	4.80	0.57	0.06338	6.87	624	30	646	54	721	50	13	0.0014	627	56	0.55
Z15*	53.6	1.33712	5.85	0.13175	5.04	0.86	0.07360	4.93	798	40	862	61	1031	51	Disc.	0.0026	–	–	0.43

Table 5
U-Pb isotopic data (LA-ICP-MS) from sample SMM-CMM-153 – Serra da Prata Complex. *Spots excluded from the calculation. Disc.: do not provide age.

SMM-CMM-153	U ppm	Isotope Ratios							Ages (Ma)						Disc %	f 206	Age (Ma)	±	$^{232}Th/^{238}U$
		$^{207}Pb^*/^{235}U$	±	$^{206}Pb^*/^{238}U$	±	Rho 1	$^{207}Pb^*/^{206}Pb^*$	±	$^{206}Pb/^{238}U$	±	$^{207}Pb/^{235}U$	±	$^{207}Pb/^{206}Pb$	±					
MA/01 A	151,7	0,63522	7,24	0,06396	5,34	0,74	0,07203	4,89	400	21,36	499	36,18	987	48,26	Disc.	0,0315	–	–	0,55
MA/02 A	201,2	1,27654	4,90	0,13950	3,87	0,79	0,06637	3,00	842	32,59	835	40,89	818	24,51	−3	0,0113	837	27	0,34
MA/03 A	769,3	0,86832	5,39	0,10514	4,58	0,85	0,05990	2,85	644	29,53	635	34,24	600	17,07	−7	0,0031	636	25	0,27
MA/004 A	221,6	1,31812	4,46	0,14184	3,61	0,81	0,06740	2,62	855	30,88	854	38,07	850	22,24	−1	0,0058	854	26	0,32
MA/05 A	176,4	1,46378	3,49	0,15712	2,31	0,66	0,06757	2,61	941	21,77	916	31,95	855	22,34	−10	0,0102	929	19	0,47
MA/06 A*	249,1	1,16054	5,00	0,12579	3,69	0,74	0,06691	3,38	764	28,18	782	39,12	835	28,19	9	0,0082	772	25	0,17
MA/07 A	53,1	1,10859	12,32	0,12328	7,74	0,63	0,06522	9,59	749	57,98	757	93,31	781	74,90	4	0,0452	751	53	0,23
MA/08 A*	207,7	0,60641	7,32	0,07295	4,83	0,66	0,06029	5,50	454	21,92	481	35,23	614	33,78	26	0,0159	457	42	0,10
MA/09 A	102,4	1,19552	12,86	0,13020	11,99	0,93	0,06659	4,65	789	94,60	799	102,69	825	38,37	4	0,0211	805	66	0,56
MA/01 B	211,6	1,42292	3,09	0,15162	2,11	0,68	0,06807	2,26	910	19,21	899	27,80	871	19,68	−5	0,0094	905	17	0,49
MA/02 B	388,3	1,19020	3,82	0,13266	2,42	0,63	0,06507	2,96	803	19,42	796	30,44	777	23,00	−3	0,0043	801	17	0,71
MA/03 B*	588,5	0,84345	3,80	0,10550	2,08	0,55	0,05798	3,18	647	13,45	621	23,60	529	16,82	−22	0,0145	642	25	0,01
MA/04 B*	473,5	1,33780	3,05	0,14808	2,33	0,76	0,06552	1,97	890	20,76	862	26,33	791	15,59	−13	0,0012	870	17	0,58
MA/05 B	3445,3	0,77966	3,81	0,09523	2,97	0,78	0,05938	2,39	586	17,39	585	22,29	581	13,88	−1	0,0011	586	16	0,69
MA/06 B*	276,0	1,44291	3,13	0,15925	2,32	0,74	0,06571	2,09	953	22,13	907	28,34	797	16,67	−19	0,0055	920	18	0,61
MA/07 B*	4124,5	1,04894	3,00	0,12668	2,06	0,69	0,06005	2,19	769	15,81	728	21,86	605	13,23	Disc.	0,0005	–	–	0,22
MA/08 B	214,9	1,34794	4,59	0,14850	2,93	0,64	0,06583	3,54	893	26,19	867	39,82	801	28,32	−11	0,0077	882	23	0,68
MA/09 B	595,7	1,18517	3,71	0,12969	2,05	0,55	0,06628	3,10	786	16,11	794	29,47	815	25,24	4	0,0023	788	15	0,54
MA/01 C*	734,2	1,62714	5,16	0,17829	4,09	0,79	0,06619	3,14	1058	43,28	981	50,60	812	25,53	−30	0,0025	982	65	1,05
MA/02 C*	584,4	1,38320	4,46	0,15296	2,85	0,64	0,06559	3,43	918	26,15	882	39,29	793	27,17	−16	0,0027	902	23	0,37
MA/03 C*	461,8	1,61811	4,35	0,17814	2,24	0,52	0,06588	3,73	1057	23,71	977	42,51	803	29,91	−32	0,0124	Disc	–	0,59
MA/04 C*	554,2	1,43576	3,91	0,15936	1,78	0,45	0,06534	3,48	953	16,92	904	35,33	785	27,35	−21	0,0041	943	15	0,88
MA/05 C	404,2	1,19397	5,38	0,13215	4,16	0,77	0,06553	3,40	800	33,31	798	42,89	791	26,92	−1	0,0046	799	29	0,42
MA/06 C*	546,3	1,54372	3,73	0,17080	1,64	0,44	0,06555	3,35	1017	16,71	948	35,39	792	26,55	−28	0,0037	1002	620	0,52
MA/07 C*	5099,1	0,93914	4,60	0,11578	2,95	0,64	0,05883	3,52	706	20,86	672	30,92	561	19,76	−26	0,0004	695	450	0,20
MA/08 C	1573,1	1,09114	7,45	0,12043	6,72	0,90	0,06571	3,22	733	49,25	749	55,80	797	25,65	8	0,0010	753	39	0,37
MA/09 C	608,0	1,54088	4,78	0,16349	2,93	0,61	0,06835	3,78	976	28,58	947	45,28	879	33,25	−11	0,0030	965	25	0,43
MA/01 D*	416,2	1,43849	3,29	0,15733	1,96	0,59	0,06631	2,65	942	18,42	905	29,82	816	21,64	−15	0,0039	929	16	0,49
MA/02 D	4667,7	0,82925	3,83	0,10149	2,82	0,74	0,05926	2,58	623	17,60	613	23,47	577	14,90	−8	0,0004	619	16	0,20
MA/03 D*	483,2	1,40437	3,86	0,15464	2,72	0,71	0,06587	2,73	927	25,22	891	34,35	802	21,91	−16	0,0040	906	21	0,68
MA/04 D*	4621,5	0,99196	3,61	0,12111	2,56	0,71	0,05941	2,54	737	18,89	700	25,23	582	14,76	−27	0,0005	718	570	0,17
MA/05 D	401,7	1,09146	4,00	0,12149	2,86	0,72	0,06516	2,79	739	21,17	749	29,96	779	21,76	5	0,0023	743	19	0,65
MA/06 D	2680,0	0,77734	5,40	0,09474	4,72	0,87	0,05951	2,62	583	27,54	584	31,53	586	15,34	0	0,0009	584	24	0,16
MA/07 D	1033,6	1,27913	12,57	0,14021	12,31	0,98	0,06617	2,53	846	104,16	836	105,17	812	20,57	−4	0,0023	820	47	0,49
MA/08 D	3171,7	1,18766	6,76	0,13235	6,33	0,94	0,06509	2,36	801	50,74	795	53,72	777	18,33	−3	0,0012	790	34	0,14
MA/09 D*	668,2	1,44953	3,00	0,15805	1,83	0,61	0,06652	2,38	946	17,35	910	27,33	823	19,57	−15	0,0024	932	15	0,59
MA/01 E	2433,3	0,75950	4,61	0,09342	3,08	0,67	0,05896	3,43	576	17,71	574	26,45	566	19,43	−2	0,0013	575	17	0,22
MA/02 E*	717,1	1,42303	4,37	0,15836	3,03	0,69	0,06517	3,15	948	28,72	899	39,27	780	24,55	−21	0,0024	919	730	0,64
MA/03 E*	6718,7	1,26505	3,61	0,15258	1,74	0,48	0,06013	3,17	915	15,91	830	30,00	608	19,27	Disc.	0,0017	–	–	0,64
MA/04 E*	727,6	1,81892	4,77	0,19607	2,97	0,62	0,06728	3,74	1154	34,24	1052	50,20	847	31,63	Disc.	0,0080	–	–	0,61
MA/05 E*	9339,6	0,66436	6,23	0,07574	4,98	0,80	0,06361	3,76	471	23,42	517	32,24	729	27,37	35	0,0067	477	850	1,79
MA/06 E*	898,8	1,27029	24,88	0,13800	5,11	0,21	0,06676	24,35	833	42,55	833	207,14	830	202,21	0	0,0058	833	40	0,06
MA/07 E	4425,6	0,72761	5,08	0,09053	3,82	0,75	0,05829	3,35	559	21,33	555	28,21	541	18,13	−3	0,0005	557	20	0,26
ME/01 A	83,6	1,34141	1,82	0,14560	1,27	0,70	0,06682	1,31	876	11,12	864	15,74	832	10,88	−5	0,0032	870	9,6	0,81
ME/02 A	447,8	0,86934	2,42	0,10401	2,19	0,91	0,06062	1,02	638	13,98	635	15,37	626	6,41	−2	0,0027	635	11	0,28
ME/03 A*	82,2	1,08955	3,21	0,11781	2,59	0,80	0,06707	1,91	718	18,56	748	24,05	840	16,03	15	0,0041	734	590	0,32
ME/04 A*	154,4	1,04534	2,33	0,12526	1,96	0,84	0,06053	1,26	761	14,91	727	16,91	622	7,81	Disc.	0,0248	–	–	0,31
ME/05 A*	41,5	1,40755	2,46	0,15424	1,72	0,70	0,06619	1,76	925	15,87	892	21,94	812	14,31	−14	0,0048	907	490	0,62
ME/06 A	249,6	0,90802	2,94	0,10792	2,04	0,69	0,06102	2,11	661	13,50	656	19,29	640	13,54	−3	0,0014	659	12	0,16
ME/07 A*	87,1	1,05503	4,24	0,11468	4,02	0,95	0,06672	1,34	700	28,15	731	31,01	829	11,13	Disc.	0,0040	–	–	0,60
ME/08 A	179,6	0,80968	4,84	0,09751	4,37	0,90	0,06023	2,06	600	26,24	602	29,13	612	12,63	2	0,0087	603	22	0,15
ME/09 A*	159,3	1,05847	2,38	0,11403	1,66	0,70	0,06733	1,70	696	11,56	733	17,44	848	14,44	Disc.	0,0023	–	–	0,69
ME/01 B	4367,1	1,12813	8,02	0,12603	7,59	0,95	0,06492	2,59	765	58,06	767	61,48	772	19,96	1	0,0003	768	39	0,07
ME/02 B	726,0	1,47710	6,92	0,15006	6,38	0,92	0,07139	2,68	901	57,50	921	63,74	969	25,97	7	0,0011	934	39	0,73
ME/03 B	2997,1	1,50085	6,68	0,15403	6,24	0,93	0,07067	2,38	923	57,64	931	62,18	948	22,59	3	0,0002	937	36	0,07
ME/04 B	2107,7	1,50773	6,93	0,15323	6,45	0,93	0,07136	2,55	919	59,27	934	64,74	968	24,67	5	0,0005	945	38	0,24
ME/05 B	365,0	1,49520	6,96	0,15427	6,45	0,93	0,07029	2,59	925	59,70	928	64,58	937	24,29	1	0,0039	931	38	0,42
ME/06 B*	119,9	1,63354	8,79	0,18427	5,47	0,62	0,06430	6,88	1090	59,65	983	86,44	751	51,70	−45	0,0100	1031	49	0,74
ME/07 B*	129,2	0,82986	13,11	0,09280	11,93	0,91	0,06486	5,44	572	68,22	614	80,42	770	41,88	26	0,0111	608	61	1,01
ME/08 B	2081,6	1,24404	9,87	0,13444	7,13	0,72	0,06711	6,82	813	58,00	821	80,97	841	57,35	3	0,0074	817	51	−0,63

(*continued on next page*)

Table 5 (*continued*)

SMM-CMM-153	U ppm	Isotope Ratios						Ages (Ma)						Disc %	f 206	Age (Ma)	±	$^{232}Th/^{238}U$
		$^{207}Pb^*/^{235}U$	±	$^{206}Pb^*/^{238}U$	±	Rho 1	$^{207}Pb^*/^{206}Pb^*$	±	$^{206}Pb/^{238}U$	±	$^{207}Pb/^{235}U$	±	$^{207}Pb/^{206}Pb$	±					
ME/09 B	460,9	1,60168	7,16	0,16697	6,05	0,84	0,06957	3,84	995	60,19	971	69,54	916	35,17	−9	0,0021	979	41	0,60
ME/01 C*	774,7	0,77462	3,93	0,09243	3,78	0,96	0,06078	1,09	570	21,53	582	22,90	632	6,91	10	0,0022	Disc	–	0,72
ME/02 C	804,5	1,43638	1,47	0,15432	0,97	0,66	0,06751	1,10	925	8,98	904	13,26	853	9,39	−8	0,0014	916	8	0,39
ME/03 C	424,0	0,83280	7,99	0,09831	7,59	0,95	0,06144	2,50	604	45,88	615	49,16	655	16,37	8	0,0213	624	34	0,10
ME/04 C*	17,2	0,95246	7,01	0,10696	4,93	0,70	0,06458	4,99	655	32,27	679	47,63	761	37,95	14	0,0197	662	30	2,01
ME/05 C*	419,9	0,96602	7,71	0,10967	7,47	0,97	0,06388	1,91	671	50,09	686	52,91	738	14,10	9	0,0003	710	31	0,13
ME/06 C*	197,8	1,51255	1,49	0,16217	1,06	0,72	0,06765	1,04	969	10,29	935	13,89	858	8,90	Disc.	0,0029	–	–	0,28
ME/07 C*	78,2	1,20389	3,09	0,13302	2,73	0,88	0,06564	1,44	0	8484,06	6	1429,28	0	5746,36	69	0,0094	802	34	1,86
ME/08 C	180,8	1,35729	1,51	0,14609	0,94	0,63	0,06738	1,17	879	8,30	871	13,11	850	9,96	−3	0,0019	876	7,4	0,67
ME/09 C	110,6	1,48470	4,83	0,15534	1,81	0,38	0,06932	4,48	931	16,89	924	44,64	908	40,66	−2	0,0136	930	15	1,36
ME/01 D	219,9	1,21981	2,01	0,13349	1,68	0,84	0,06627	1,10	808	13,58	810	16,28	815	8,99	1	0,0009	809	11	0,17
ME/02 D	99,5	1,22256	2,15	0,13321	1,19	0,55	0,06656	1,79	806	9,58	811	17,40	824	14,72	2	0,0026	807	8,8	0,51
ME/03 D	228,7	1,19376	3,37	0,13151	2,35	0,70	0,06584	2,41	796	18,71	798	26,86	801	19,32	1	0,0017	797	17	0,71
ME/04 D	930,3	0,78498	1,89	0,09551	1,61	0,85	0,05961	0,99	588	9,49	588	11,13	589	5,82	0	0,0004	588	8,4	0,26
ME/05 D	461,5	0,84732	5,08	0,10225	4,81	0,95	0,06010	1,62	628	30,21	623	31,65	607	9,81	−3	0,0087	619	22	0,20
ME/06 D*	4,5	1,23740	47,00	0,14816	40,57	0,86	0,06057	23,75	891	361,30	818	384,36	624	148,20	−43	0,2171	801	270	−0,18
ME/07 D	262,7	1,21572	1,79	0,13346	1,21	0,68	0,06607	1,31	808	9,80	808	14,45	809	10,62	0	0,0017	808	8,7	0,35
ME/08 D	182,0	0,73740	2,99	0,08984	2,57	0,86	0,05953	1,53	555	14,27	561	16,78	586	8,95	5	0,0335	559	13	−0,22
ME/09 D	58,6	1,25229	3,18	0,13749	1,82	0,57	0,06606	2,60	830	15,15	824	26,21	808	21,04	−3	0,0070	829	14	0,30
ME/01 E*	119,9	1,15125	8,71	0,08249	4,58	0,53	0,10122	7,41	511	23,41	778	67,74	1647	121,94	Disc.	0,1943	–	–	0,86
ME/02 E	257,5	0,81567	3,17	0,09776	2,81	0,89	0,06051	1,47	601	16,92	606	19,22	622	9,13	3	0,2821	605	14	−0,53
ME/03 E	1274,3	0,81705	2,72	0,09907	2,51	0,92	0,05981	1,06	609	15,28	606	16,52	597	6,32	−2	0,0004	605	12	0,28
ME/04 E	85,0	1,34155	1,87	0,14349	1,03	0,55	0,06781	1,56	864	8,86	864	16,13	863	13,47	0	0,0039	864	8	0,54
ME/05 E*	1,3	1,77148	56,83	0,20224	27,82	0,49	0,06353	49,55	1187	330,27	1035	588,18	726	359,72	−64	0,3478	1122	270	1,95
ME/06 E*	188,6	1,28363	1,57	0,14102	1,06	0,68	0,06602	1,15	850	9,05	838	13,14	807	9,29	−5	0,0019	845	8	0,17
ME/07 E*	102,4	0,99200	2,56	0,10841	1,74	0,68	0,06636	1,87	664	11,57	700	17,90	818	15,31	Disc.	0,0044	–	–	0,26

The preserved cores from five zircons yielded a concordant age of 859 ± 31 Ma interpreted as the crystallization age of the amphibolite (Fig. 11e). This result is very similar to the reported U-Pb TIMS age of 848 ± 11 Ma (Heilbron and Machado, 2003) for an amphibolite sample collected nearby the Italva town.

The second analyzed population consists of grains with rounded and ovoid shapes, with a diameter less than 90 μm and chaotic internal structures (Fig. 11c, d). According to Hoskin and Black (2000), Hoskin & Schaltegger (2003), Corfu et al. (2003) and Kroner et al. (2014), this texture is typical of zircons that grew during high-grade metamorphism. These zircon grains yielded the concordant age of 584 ± 14 Ma, corroborating the age of the high-temperature metamorphic episode (Fig. 11f) previously reported by Heilbron and Machado (2003).

6.4. Serra da Prata Complex

Five samples of representative varieties of the orthogneisses from the Serra da Prata complex were collected: four are hornblende biotite orthogneisses (SM-CB-85, SM-CM-70A, SM-CM-69, SMM-CMM-153); one is representative of the biotite orthogneisses of granitic composition (SM-CM-70B). The numerical data are given in Tables 5–9.

The majority of the zircon grains are vitreous and translucent with pale pink color, and rounded, elongate and prismatic shapes with variable sizes between 50 μm and 320 μm and with width-to-length ratios of 1:1 to 6:1. CL images (Fig. 12a) show that most zircon grains display internal igneous structures with the concentric and parallel zoning of different widths. Subordinated grains show chaotic cores surrounded by oscillatory zoning.

The analyses of the Serra da Prata Complex furnished ages between 856 ± 9 and 588 ± 12 Ma that reveals both Tonian and Ediacaran geological episodes (see Fig. 12).

The analyses of the igneous cores from zoned zircons grains yielded Tonian concordant ages of 856 ± 9 Ma, 848 ± 7 Ma, 839 ± 17 Ma 838 ± 8 Ma and 807 ± 4 Ma. These data are interpreted to reflect the age of magmatic crystallization for this complex (Fig. 12b–f) which is corroborated by Th/U > 0.1 according to Rubatto et al. (1999) to classify igneous zircons (see Tables 5–9).

Analyzes from chaotic cores and some rims with Th/U < 0.1 provided concordant ages of 629 ± 6 Ma and 620 ± 16 Ma (Fig. 12g, h), indicating the Ediacaran age of metamorphism which disordered the internal structure of these Tonian zircons.

These ages are coincident with both new ages presented in this work, and the previously cited published interval between 790 and 620 Ma of the Rio Negro Complex crystallization ages. These data suggest that there are both Tonian and Ediacaran stages for arc evolution in the Ribeira Belt.

Finally, analyzed metamorphic rims produced concordant ages of 602 ± 7 Ma and 580 ± 12 Ma (Fig. 12a, i, j) suggesting a regionally extensive metamorphic interval of 602–567 Ma in Costeiro and Italva Domain.

6.5. Granitoid rocks from the Morro do Escoteiro Suite

Three granitic samples from the Morro do Escoteiro Suite were collected: SM-CM-07, SM-CM-02 and IT-NM-15 (Tables 10–12). The zircons grains exhibit vitreous with pink and yellow colors and dull brownish ones. Their shape is prismatic to elongate with a size between 130 μm and 425 μm and width-to-length ratios of 1:1 to 5:1. The CL images showed both igneous and inherited zircons grains with oscillatory rims (Fig. 13a).

The inherited ages from igneous cores yield Paleoproterozoic to Neoproterozoic concordant ages between 2009 and 1212 Ma, and of 805 ± 24 Ma and 669 ± 20 Ma (Fig. 13b–d). The non-inherited ages from igneous cores furnish concordant ages of 602 ± 6 Ma and 600 ± 8 Ma and their real metamorphic rims provide concordant ages

Table 6
U-Pb isotopic data (LA-ICP-MS) from sample SM-CB-85 – Serra da Prata Complex. *Spots excluded from the calculation.

SM-CM-85	U ppm	Ratios							Age (Ma)						Disc. %	f 206	Age (Ma)	±	$^{232}Th/^{238}U$
		$^{207}Pb^*/^{235}U$	±	$^{206}Pb^*/^{238}U$	±	Rho 1	$^{207}Pb^*/^{206}Pb^*$	±	$^{206}Pb/^{238}U$	±	$^{207}Pb/^{235}U$	±	$^{207}Pb/^{206}Pb$	±					
Z1	26.0	1.25055	6.56	0.13644	4.58	0.70	0.06647	4.70	825	38	824	54	821	39	0	0.0019	824	67	0.87
Z2	24.2	1.26804	6.27	0.13750	3.93	0.63	0.06689	4.89	831	33	832	52	834	41	0	0.0026	831	59	0.72
Z3B	298.3	0.79205	3.07	0.09533	1.64	0.53	0.06026	2.60	587	10	592	18	613	16	4	0.0003	588	18	0.10
Z3N	48.3	1.27613	4.71	0.13819	2.38	0.51	0.06698	4.06	834	20	835	39	837	34	0	0.0011	835	36	0.83
Z4	22.9	1.29532	6.34	0.14000	4.05	0.64	0.06710	4.88	845	34	844	54	841	41	0	0.0012	844	61	0.70
Z5	19.4	1.34230	6.72	0.14361	4.73	0.70	0.06779	4.77	865	41	864	58	862	41	0	0.0012	865	71	0.74
Z6	24.4	1.33631	5.52	0.14296	3.24	0.59	0.06780	4.46	861	28	862	48	862	38	0	0.0013	861	50	0.73
Z7	12.6	1.15679	6.84	0.12874	4.79	0.70	0.06517	4.88	781	37	780	53	780	38	0	0.0029	781	67	0.63
Z8	23.3	1.30827	5.78	0.14037	4.80	0.83	0.06760	3.22	847	41	849	49	856	28	1	0.0027	849	66	0.47
Z9	42.3	1.22465	6.19	0.13477	3.88	0.63	0.06591	4.83	815	32	812	50	803	39	−1	0.0015	814	57	0.52
Z10	32.5	1.36357	5.95	0.14485	4.25	0.71	0.06827	4.16	872	37	873	52	877	36	1	0.0019	873	64	0.58
Z11N	40.4	1.33484	5.44	0.14293	2.39	0.44	0.06774	4.89	861	21	861	47	860	42	0	0.0026	861	38	0.63
Z11B	38.7	1.34317	5.61	0.14333	2.39	0.43	0.06797	5.08	863	21	865	49	867	44	0	0.0012	864	38	0.53
Z12	33.1	1.28456	5.00	0.13814	3.30	0.66	0.06744	3.76	834	27	839	42	851	32	2	0.0008	836	49	0.69
Z13	37.9	1.38914	5.16	0.14686	2.69	0.52	0.06860	4.41	883	24	884	46	887	39	0	0.0009	884	43	0.43
Z14N	55.0	1.33003	4.35	0.14271	2.90	0.67	0.06759	3.24	860	25	859	37	856	28	0	0.0008	860	44	0.74
Z14B	576.9	0.82013	3.19	0.09882	1.34	0.42	0.06019	2.89	607	8	608	19	610	18	0	0.0001	608	15	0.06
Z15N	49.5	1.35377	4.69	0.14448	2.93	0.63	0.06795	3.66	870	26	869	41	867	32	0	0.0012	870	46	0.45
Z15B	101.3	0.86029	4.72	0.10166	3.01	0.64	0.06138	3.63	624	19	630	30	652	24	4	0.0008	625	35	0.20
Z16	61.4	1.33798	4.45	0.14301	2.66	0.60	0.06785	3.57	862	23	862	38	864	31	0	0.0007	862	41	0.63
Z17N*	−4286.2	1.35395	5.68	0.14350	3.19	0.56	0.06843	4.70	864	28	869	49	882	41	2	0.0017	866	50	0.63
Z17B*	−41974.5	0.80391	3.43	0.09738	1.38	0.40	0.05987	3.14	599	8	599	21	599	19	0	0.0002	599	16	0.09
Z18*	−10559.1	1.33059	4.05	0.14158	2.42	0.60	0.06816	3.25	854	21	859	35	874	28	2	0.0007	855	37	0.62
Z19*	−7075.1	1.31521	5.70	0.14041	3.46	0.61	0.06793	4.53	847	29	852	49	867	39	2	0.0009	848	53	0.66
Z20	165.3	1.32504	4.31	0.14196	2.69	0.62	0.06770	3.36	856	23	857	37	859	29	0	0.0007	856	41	0.73
Z21	128.0	1.36566	4.38	0.14586	2.66	0.61	0.06790	3.47	878	23	874	38	866	30	−1	0.0007	877	42	0.69
Z22	101.4	1.35163	3.86	0.14607	1.60	0.42	0.06711	3.51	879	14	868	34	841	30	−4	0.0011	878	26	0.76
Z23N	95.0	1.40386	6.03	0.14810	3.88	0.64	0.06875	4.62	890	35	891	54	891	41	0	0.0011	890	61	0.77
Z23B	594.0	0.81446	2.42	0.09881	1.25	0.52	0.05978	2.08	607	8	605	15	596	12	−2	0.0001	607	14	0.10
Z24	58.2	1.27039	4.75	0.13794	2.45	0.52	0.06679	4.07	833	20	833	40	831	34	0	0.0014	833	37	0.24
Z25	58.5	1.32276	4.84	0.14222	3.19	0.66	0.06746	3.65	857	27	856	41	852	31	−1	0.0010	857	48	0.60
Z26	64.0	1.37150	5.52	0.14671	3.11	0.56	0.06780	4.56	882	27	877	48	862	39	−2	0.0012	841	49	0.76
Z27	68.6	1.36621	3.38	0.14587	2.75	0.81	0.06793	1.96	878	24	875	30	866	17	−1	0.0007	875	39	0.67
Z28	79.5	1.35224	3.72	0.14487	2.51	0.68	0.06770	2.74	872	22	869	32	859	24	−1	0.0005	871	38	0.54
Z29	78.4	1.40968	4.15	0.15050	1.59	0.38	0.06793	3.84	904	14	893	37	866	33	−4	0.0005	906	23	0.77

Table 7
U-Pb isotopic data (LA-ICP-MS) from sample SM-CM-70A – Serra da Prata Complex. *Spots excluded from the calculation.

SM-CM-70A	U ppm	Isotope Ratios							Ages (Ma)						Disc. %	f 206	Age (Ma)	±	$^{232}Th/^{238}U$
		$^{207}Pb^*/^{235}U$	±	$^{206}Pb^*/^{238}U$	±	Rho 1	$^{207}Pb^*/^{206}Pb^*$	±	$^{206}Pb/^{238}U$	±	$^{207}Pb/^{235}U$	±	$^{207}Pb/^{206}Pb$	±					
003-Z1	59.5	1.36527	3.71	0.14753	2.10	0.56	0.06712	3.07	887	19	874	32	841	26	−5	0.0005	884	36	0.72
004-Z2	86.4	1.32485	4.55	0.14216	2.82	0.62	0.06759	3.57	857	24	857	39	856	31	0	0.0005	857	43	0.88
005-Z3	33.2	1.34879	6.58	0.14460	4.83	0.73	0.06765	4.47	871	47	867	57	858	38	−1	0.0011	869	72	0.80
006-Z4	18.2	1.27857	7.42	0.13853	5.60	0.75	0.06694	4.87	836	47	836	62	836	41	0	0.0021	836	81	0.60
009-Z5	29.9	1.23446	5.69	0.13487	4.27	0.75	0.06638	3.75	816	35	816	46	818	31	0	0.0007	816	60	0.57
010-Z6N	53.4	1.22699	4.78	0.13439	3.25	0.68	0.06622	3.51	813	26	813	39	813	29	0	0.0008	813	47	0.72
011-Z6B	77.6	1.27214	3.71	0.13802	2.71	0.73	0.06685	2.53	833	23	833	31	833	21	0	0.0005	833	39	0.42
012-Z7*	−0.2	5.33722	31.48	0.04700	27.40	0.87	0.82363	15.50	296	81	1875	590	4963	769	94	0.1989	80	85	-2
015-Z8	39.0	1.26499	5.54	0.13756	3.36	0.61	0.06670	4.40	831	28	830	46	828	36	0	0.0012	831	50	0.58
016-Z9	55.6	1.28926	4.88	0.14000	3.24	0.66	0.06679	3.65	845	27	841	41	831	30	−2	0.0006	843	48	0.64
017-Z10	33.6	1.22110	6.77	0.13441	4.69	0.69	0.06589	4.89	813	38	810	55	803	39	−1	0.0018	812	67	0.48
018-Z11	76.9	1.23988	3.81	0.13540	2.82	0.74	0.06641	4.87	819	23	819	31	819	21	0	0.0005	819	40	0.53
021-Z12	58.3	1.26478	5.23	0.13711	2.25	0.43	0.06690	4.72	828	19	830	43	835	39	1	0.0009	828	34	0.64
022-Z13	42.1	1.23623	6.72	0.13525	4.94	0.73	0.06629	4.55	818	40	817	55	816	37	0	0.0011	817	70	0.40
023-Z14	53.1	1.31860	5.70	0.14156	3.70	0.65	0.06756	4.34	853	32	854	49	855	37	0	0.0006	854	56	0.46
024-Z15B*	208.2	0.92827	3.48	0.10895	2.25	0.65	0.06180	2.65	667	15	667	23	667	18	0	0.0003	667	28	0.21
027-Z15N	65.7	1.28544	4.03	0.13920	2.70	0.67	0.06698	3.00	840	23	839	34	837	25	0	0.0008	840	40	0.64
028-Z16	43.9	1.33343	5.21	0.14398	3.14	0.60	0.06717	4.16	867	27	860	45	843	35	−3	0.0010	865	49	0.68
029-Z17	40.6	1.29809	5.31	0.14139	3.49	0.66	0.06659	4.00	853	30	845	45	825	33	−3	0.0010	850	53	0.48
030-Z18	43.2	1.25730	5.19	0.13721	4.24	0.82	0.06646	2.99	829	35	827	43	821	25	−1	0.0014	827	58	0.49
033-Z19	63.7	1.30815	4.39	0.14084	3.13	0.71	0.06737	3.08	849	27	849	37	849	26	0	0.0007	849	46	0.48
034-Z20	56.1	1.34771	3.95	0.14405	3.33	0.84	0.06786	2.12	868	29	867	34	864	18	0	0.0008	867	46	0.56
035-Z21	79.9	1.31111	3.92	0.14120	2.59	0.66	0.06734	2.94	851	22	851	33	848	25	0	0.0005	851	39	0.50
036-Z22	64.6	1.31718	4.10	0.14154	2.95	0.72	0.06750	2.86	853	25	853	35	853	24	0	0.0007	853	44	0.49
ZR1N*	69.2	1.04058	3.94	0.11681	3.21	0.82	0.06461	2.27	712	23	724	29	762	17	6	0.0043	720	40	0.26
ZR1B	72.9	1.34945	3.35	0.14639	2.62	0.78	0.06686	2.09	881	23	867	29	833	17	-6	0.0027	871	38	0.38
ZR2N*	47.3	1.02753	5.71	0.11396	3.13	0.55	0.06539	4.77	696	22	718	41	787	38	12	0.0068	699	41	0.40
ZR2B	45.8	1.26294	7.24	0.13668	3.25	0.45	0.06702	6.47	826	27	829	60	838	54	1	0.0060	826	50	0.38
ZR3B	111.3	1.29857	3.18	0.13900	1.98	0.62	0.06776	2.49	839	17	845	27	861	21	3	0.0012	841	30	0.36
ZR4N	67.9	1.21041	2.81	0.13061	1.74	0.62	0.06721	2.20	791	14	805	23	844	19	6	0.0042	795	25	0.16
ZR4B*	48.1	0.89810	11.85	0.09891	9.55	0.81	0.06585	7.02	608	58	651	77	802	56	24	0.0097	623	110	0.35
ZR5N*	38.1	0.99251	11.36	0.10634	9.53	0.84	0.06770	6.17	651	62	700	79	859	53	24	0.0051	676	56	0.52
ZR5B	47.9	1.37773	6.00	0.14391	4.20	0.70	0.06944	4.28	867	36	879	53	912	39	5	0.0153	872	32	0.30
ZR6N*	55.7	1.17765	5.06	0.12540	3.29	0.65	0.06811	3.84	762	25	790	40	872	34	13	0.0026	769	23	0.62
ZR6B	72.5	1.25885	4.52	0.13642	3.15	0.70	0.06692	3.25	824	26	827	37	835	27	1	0.0018	826	23	0.39
ZR7B	412.0	0.82558	3.06	0.09764	2.18	0.71	0.06132	2.15	601	13	611	19	651	14	8	0.0005	604	24	0.09
ZR8B	132.3	0.83235	4.09	0.09924	2.97	0.73	0.06083	2.82	610	18	615	25	633	18	4	0.0015	612	27	0.08
ZR9N	51.6	1.25773	8.89	0.13415	5.72	0.64	0.06800	6.81	811	46	827	74	869	59	7	0.0040	816	42	0.66
ZR9B	231.2	0.90990	3.34	0.10488	2.32	0.70	0.06292	2.40	643	15	657	22	706	17	9	0.0015	647	28	0.12

Table 8
U-Pb isotopic data (LA-ICP-MS) from sample SM-CM-70B – Serra da Prata Complex. *Spots excluded from the calculation. Disc.: do not provide age.

SM-CM-70B	U ppm	Isotope Ratios							Ages (Ma)						Disc. %	f 206	Age (Ma)	±	$^{232}Th/^{238}U$
		$^{207}Pb^*/^{235}U$	±	$^{206}Pb^*/^{238}U$	±	Rho 1	$^{207}Pb^*/^{206}Pb^*$	±	$^{206}Pb/^{238}U$	±	$^{207}Pb/^{235}U$	±	$^{207}Pb/^{206}Pb$	±					
Z1	35.2	1.28597	6.56	0.13831	4.82	0.73	0.06743	4.45	835	40	840	55	851	38	2	0.0013	837	70	0.51
Z2	37.2	1.25156	5.71	0.13563	4.72	0.83	0.06693	3.21	820	39	824	47	836	27	2	0.0014	823	64	0.54
Z3	40.3	1.27388	5.04	0.13767	2.70	0.54	0.06711	4.25	831	22	834	42	841	36	1	0.0013	832	41	0.67
Z4*	68.2	1.28229	2.65	0.13540	1.58	0.60	0.06868	2.13	819	13	838	22	889	19	8	0.0008	823	24	0.63
Z5	84.1	1.26164	3.54	0.13734	3.09	0.87	0.06662	1.73	830	26	829	29	826	14	0	0.0005	829	40	0.93
Z6	20.1	1.29668	5.52	0.13994	4.58	0.83	0.06720	3.07	844	39	844	47	844	26	0	0.0015	844	63	0.51
Z7	27.4	1.28563	5.19	0.13717	3.51	0.68	0.06798	3.81	829	29	839	44	868	33	5	0.0014	833	52	0.71
Z8	14.5	1.30272	8.43	0.13771	5.93	0.70	0.06861	6.00	832	49	847	71	887	53	6	0.0024	838	87	0.45
Z9*	28.4	1.03558	4.92	0.11812	3.39	0.69	0.06358	3.57	720	24	722	36	728	26	1	0.0009	720	44	0.53
Z10	36.4	1.28449	3.80	0.13902	1.92	0.50	0.06701	3.29	839	16	839	32	838	28	0	0.0006	839	29	0.77
Z11	9.9	1.32384	5.96	0.14190	3.87	0.65	0.06766	4.53	855	33	856	51	858	39	0	0.0026	856	59	0.48
Z12	12.5	1.31506	5.93	0.14033	4.10	0.69	0.06797	4.28	847	35	852	51	868	37	2	0.0019	849	61	0.62
Z13	19.1	1.30542	4.79	0.14054	3.08	0.64	0.06737	3.67	848	26	848	41	849	31	0	0.0009	848	47	0.74
Z14	21.4	1.27531	3.35	0.13713	2.31	0.69	0.06745	2.43	828	19	835	28	852	21	3	0.0010	832	34	0.66
Z15B*	36.7	1.26033	2.41	0.13142	1.73	0.72	0.06956	1.68	796	14	828	20	915	15	13	0.0008	808	500	0.46
Z15N	24.7	1.26667	4.98	0.13750	2.56	0.51	0.06681	4.28	830	21	831	41	832	36	0	0.0010	831	39	0.50
Z16	26.6	1.28653	3.35	0.13813	1.92	0.57	0.06755	2.75	834	16	840	28	855	24	2	0.0008	835	29	0.43
Z17N	22.6	1.29808	3.54	0.13988	2.55	0.72	0.06730	2.46	844	21	845	30	847	21	0	0.0006	844	38	0.56
Z17B*	46.2	1.20949	2.02	0.12923	1.06	0.53	0.06788	1.72	783	8	805	16	865	15	9	0.0007	787	210	0.83
Z18	131.9	1.32365	2.63	0.14150	2.10	0.80	0.06784	1.57	853	18	856	22	864	14	1	0.0002	855	30	0.45
Z19	84.0	1.35741	2.49	0.14452	1.35	0.54	0.06812	2.09	870	12	871	22	872	18	0	0.0001	870	21	0.65
Z20N*	108.8	0.88373	3.33	0.10481	2.30	0.69	0.06115	2.41	643	15	643	21	645	16	0	0.0002	643	27	0.44
Z20B*	825.0	0.77074	3.25	0.09440	2.76	0.85	0.05922	1.71	581	16	580	19	575	10	-1	0.0002	581	28	0.45
Z21	37.9	1.29193	3.60	0.14011	2.33	0.65	0.06687	2.74	845	20	842	30	834	23	-1	0.0004	844	35	0.45
Z22*	185.1	1.06351	3.10	0.12132	1.73	0.56	0.06358	2.57	738	13	736	23	728	19	-1	0.0002	738	24	0.28
Z23	82.4	1.32383	2.44	0.14198	1.23	0.50	0.06762	2.10	856	11	856	21	857	18	0	0.0002	856	19	0.53
Z24	151.8	1.29968	2.18	0.13997	1.28	0.59	0.06734	1.76	845	11	846	18	848	15	0	0.0001	845	20	0.63
Z25	76.4	1.30652	2.90	0.14079	1.87	0.64	0.06730	2.22	849	16	849	25	847	19	0	0.0002	849	28	0.50
ZR1	121.2	1.31938	6.14	0.13901	2.78	0.45	0.06884	5.47	839	23	854	52	894	49	6	0.0027	841	43	0.78
ZR2N	380.4	1.36607	3.14	0.14407	1.87	0.59	0.06877	2.53	868	16	874	27	892	23	3	0.0015	869	29	0.82
ZR2B*	91.9	1.20514	8.14	0.12725	4.13	0.51	0.06869	7.02	772	32	803	65	889	62	13	0.0037	776	59	0.16
ZR3N*	153.6	4.45949	4.31	0.27210	3.09	0.72	0.11887	3.00	1551	48	1723	74	1939	58	Disc.	0.0021	–	–	1.07
ZR3B*	167.5	3.33375	5.01	0.19983	3.68	0.74	0.12099	3.39	1174	43	1489	75	1971	67	Disc.	0.0012	–	–	0.43
ZR4N*	142.0	0.92627	6.73	0.10023	4.50	0.67	0.06703	5.01	616	28	666	45	839	42	27	0.0036	623	52	0.39
ZR4B*	184.9	0.87965	4.82	0.09841	3.01	0.62	0.06483	3.76	605	18	641	31	769	29	21	0.0033	610	34	0.71

Table 9
U-Pb isotopic data (LA-ICP-MS) from sample SM-CM-69 – Serra da Prata Complex. *Spots excluded from the calculation. Disc.: do not provide age.

SM-CM-69	U ppm	Isotope Ratios							Ages (Ma)						Disc. %	f 206	Age (Ma)	±	$^{232}Th/^{238}U$
		$^{207}Pb^*/^{235}U$	±	$^{206}Pb^*/^{238}U$	±	Rho 1	$^{207}Pb^*/^{206}Pb^*$	±	$^{206}Pb/^{238}U$	±	$^{207}Pb/^{235}U$	±	$^{207}Pb/^{206}Pb$	±					
Z1*	36.2	1.05844	6.14	0.08537	4.67	0.76	0.08992	3.9841	528	25	733	45	1424	57	Disc.	0.0024	–	–	0.56
Z2	164.9	0.82384	3.81	0.09952	2.78	0.73	0.06004	2.62	612	17	610	23	605	16	−1	0.0001	611	16	0.13
Z3	45.9	1.33502	6.21	0.14335	4.91	0.79	0.06755	3.80	864	42	861	53	855	32	−1	0.0009	862	35	0.25
Z4	77.0	1.32066	4.45	0.14188	3.35	0.75	0.06751	2.93	855	29	855	38	854	25	0	0.0005	855	25	0.78
Z5	34.8	1.26012	4.59	0.13794	3.92	0.85	0.06625	2.38	833	33	828	38	814	19	−2	0.0006	828	26	0.48
Z6	173.5	0.93478	4.12	0.10863	3.32	0.81	0.06241	2.44	665	22	670	28	688	17	3	0.0003	688	20	1.87
Z7	83.7	1.25569	4.65	0.13589	3.87	0.83	0.06702	2.58	821	32	826	38	838	22	2	0.0004	825	26	0.84
Z8	155.4	0.81368	4.83	0.09785	3.72	0.77	0.06031	3.07	602	22	605	29	615	19	2	0.0003	603	20	0.21
Z9*	61.8	1.13927	7.45	0.12685	6.26	0.84	0.06514	4.03	770	48	772	57	779	31	1	0.0012	772	80	0.47
Z10	955.9	0.94170	3.22	0.11104	2.69	0.83	0.06151	1.78	679	18	674	22	657	12	−3	0.0001	675	16	0.01
Z11	102.6	1.22113	5.11	0.13373	4.38	0.86	0.06623	2.64	809	35	810	41	814	22	1	0.0007	810	29	1.02
Z12	436.8	0.86159	3.30	0.10235	2.39	0.72	0.06105	2.27	628	15	631	21	641	15	2	0.0001	629	14	0.01
Z13*	100.5	0.77479	4.21	0.09400	2.72	0.65	0.05978	3.21	579	16	583	25	596	19	3	0.0004	580	29	0.17
Z14*	15.7	1.33320	9.95	0.08391	9.01	0.91	0.11523	4.23	519	47	860	86	1883	80	Disc.	0.0067	–	–	1.27
Z15*	32.8	0.94118	4.95	0.08546	3.14	0.64	0.07988	3.82	529	17	673	33	1194	46	Disc.	0.0031	–	–	2.77
Z16*	36.5	0.96289	4.20	0.08595	3.31	0.79	0.08126	2.59	532	18	685	29	1228	32	Disc.	0.0025	–	–	2.72
Z17	497.6	0.88165	3.31	0.10471	2.40	0.73	0.06107	2.28	642	15	642	21	642	15	0	0.0001	642	14	0.01
Z18	160.3	0.88793	4.76	0.10539	3.65	0.77	0.06110	3.05	646	24	645	31	643	20	0	0.0002	646	21	0.01
Z19	18.7	1.32123	6.12	0.14179	4.60	0.75	0.06758	4.03	855	39	855	52	856	35	0	0.0023	855	34	0.38
Z20	96.2	1.36952	5.84	0.14607	4.48	0.74	0.06800	3.74	879	39	876	51	869	33	−1	0.0011	877	33	1.02
Z21	142.7	1.32595	5.09	0.14255	3.37	0.66	0.06746	3.81	859	29	857	44	852	32	−1	0.0014	858	26	1.04
Z22*	60.9	1.50766	10.09	0.08402	9.02	0.13	0.13015	4.53	520	47	933	94	2100	95	Disc.	0.0076	–	–	0.37
ZR1B	294.0	0.76194	3.01	0.09229	2.29	0.76	0.05988	1.96	569	13	575	17	599	12	5	0.0013	571	12	0.13
ZR1N*	223.6	1.05471	7.75	0.11322	5.60	0.72	0.06756	5.35	691	39	731	57	855	46	19	0.0109	703	71	0.58
ZR2B*	139.8	0.75717	3.75	0.09327	2.98	0.80	0.05887	2.27	575	17	572	21	562	13	−2	0.0184	574	16	0.18
ZR3B	156.4	0.79312	2.95	0.09451	2.11	0.72	0.06087	2.06	582	12	593	17	635	13	8	0.0010	585	11	0.46
ZR4B*	67.2	0.84337	5.47	0.09718	2.31	0.42	0.06294	4.96	598	14	621	34	706	35	15	0.0203	599	13	0.12
ZR5N*	416.3	0.87101	3.20	0.09345	2.39	0.75	0.06760	2.13	576	14	636	20	856	18	Disc.	0.0076	–	–	2.09
ZR6B	250.2	0.83511	3.73	0.10125	3.19	0.85	0.05982	1.94	622	20	616	23	597	12	−4	0.0046	617	17	0.06
ZR7N*	44.8	1.36604	6.33	0.15120	4.75	0.75	0.06553	4.18	908	43	874	55	791	33	−15	0.0021	885	71	0.49
ZR7B	262.6	0.83253	2.28	0.10123	1.32	0.58	0.05965	1.86	622	8	615	14	591	11	−5	0.0041	620	8	0.08
ZR8B	785.2	0.88992	2.00	0.10542	1.15	0.57	0.06123	1.64	646	7	646	13	647	11	0	0.0017	646	7	0.02
ZR9B*	243.7	1.07117	3.48	0.12138	1.26	0.36	0.06401	3.25	738	9	739	26	742	24	0	0.0030	739	8	0.24
ZR10B	192.3	0.77018	3.30	0.09433	2.26	0.68	0.05922	2.41	581	13	580	19	575	14	−1	0.0061	581	12	0.09
ZR11B1	574.8	0.83425	2.93	0.09969	2.33	0.80	0.06069	1.77	613	14	616	18	628	11	3	0.0012	614	13	0.03
ZR11B2*	309.0	0.77643	3.16	0.09035	1.98	0.63	0.06233	2.46	558	11	583	18	685	17	19	0.0052	561	310	0.19
ZR12N*	349.1	0.91005	3.47	0.10736	2.70	0.78	0.06148	2.19	657	18	657	23	656	14	0	0.0038	657	16	0.36
ZR12B1	186.7	0.76121	4.65	0.09313	3.88	0.83	0.05928	2.57	574	22	575	27	577	15	1	0.0048	574	20	0.27
ZR12B2	299.1	0.77663	3.06	0.09555	2.33	0.76	0.05895	1.98	588	14	584	18	565	11	−4	0.0042	586	12	0.12
ZR13N	157.9	0.93144	8.45	0.10793	8.07	0.96	0.06259	2.51	661	53	668	56	694	17	5	0.0019	677	37	0.31
ZR13B	194.6	0.82197	3.20	0.10029	2.07	0.65	0.05944	2.45	616	13	609	19	583	14	−6	0.0020	614	12	0.15
ZR14N	52.7	1.24970	4.80	0.13675	3.44	0.72	0.06628	3.36	826	28	823	40	815	27	−1	0.0028	825	25	0.45
ZR14B	199.4	0.81882	2.96	0.09918	2.18	0.73	0.05988	2.01	610	13	607	18	599	12	−2	0.0037	609	12	0.10
ZR15N*	211.0	1.18181	6.34	0.13068	1.59	0.25	0.06559	6.14	792	13	792	50	793	49	0	0.0063	792	12	0.48
ZR15B	529.6	0.83055	2.98	0.10066	2.04	0.69	0.05984	2.17	618	13	614	18	598	13	−3	0.0013	617	12	0.11
ZR16N*	141.9	1.42240	3.35	0.15327	2.14	0.64	0.06731	2.57	919	20	898	30	847	22	−9	0.0042	911	17	0.63
ZR16B*	118.8	0.88250	3.30	0.09958	2.20	0.66	0.06427	2.47	612	13	642	21	751	19	18	0.0180	617	400	0.25
ZR17N	96.3	1.26380	4.93	0.13763	2.70	0.55	0.06660	4.12	831	22	830	41	825	34	−1	0.0027	831	20	0.66
ZR17b*	156.1	0.97163	2.88	0.11301	2.03	0.70	0.06236	2.05	690	14	689	20	686	14	−1	0.0017	690	13	0.16

Table 10
U-Pb isotopic data (LA-ICP-MS) from sample SM-CM-07 – Morro do Escoteiro Suite. *Spots excluded from the calculation. Disc.: do not provide age.

SM-CM-07	U ppm	Isotope Ratios							Ages (Ma)						Disc. %	f 206	Age (Ma)	±	$^{232}Th/^{238}U$
		$^{207}Pb^*/^{235}U$	±	$^{206}Pb^*/^{238}U$	±	Rho 1	$^{207}Pb^*/^{206}Pb^*$	±	$^{206}Pb/^{238}U$	±	$^{207}Pb/^{235}U$	±	$^{207}Pb/^{206}Pb$	±					
Z1*	21.4	0.78201	13.34	0.09412	12.15	0.91	0.06026	5.50	580	70	587	78	613	34	5	0.0090	588	120	0.83
Z2*	214.8	0.74194	5.37	0.08814	3.93	0.73	0.06105	3.66	545	21	564	30	641	23	15	0.0011	549	40	0.41
Z3*	94.6	0.74172	6.46	0.08783	4.53	0.70	0.06125	4.60	543	25	563	36	648	30	16	0.0019	547	46	0.81
Z4*	170.2	1.09802	5.77	0.12616	4.18	0.72	0.06312	3.98	766	32	752	43	712	28	−8	0.0023	759	56	0.50
Z5*	646.9	0.89754	3.46	0.10363	2.78	0.80	0.06281	2.06	636	18	650	22	702	14	9	0.0004	643	32	0.02
Z6	143.0	0.80614	4.68	0.09757	3.60	0.77	0.05992	2.99	600	22	600	28	601	18	0	0.0003	600	39	0.05
Z7*	12.7	0.63307	12.01	0.08018	9.62	0.80	0.05726	7.19	497	48	498	60	502	36	1	0.0025	488	88	0.71
Z8*	5.4	0.70297	15.86	0.08732	10.93	0.69	0.05839	11.50	540	59	541	86	544	63	1	0.0078	540	110	1.02
Z9	20.4	0.82820	7.17	0.10066	4.86	0.68	0.05967	5.27	618	30	613	44	592	31	−4	0.0009	617	55	0.66
Z10	17.2	0.79814	6.79	0.09603	4.79	0.71	0.06028	4.80	591	28	596	40	614	29	4	0.0018	592	53	0.80
Z11	109.4	0.82253	2.78	0.09950	1.71	0.62	0.05995	2.19	611	10	609	17	602	13	−2	0.0004	611	20	0.01
Z12	23.4	0.75108	5.88	0.09230	3.29	0.56	0.05902	4.88	569	19	569	33	568	28	0	0.0019	569	35	0.92
Z13*	215.4	2.35337	2.56	0.20452	1.88	0.73	0.08345	1.75	1200	23	1229	31	1280	22	6	0.0008	1220	460	0.56
Z14*	26.5	0.79682	8.52	0.09674	6.59	0.77	0.05974	5.40	595	39	595	51	594	32	0	0.0021	595	71	0.86
Z22	77.1	0.85509	5.43	0.10225	4.36	0.80	0.06065	3.23	628	27	627	34	627	20	0	0.0003	627	49	0.20
ZR1B*	21.3	0.59890	15.68	0.07596	12.42	0.79	0.05718	9.58	472	59	477	75	499	48	5	0.0084	474	55	0.75
ZR2	534.4	0.78915	2.59	0.09537	1.34	0.52	0.06001	2.22	587	8	591	15	604	13	3	0.0029	588	15	0.01
ZR3N*	352.1	2.41600	3.81	0.18353	1.68	0.44	0.09547	3.42	1086	18	1247	48	1537	53	Disc.	0.0346	–	–	0.18
ZR3B	357.6	0.84685	3.12	0.10001	2.14	0.69	0.06142	2.27	614	13	623	19	654	15	6	0.0045	617	24	0.03
ZR4N	294.0	0.92230	6.28	0.10717	2.29	0.37	0.06242	5.84	656	15	664	42	688	40	5	0.0197	657	28	0.10
ZR4B*	846.7	1.35156	2.88	0.09581	2.07	0.72	0.10231	2.01	590	12	868	25	1666	33	Disc.	0.0665	–	–	0.03
ZR5N	152.6	0.77493	4.45	0.09375	2.93	0.66	0.05995	3.35	578	17	583	26	602	20	4	0.0046	579	32	0.23
ZR5B*	519.4	0.88511	5.23	0.09482	2.57	0.49	0.06770	4.56	584	15	644	34	859	39	32	0.0149	586	27	0.01
ZR6N*	37.2	1.02714	11.17	0.09855	8.87	0.79	0.07559	6.79	606	54	717	80	1084	74	44	0.0182	608	100	0.89
ZR6B*	173.9	0.75523	4.44	0.08806	2.72	0.61	0.06220	3.51	544	15	571	25	681	24	20	0.0077	547	28	0.09
ZR7*	193.0	1.14003	5.57	0.08279	2.30	0.41	0.09987	5.07	513	12	773	43	1622	Disc.	68	0.0651	–	–	0.09
ZR8B*	24.1	0.87355	24.73	0.10343	15.91	0.64	0.06125	18.93	634	101	637	158	648	123	2	0.0106	635	190	0.95
ZR9N*	17.5	0.89191	21.49	0.10528	12.99	0.60	0.06144	17.12	645	84	647	139	655	112	1	0.0194	646	160	1.16
ZR9B*	15.7	1.00314	24.45	0.10184	15.85	0.65	0.07144	18.61	625	99	705	172	970	181	36	0.0302	6311	19	0.76
ZR10N	45.0	0.95478	5.50	0.11165	2.35	0.43	0.06202	4.98	682	16	681	37	675	34	−1	0.0091	682	30	0.53
ZR11	359.6	0.93750	6.61	0.10799	6.06	0.92	0.06296	2.63	661	40	672	44	707	19	6	0.0217	675	32	0.10
ZR12*	16.6	0.88510	33.27	0.10067	20.99	0.63	0.06377	25.81	618	130	644	214	734	189	16	0.0231	623	240	0.83
ZR13B	1070.9	0.82364	2.19	0.09844	1.31	0.60	0.06068	1.76	605	8	610	13	628	11	4	0.0015	606	15	0.02

Table 11
U-Pb isotopic data (LA-ICP-MS) from sample SM-CM-02 – Morro do Escoteiro Suite. *Spots excluded from the calculation. Disc.: do not provide age.

SM-CM-02	U ppm	Isotope Ratios							Ages (Ma)						Disc. %	f 206	Age (Ma)	±	$^{232}Th/^{238}U$
		$^{207}Pb^*/^{235}U$	±	$^{206}Pb^*/^{238}U$	±	Rho 1	$^{207}Pb^*/^{206}Pb^*$	±	$^{206}Pb/^{238}U$	±	$^{207}Pb/^{235}U$	±	$^{207}Pb/^{206}Pb$	±					
Z1*	192.3	0.94646	5.73	0.10952	3.64	0.64	0.06267	4.43	670	24	676	39	697	31	4	0.0007	671	45	0.02
Z2*	321.5	2.73747	8.09	0.21523	4.80	0.59	0.09225	6.51	1257	60	1339	108	1472	96	15	0.0002	1283	100	0.36
Z3	95.8	6.89687	5.41	0.37672	3.85	0.71	0.13278	3.80	2061	79	2098	113	2135	81	3	0.0007	2098	96	0.39
Z4	104.5	5.03560	3.66	0.33261	2.59	0.71	0.10980	2.59	1851	48	1825	67	1796	47	−3	0.0008	1827	62	0.61
Z5B*	453.5	0.72539	5.00	0.08828	3.83	0.77	0.05960	3.21	545	21	554	28	589	19	7	0.0003	548	39	0.04
Z5N*	34.2	0.85911	14.28	0.10182	12.72	0.89	0.06120	6.48	625	79	630	90	646	42	3	0.0036	630	130	0.80
Z6	301.1	0.79822	4.66	0.09634	2.78	0.60	0.06009	3.73	593	17	596	28	607	23	2	0.0004	593	31	0.05
Z7	54.0	0.74174	8.56	0.09126	4.65	0.54	0.05895	7.19	563	26	563	48	565	41	0	0.0024	563	50	0.77
Z8N	194.1	4.15531	5.51	0.29203	3.58	0.65	0.10320	4.19	1652	59	1665	92	1682	70	2	0.0008	1661	87	0.45
Z8B	199.5	0.71742	4.73	0.08884	3.02	0.64	0.05857	3.64	549	17	549	26	551	20	0	0.0006	549	31	0.03
Z9	481.9	0.81532	4.00	0.09790	1.77	0.44	0.06040	3.59	602	11	605	24	618	22	3	0.0003	602	20	0.07
Z10*	331.1	0.82063	3.92	0.09848	1.79	0.46	0.06043	3.49	606	11	608	24	619	22	2	0.0003	606	21	0.09
Z11B	22.5	0.76902	9.00	0.09480	4.08	0.45	0.05884	8.03	584	24	579	52	561	45	−4	0.0030	583	45	0.61
Z11N	21.7	0.75623	8.72	0.09319	6.87	0.79	0.05886	5.37	574	39	572	50	562	30	−2	0.0030	573	72	0.68
Z12*	172.1	0.77239	4.91	0.09393	2.40	0.49	0.05964	4.29	579	14	581	29	591	25	2	0.0003	579	26	0.02
Z13B*	237.0	0.76466	3.71	0.09010	1.52	0.41	0.06155	3.38	556	8	577	21	658	22	16	0.0005	557	16	0.02
Z13N*	18.2	0.72024	9.98	0.08715	8.14	0.82	0.05994	5.78	539	44	551	55	601	35	10	0.0061	544	81	0.55
Z14*	7.1	1.10830	25.37	0.12572	23.14	0.91	0.06394	10.40	763	177	757	192	740	77	−3	0.0188	755	260	1.36
Z15B	80.1	0.74650	6.28	0.09140	3.64	0.58	0.05923	5.12	564	21	566	36	576	29	2	0.0014	564	39	0.03
Z15N	14.7	0.90020	7.35	0.10564	6.57	0.89	0.06180	3.30	647	43	652	48	667	22	3	0.0055	652	71	2.04
Z16	84.9	4.49291	3.99	0.29275	2.84	0.71	0.11131	2.80	1655	47	1730	69	1821	51	9	0.0019	1717	1100	1.04
Z17*	158.4	2.76790	4.94	0.20475	3.17	0.64	0.09805	3.79	1201	38	1347	67	1587	60	Disc.	0.0017	–	–	0.26
Z18N*	43.0	0.64047	11.27	0.08357	9.97	0.89	0.05558	5.24	517	52	503	57	436	23	−19	0.0038	503	89	0.73
Z18B*	344.7	1.02326	5.40	0.08978	3.14	0.58	0.08266	4.39	554	17	716	39	1261	55	Disc.	0.0032	–	–	0.06
Z19	40.0	2.56435	7.56	0.20757	6.83	0.90	0.08960	3.25	1216	83	1291	98	1417	46	14	0.0022	1338	1300	0.57
Z20*	37.5	0.75244	8.46	0.09283	3.63	0.43	0.05879	7.64	572	21	570	48	559	43	−2	0.0022	572	39	0.85
Z21	30.9	1.90315	7.32	0.18110	4.76	0.65	0.07622	5.56	1073	51	1082	79	1101	61	3	0.0034	1077	87	0.55
Z22	136.9	0.85715	4.77	0.10116	1.68	0.35	0.06145	4.46	621	10	629	30	655	29	5	0.0005	622	20	0.74
ZR1	157.6	0.77057	3.91	0.09432	3.06	0.78	0.05925	2.43	581	18	580	23	576	14	−1	0.0070	581	16	0.03
ZR2N*	111.0	0.80854	5.10	0.09484	3.76	0.74	0.06183	3.45	584	22	602	31	668	23	13	0.0165	589	20	0.05
ZR2B*	58.0	0.79332	13.24	0.09480	4.38	0.33	0.06070	12.49	584	26	593	79	628	79	7	0.0796	584	24	0.02
ZR3B	157.5	0.73608	4.16	0.09094	3.62	0.87	0.05870	2.05	561	20	560	23	556	11	−1	0.0124	560	18	0.03
ZR4B*	193.1	1.07057	4.82	0.11883	4.20	0.87	0.06534	2.37	724	30	739	36	785	19	8	0.0116	738	25	0.10
ZR5B*	129.1	1.00392	5.48	0.11545	4.44	0.81	0.06307	3.21	704	31	706	39	710	23	1	0.0138	705	27	0.03
ZR6N	158.4	0.79722	4.11	0.09635	3.28	0.80	0.06001	2.48	593	19	595	24	604	15	2	0.0077	594	18	0.05
ZR6B*	64.3	0.84708	18.00	0.09918	11.02	0.61	0.06194	14.23	610	67	623	112	672	96	9	0.0158	612	63	0.03
ZR7	83.6	0.75849	7.72	0.09273	6.07	0.79	0.05932	4.76	572	35	573	44	579	28	1	0.0113	572	32	0.02
ZR8N	225.1	0.77752	5.40	0.09503	4.85	0.90	0.05934	2.38	585	28	584	32	580	14	−1	0.0035	584	24	0.03
ZR8B*	98.1	0.85552	4.80	0.09670	3.52	0.73	0.06416	3.26	595	21	628	30	747	24	20	0.0166	603	39	0.02
ZR9B	145.0	0.81005	6.03	0.09863	5.23	0.87	0.05957	2.99	606	32	602	36	588	18	−3	0.0037	603	27	0.02
ZR9N	156.4	1.09609	7.62	0.12293	4.69	0.62	0.06467	6.01	747	35	751	57	764	46	2	0.0055	748	32	0.09
ZR9B2	244.3	0.90551	6.05	0.10696	4.41	0.73	0.06140	4.13	655	29	655	40	653	27	0	0.0058	655	26	0.08
ZR10	156.7	0.84300	5.24	0.10209	3.76	0.72	0.05989	3.65	627	24	621	33	599	22	−5	0.0017	625	22	0.35
ZR11N*	125.9	0.97810	7.70	0.11410	3.76	0.49	0.06217	6.72	697	26	693	53	680	46	−2	0.0083	696	24	0.24
ZR11B	280.3	0.90922	5.80	0.10713	4.30	0.74	0.06156	3.90	656	28	657	38	659	26	0	0.0032	656	26	0.07
ZR12N*	202.1	1.14762	13.91	0.12559	2.51	0.18	0.06627	13.68	763	19	776	108	815	112	6	0.0031	763	18	0.10
ZR12B	160.8	0.92263	6.28	0.10718	5.53	0.88	0.06243	2.97	656	36	664	42	689	20	5	0.0105	664	31	0.04
ZR13B1	42.7	0.77804	9.22	0.09488	6.68	0.73	0.05947	6.35	584	39	584	54	584	37	0	0.0054	584	36	0.72
ZR13B2	51.8	0.83019	8.61	0.09940	5.41	0.63	0.06058	6.70	611	33	614	53	624	42	2	0.0045	611	31	0.69
ZR14N	261.3	0.73715	4.89	0.09056	3.16	0.65	0.05904	3.72	559	18	561	27	568	21	2	0.0016	559	17	0.08
ZR14B	227.4	0.76391	4.63	0.09395	3.29	0.71	0.05898	3.26	579	19	576	27	566	18	−2	0.0020	578	18	0.08
ZR15	101.2	0.79066	6.48	0.09699	4.72	0.73	0.05912	4.44	597	28	592	38	572	25	−4	0.0041	595	23	0.31
ZR16N	105.8	0.87552	5.29	0.10320	3.69	0.70	0.06153	3.80	633	23	639	34	658	25	4	0.0022	635	22	1.00
ZR16B	289.9	0.75142	5.21	0.09160	4.26	0.82	0.05950	3.00	565	24	569	30	585	18	3	0.0014	567	22	0.02
ZR17	51.1	0.77268	8.56	0.09435	6.29	0.74	0.05939	5.80	581	37	581	50	582	34	0	0.0051	581	34	0.40
ZR18N*	139.2	0.83990	8.14	0.09926	4.93	0.61	0.06137	6.48	610	30	619	50	652	42	6	0.0076	612	28	0.18
ZR18B*	125.1	1.19276	6.56	0.11754	4.19	0.64	0.07360	5.05	716	30	797	52	1030	52	30	0.0139	726	56	0.13
ZR19B	109.1	1.20210	7.06	0.13207	4.65	0.66	0.06601	5.30	800	37	802	57	807	43	1	0.0086	800	33	0.09
ZR19N*	156.2	7.66344	2.09	0.44807	0.80	0.38	0.12405	1.93	2387	19	2192	46	2015	39	Disc.	0.0005	–	–	0.35
ZR20N*	265.3	0.95807	5.56	0.10893	4.81	0.87	0.06379	2.78	667	32	682	38	735	20	9	0.0061	680	28	0.13

(continued on next page)

Table 11 (*continued*)

SM-CM-02	U ppm	Isotope Ratios							Ages (Ma)						Disc. %	f 206	Age (Ma)	±	$^{232}Th/^{238}U$
		$^{207}Pb^*/^{235}U$	±	$^{206}Pb^*/^{238}U$	±	Rho 1	$^{207}Pb^*/^{206}Pb^*$	±	$^{206}Pb/^{238}U$	±	$^{207}Pb/^{235}U$	±	$^{207}Pb/^{206}Pb$	±					
ZR20B	341.8	0.78263	3.90	0.09502	2.52	0.65	0.05974	2.98	585	15	587	23	594	18	2	0.0031	586	14	0.02
ZR21B*	906.7	0.93555	3.99	0.09026	3.24	0.81	0.07517	2.33	557	18	671	27	1073	25	Disc.	0.0172	–	–	0.06
ZR22B	487.0	1.24301	6.15	0.13632	2.01	0.33	0.06613	5.81	824	17	820	50	811	47	−2	0.0102	824	15	0.09
ZR23N	183.6	1.16769	10.40	0.12854	5.37	0.52	0.06589	8.91	780	42	786	82	803	72	3	0.0020	780	19	0.20
ZR24N*	54.1	1.09815	7.67	0.12607	3.58	0.47	0.06317	6.79	765	27	752	58	714	48	−7	0.0071	764	13	0.09

Table 12
U-Pb isotopic data (SHRIMP) from sample IT-NM-15 – Morro do Escoteiro Suite.

IT-NM-15			Ratios							Age (Ma)				Disc.
Grain#	^{206}Pb cps	$^{206}Pb/^{204}Pb$	$^{207}Pb/^{206}Pb$	2 s error	$^{207}Pb/^{235}U$	2s error	$^{206}Pb/^{238}U$	2 s error	rho	$^{207}Pb/^{206}Pb$	2s error	$^{206}Pb/^{238}U$		%
1	181,087	Infinite	0.06138	0.00097	0.7965	0.0335	0.0926	0.0037	0.927	653	34	571	23	12.5
2	235,059	Infinite	0.05990	0.00067	0.7708	0.0281	0.0933	0.0034	0.952	600	24	575	21	4.1
3	158,875	Infinite	0.06027	0.00066	0.8097	0.0299	0.0963	0.0035	0.955	613	24	593	22	3.3
4	205,833	Infinite	0.06141	0.00072	0.7786	0.0289	0.0910	0.0033	0.949	654	25	561	21	14.1
5	512,881	Infinite	0.05961	0.00065	0.7919	0.0327	0.0966	0.0040	0.965	590	24	595	24	−0.9
6	132,300	Infinite	0.06033	0.00073	0.8183	0.0404	0.0975	0.0048	0.970	615	26	600	29	2.5
7	334,380	Infinite	0.06005	0.00066	0.7696	0.0246	0.0926	0.0029	0.941	605	24	571	18	5.7
8	134,260	Infinite	0.05977	0.00068	0.7841	0.0281	0.0943	0.0033	0.949	595	25	581	21	2.4
9	379,986	Infinite	0.05880	0.00061	0.7003	0.0294	0.0864	0.0036	0.969	560	23	534	22	4.6
10	344,076	Infinite	0.06022	0.00069	0.7595	0.0281	0.0918	0.0033	0.951	611	25	566	21	7.4
11	147,173	Infinite	0.06280	0.00139	0.7613	0.0301	0.0872	0.0030	0.830	702	47	539	18	23.2
12	122,361	Infinite	0.06101	0.00072	0.7967	0.0371	0.0940	0.0043	0.968	640	25	579	27	9.5
13	110,033	Infinite	0.06185	0.00093	0.7980	0.0270	0.0923	0.0029	0.897	669	32	569	18	14.9
14	434,372	Infinite	0.06000	0.00068	0.7603	0.0245	0.0920	0.0029	0.938	603	24	567	18	6.0
15	129,018	Infinite	0.06040	0.00077	0.7878	0.0296	0.0929	0.0034	0.941	618	28	573	21	7.3
16	83,779	Infinite	0.06002	0.00070	0.8154	0.0302	0.0975	0.0036	0.950	604	25	600	22	0.8
17	228,951	Infinite	0.05947	0.00068	0.7603	0.0237	0.0922	0.0028	0.932	584	25	569	17	2.7
18	95,055	Infinite	0.05955	0.00068	0.8546	0.0332	0.1028	0.0040	0.956	587	25	631	24	−7.4
19	282,119	Infinite	0.06057	0.00071	0.7761	0.0301	0.0929	0.0036	0.954	624	25	573	22	8.2
20	259,550	Infinite	0.05958	0.00062	0.8096	0.0270	0.0984	0.0033	0.951	588	23	605	20	−2.8
21	254,793	Infinite	0.06008	0.00071	0.8249	0.0291	0.0991	0.0034	0.943	606	26	609	21	−0.4
22	235,356	Infinite	0.06028	0.00064	0.7917	0.0313	0.0949	0.0037	0.964	614	23	585	23	4.7
23	366,794	Infinite	0.05987	0.00064	0.8091	0.0293	0.0980	0.0035	0.956	599	23	602	22	−0.6
24	191,073	11,942	0.05989	0.00144	0.8192	0.0330	0.0984	0.0033	0.803	600	52	605	20	−0.9

Table 13
U-Pb isotopic data (LA-ICP-MS) from sample SM-CM-172 – Rio Negro Complex. *Spots excluded from the calculation.

SMM-CMM-172	U ppm	Isotope Ratios							Ages (Ma)						Disc. %	f 206	Age (Ma)	±	$^{232}Th/^{238}U$
		$^{207}Pb^*/^{235}U$	±	$^{206}Pb^*/^{238}U$	±	Rho 1	$^{207}Pb^*/^{206}Pb^*$	±	$^{206}Pb/^{238}U$	±	$^{207}Pb/^{235}U$	±	$^{207}Pb/^{206}Pb$	±					
001 A	476.9	0.88348	3.28	0.10584	2.31	0.71	0.06054	2.32	649	15	643	21	623	14	−4	0.0034	647	27	0.13
002 A	173.0	0.73815	5.62	0.09060	3.47	0.62	0.05909	4.41	559	19	561	32	571	25	2	0.0062	559	37	0.84
003 A	92.1	0.72755	5.69	0.08974	2.74	0.48	0.05880	4.99	554	15	555	32	560	28	1	0.0167	554	29	0.72
004 A*	142.6	0.77815	7.06	0.09598	5.21	0.74	0.05880	4.77	591	31	584	41	560	27	−6	0.0146	588	56	0.86
005 A	925.8	0.81027	2.86	0.09845	1.95	0.68	0.05969	2.09	605	12	603	17	592	12	−2	0.0010	605	22	0.28
006 A	609.7	0.77626	3.56	0.09472	1.57	0.44	0.05944	3.19	583	9	583	21	583	19	0	0.0015	583	17	0.18
007 A	447.8	0.73751	4.01	0.09013	2.08	0.52	0.05934	3.43	556	12	561	22	580	20	4	0.0023	557	22	0.19
008 A	952.0	0.80794	5.75	0.09771	3.67	0.64	0.05997	4.43	601	22	601	35	603	27	0	0.0035	601	41	0.89
009 A	209.3	0.72604	4.61	0.08993	3.18	0.69	0.05855	3.34	555	18	554	26	551	18	−1	0.0053	555	33	0.74
001 B*	1881.3	0.83943	6.49	0.09881	3.41	0.53	0.06161	5.52	607	21	619	40	661	36	8	0.0011	609	39	0.17
002 B	1086.6	0.86174	6.77	0.10207	3.46	0.51	0.06123	5.81	627	22	631	43	647	38	3	0.0017	627	41	0.21
003 B	978.6	0.84907	6.76	0.10051	3.73	0.55	0.06127	5.64	617	23	624	42	649	37	5	0.0028	618	43	0.23
004 B*	733.4	1.13414	5.40	0.12189	2.87	0.53	0.06748	4.58	741	21	770	42	853	39	13	0.0026	745	20	1.7
005 B*	140.7	0.72474	12.18	0.09009	3.94	0.32	0.05834	11.53	556	22	553	67	543	63	−2	0.0161	556	42	0.88
006 B	774.4	0.84128	6.77	0.09925	4.01	0.59	0.06147	5.46	610	24	620	42	656	36	7	0.0027	612	46	0.12
007 B	319.1	0.93727	6.77	0.10843	4.49	0.66	0.06269	5.07	664	30	671	45	698	35	5	0.0071	666	55	0.57
008 B	189.4	0.76776	7.97	0.09192	4.05	0.51	0.06058	6.87	567	23	578	46	624	43	9	0.0162	568	44	0.84
009 B*	1109.1	0.77730	7.23	0.09203	4.71	0.65	0.06125	5.49	568	27	584	42	648	36	12	0.0024	570	50	0.28
001 C	1763.9	0.84642	6.99	0.10013	5.09	0.73	0.06131	4.80	615	31	623	44	650	31	5	0.0036	618	58	0.28
002 C	617.3	0.84210	7.64	0.09928	5.44	0.71	0.06152	5.36	610	33	620	47	657	35	7	0.0080	613	61	1.03
003 C*	169.1	0.76177	9.92	0.09035	7.03	0.71	0.06115	7.00	558	39	575	57	645	45	13	0.0382	562	74	1.26
004 C	1862.8	0.90377	6.84	0.10602	4.80	0.70	0.06182	4.87	650	31	654	45	668	33	3	0.0032	651	57	0.11
005 C*	333.1	0.79956	8.28	0.09526	6.17	0.75	0.06087	5.51	587	36	597	49	635	35	8	0.0137	590	67	1.25
006 C*	1143.4	0.78246	7.22	0.09266	5.49	0.76	0.06124	4.70	571	31	587	42	648	30	12	0.0049	576	58	0.21
007 C*	999.2	0.85286	8.01	0.09958	6.49	0.81	0.06212	4.70	612	40	626	50	678	32	10	0.0048	619	72	1.91
008 C	860.2	0.88260	6.80	0.10469	4.94	0.73	0.06114	4.67	642	32	642	44	644	30	0	0.0074	642	58	0.25
009 C	1451.9	0.89668	7.62	0.10546	6.19	0.81	0.06166	4.44	646	40	650	50	662	29	2	0.0038	649	71	0.19
001 D*	166.5	0.80589	10.51	0.09882	6.69	0.64	0.05915	8.10	607	41	600	63	573	46	−6	0.0367	606	75	1.52
002 D	3434.0	0.92021	6.93	0.10842	4.46	0.64	0.06155	5.30	664	30	662	46	659	35	−1	0.0015	663	55	0.34
004 D*	155.1	0.86161	10.13	0.10025	4.96	0.49	0.06234	8.83	616	31	631	64	686	61	10	0.0580	617	58	0.91
005 D	1705.8	0.87122	6.86	0.10309	4.27	0.62	0.06129	5.37	632	27	636	44	650	35	3	0.0032	633	50	0.19
006 D	392.7	0.89594	8.61	0.10675	4.47	0.52	0.06087	7.35	654	29	650	56	635	47	−3	0.0158	653	55	1
007 D	1686.5	0.89576	7.24	0.10661	4.54	0.63	0.06094	5.64	653	30	649	47	637	36	−3	0.0109	652	55	0.36
008 D	464.7	0.85031	9.26	0.10155	7.06	0.76	0.06073	5.99	623	44	625	58	630	38	1	0.0177	624	80	0.62
009 D	1474.5	0.93391	7.36	0.11127	4.46	0.61	0.06087	5.85	680	30	670	49	635	37	−7	0.0041	678	56	0.27
001 E*	406.0	0.98116	18.69	0.11059	6.75	0.36	0.06434	17.42	676	46	694	130	753	131	10	0.0245	677	86	0.24
002 E*	783.4	0.91021	20.76	0.10793	9.32	0.45	0.06116	18.55	661	62	657	136	645	120	−2	0.0110	660	120	0.38
003 E*	219.1	0.61703	20.15	0.07134	8.46	0.42	0.06273	18.29	444	38	488	98	699	128	36	0.0451	445	73	0.22
004 E*	44.4	0.61532	54.72	0.08055	25.93	0.47	0.05540	48.19	499	129	487	266	429	206	−17	0.1229	498	250	0.47

Table 14
U-Pb isotopic data (SHRIMP) from sample THE-02 – Rio Negro Complex.

THE-02						Age			Ration					
Grain.Spot	% 206Pbc	ppm U	$^{232}Th/^{238}U$	± %	ppm $206Pb^*$	$^{206}Pb/^{238}U$	$^{207}Pb/^{206}Pb$	% Disc.	$^{207}Pb^*/^{206}Pb^*$	± %	$^{207}Pb^*/^{235}U$	± %	$^{206}Pb^*/^{238}U$	± %	err Corr
1.1	–	1152	0.06	0.79	100	619 ± 6	605 ± 14	−2	0.06004	0.67	0.835	1.3	0.1009	1.1	0.85
1.2	–	1414	0.98	0.15	123	622 ± 6	649 ± 12	+4	0.06127	0.55	0.856	1.2	0.1014	1.1	0.89
2.1	0.04	296	0.49	0.31	25	606 ± 7	611 ± 29	+1	0.06020	1.34	0.818	1.8	0.0986	1.2	0.66
3.1	0.01	895	1.29	1.31	79	627 ± 6	635 ± 16	+1	0.06088	0.74	0.858	1.3	0.1022	1.1	0.82
4.1	–	493	0.27	0.91	43	623 ± 7	603 ± 23	−3	0.05999	1.05	0.839	1.5	0.1014	1.1	0.73
5.1	–	836	0.11	0.38	60	521 ± 7	537 ± 19	+3	0.05819	0.87	0.676	1.6	0.0842	1.4	0.84
5.2	0.07	373	0.75	0.25	32	612 ± 8	589 ± 28	−4	0.05960	1.28	0.819	1.9	0.0997	1.4	0.73
6.1	–	1645	0.74	0.15	145	631 ± 6	622 ± 11	−1	0.06052	0.50	0.858	1.2	0.1028	1.1	0.90
7.1	0.01	801	0.24	0.25	69	616 ± 7	636 ± 16	+3	0.06090	0.72	0.842	1.5	0.1003	1.3	0.87
8.1	0.07	806	0.10	1.13	71	627 ± 7	600 ± 18	−5	0.05991	0.85	0.844	1.4	0.1022	1.1	0.79
9.1	–	771	0.57	0.20	68	628 ± 7	628 ± 16	+0	0.06067	0.75	0.855	1.3	0.1023	1.1	0.82
10.1	0.06	483	0.31	0.30	42	628 ± 7	609 ± 41	−3	0.06014	1.89	0.849	2.2	0.1024	1.1	0.51
11.1	0.02	1898	0.78	0.15	164	618 ± 6	628 ± 11	+2	0.06069	0.50	0.841	1.2	0.1005	1.1	0.90
12.1	0.05	746	0.24	0.49	66	629 ± 6	614 ± 16	−3	0.06029	0.74	0.852	1.3	0.1025	1.1	0.83
13.1	0.02	890	0.04	1.03	79	631 ± 7	632 ± 23	+0	0.06080	1.06	0.862	1.6	0.1028	1.2	0.75
14.1	0.09	1297	0.89	0.16	110	606 ± 6	624 ± 14	+3	0.06058	0.65	0.823	1.2	0.0986	1.1	0.85
15.1	0.00	752	0.31	0.49	66	624 ± 7	609 ± 17	−3	0.06015	0.79	0.843	1.3	0.1017	1.1	0.81
16.1	0.02	2017	0.91	0.39	172	610 ± 7	616 ± 10	+1	0.06033	0.48	0.826	1.2	0.0993	1.1	0.92
17.1	0.00	2101	0.93	0.14	183	622 ± 6	637 ± 10	+3	0.06095	0.46	0.851	1.1	0.1013	1.0	0.91

of 593 ± 7 Ma (Fig. 13e–g).

These data suggest that the Morro do Escoteiro Suite represents syn-collisional granites and is the result of a high-grade metamorphic event, associated with melting of the Italva Group and the Serra da Prata Complex around ca. 0.60 Ga.

6.6. Rio Negro complex

Both samples selected for analysis (THE-02 and SMM-CMM-172 – Tables 13 and 14) are porphyritic hornblende biotite orthogneisses with granodiorite composition (see location in Fig. 4). In the map, the location of THE-02 outcrop is hidden in the Serra da Prata Complex mapped area and represents the Rio Negro Complex enclosed within the Serra da Prata Complex.

The zircon grains from both samples display vitreous translucent light gray colors, and prismatic shape, variable widths between 150 μm and 670 μm and width-to-length ratios of 2:1 to 6:1. The internal structures from CL images show concentric igneous cores surrounded by metamorphic rims (Fig. 14a).

Analyzes from igneous cores yield two concordant ages of 629 ± 10 Ma and 622 ± 5 Ma, interpreted as the magmatic age (Fig. 14b, c). These data support the interpretations for Ediacaran age of arc evolution. The concordant ages obtained from the metamorphic rim is 567 ± 11 Ma represent the youngest age of metamorphism documented in the studied area (Fig. 14d).

6.7. Euclidelândia unit

The biotite-muscovite gneiss collected from this unit yield clear and translucent zircon grains with yellow color, a prismatic shape, sizes between 100 μm and 150 μm and with width-to-length ratios of 2:1 to 3:1. CL images (Fig. 15a) show an internal igneous structure with the concentric zoning of different widths with metamorphic overgrowth surrounding cores.

The histogram with the $^{206}Pb/^{238}U$ ages obtained for 68 analyzes show a bimodal distribution (Fig.15b; Table 15): the results from cores indicate zircon ages between ~940 and ~720 Ma with the higher frequency for ca. 850 Ma. The results from metamorphic rims provided concentrations of ages between ~680 and 500 Ma.

The data indicate that primary sedimentary sources for the Euclidelândia unit are the Tonian rocks, probably from the Serra da Prata complex. The Cryogenian-Ediacaran interval encompasses metamorphic ages recorded during both Rio Negro stage (~620–630 Ma) and high-grade metamorphic event previously described (~600 Ma).

7. Sm-Nd Isotopic data

7.1. Sm-Nd and Sr isotopic analyses

The isotopic (Sm-Nd and Sr-Sr) analyses were obtained at the Geochronology and Radiogenic Isotopes Laboratory (LAGIR), of the Rio de Janeiro State University. All chemical procedures were performed in clean rooms with positive air pressure (Valeriano et al., 2008).

Each sample weighing approximately 25 mg was mixed with proportional amounts of a ^{149}Sm-^{150}Nd double tracer solution. Sample dissolution was done in high-pressure PTFE bombs during two 5-day cycles using a mixture of HF (6 mL) and HNO_3 6 N (0.5 mL). Separation of Sm and Nd was performed using HCl in two ion exchange columns, the primary ones with AG 50 W-X8 (100–200 mesh) resin for the extraction of Sr and REE and the secondary columns with LN-spec (150 mesh) resin for the extraction of Sm and Nd.

Strontium, Samarium, and Neodymium are separately loaded onto a previously degassed double Re filament mounts, using H_3PO_4 as the ionization activator. The isotope ratios were measured with a TRITON thermal ionization mass spectrometer (TIMS). Data acquisition was performed in multi-collector static mode using arrays of up to 8 Faraday

Table 15
U-Pb isotopic data (LA-ICP-MS) from sample SM-CMB-148 – Euclidelândia unit. *Spots excluded from the calculation.

SM-CMB-148	U ppm	Isotope Ratios							Ages (Ma)						Disc.%	f 206	Age (Ma)	±	$^{232}Th/^{238}U$
		$^{207}Pb^*/^{235}U$	±	$^{206}Pb^*/^{238}U$	±	Rho 1	$^{207}Pb^*/^{206}Pb^*$	±	$^{206}Pb/^{238}U$	±	$^{207}Pb/^{235}U$	±	$^{207}Pb/^{206}Pb$	±					
Z1*	−274.4758	1.3211	7.70	0.13847	5.37	0.70	0.0692	5.52	836	45	855	66	905	50	8	0.0014	843	40	0.48
Z2	−91.3811	1.3249	10.95	0.13874	9.20	0.84	0.0693	5.93	838	77	857	94	906	54	8	0.0041	854	63	0.66
Z3B*	−142.7315	0.6164	9.77	0.07261	7.55	0.77	0.0616	6.20	452	34	488	48	659	41	31	0.0011	457	65	0.21
Z3N*	−212.0141	0.6697	8.00	0.07930	5.61	0.70	0.0612	5.70	492	28	521	42	648	37	24	0.0010	496	53	0.31
Z4	158.4868	1.2617	6.78	0.13473	5.00	0.74	0.0679	4.58	815	41	829	56	866	40	6	0.0010	821	36	0.63
Z5	112.0645	1.2528	7.42	0.13628	5.74	0.77	0.0667	4.70	824	47	825	61	828	39	0	0.0015	824	40	0.55
Z6	269.5596	1.3056	4.50	0.13997	3.05	0.68	0.0677	3.31	844	26	848	38	858	28	2	0.0008	846	23	0.64
Z7	46.2007	1.4690	10.87	0.13890	7.72	0.71	0.0767	7.65	838	65	918	100	1113	85	25	0.0061	860	120	1.71
Z8	27.6979	0.9444	17.79	0.09794	16.67	0.94	0.0699	6.22	602	100	675	120	926	58	35	0.0096	686	170	0.42
Z9	33.6631	1.4312	9.99	0.14871	7.63	0.76	0.0698	6.45	894	68	902	90	922	59	3	0.0051	899	58	0.47
Z10	90.8504	1.3545	5.85	0.14151	3.57	0.61	0.0694	4.64	853	30	869	51	911	42	6	0.0020	857	28	0.82
Z11	91.1489	1.4249	6.12	0.14585	3.70	0.60	0.0709	4.88	878	33	899	55	953	46	8	0.0017	883	29	0.37
Z12B	291.5513	0.6908	5.92	0.08368	2.78	0.47	0.0599	5.23	518	14	533	32	599	31	14	0.0005	519	14	0.31
Z12N	96.5220	1.1849	8.02	0.12840	4.93	0.61	0.0669	6.33	779	38	794	64	836	53	7	0.0020	782	35	1.04
Z13	72.4985	1.2830	10.36	0.13784	8.11	0.78	0.0675	6.44	832	68	838	87	853	55	2	0.0021	836	58	0.36
Z14B	281.3255	0.7526	4.74	0.08731	2.33	0.49	0.0625	4.12	540	13	570	27	692	29	22	0.0006	541	24	0.16
Z14N	181.3186	1.3481	5.58	0.14411	3.63	0.65	0.0678	4.24	868	31	867	48	864	37	0	0.0017	867	28	0.38
Z15	86.1455	1.2113	11.47	0.13079	7.98	0.70	0.0672	8.24	792	63	806	92	843	69	6	0.0032	797	57	0.60
Z16	386.3755	1.2374	4.81	0.12987	1.89	0.39	0.0691	4.43	787	15	818	39	902	40	13	0.0016	789	14	0.38
Z17*	1376.0413	0.9846	3.49	0.10689	1.74	0.50	0.0668	3.02	655	11	696	24	832	25	21	0.0005	658	22	0.91
Z18	886.3846	0.7414	4.09	0.09143	2.05	0.50	0.0588	3.54	564	12	563	23	560	20	−1	0.0002	564	11	0.04
Z19*	119.2942	1.0260	5.60	0.11547	3.26	0.58	0.0644	4.55	704	23	717	40	756	34	7	0.0020	707	21	0.47
Z20*	484.9377	1.0429	4.50	0.11484	2.37	0.53	0.0659	3.83	701	17	725	33	802	31	13	0.0004	704	16	0.30
Z21	999.1393	1.3901	3.37	0.14815	1.33	0.40	0.0681	3.09	891	12	885	30	870	27	−2	0.0002	890	11	0.89
Z22	70.3715	1.2535	4.84	0.13570	2.35	0.49	0.0670	4.23	820	19	825	40	838	35	2	0.0004	821	18	0.52
Z23	98.9534	1.3016	6.85	0.13979	1.83	0.27	0.0675	6.60	843	15	846	58	854	56	1	0.0004	844	14	1.02
Z24	131.6318	1.3365	4.28	0.14371	1.96	0.46	0.0675	3.80	866	17	862	37	852	32	−2	0.0003	865	16	0.85
Z25	109.5158	1.4830	4.74	0.15475	1.94	0.41	0.0695	4.33	928	18	923	44	914	40	−2	0.0005	927	16	0.87
ZR1N	94.5759	1.1847	5.14	0.12937	3.82	0.74	0.0664	3.45	784	30	793	41	819	28	4	0.0047	789	26	0.56
ZR1B	81.8209	1.1052	5.66	0.12147	4.24	0.75	0.0660	3.76	739	31	756	43	806	30	8	0.0042	746	28	0.45
ZR2N	151.3457	1.1776	6.41	0.12637	5.27	0.82	0.0676	3.64	767	40	790	51	856	31	10	0.0047	783	35	0.71
ZR2B	271.0344	0.9477	5.08	0.10961	1.86	0.37	0.0627	4.73	670	12	677	34	698	33	4	0.0025	671	12	0.20
ZR3N	93.2536	1.2492	5.83	0.13849	3.51	0.60	0.0654	4.65	836	29	823	48	788	37	−6	0.0127	832	26	0.31
ZR3B	145.2919	0.8610	5.28	0.10260	4.27	0.81	0.0609	3.11	630	27	631	33	634	20	1	0.0225	630	24	0.03
ZR4N	134.2470	1.3969	3.97	0.14757	2.51	0.63	0.0687	3.08	887	22	888	35	888	27	0	0.0048	887	20	0.72
ZR5N	178.0079	1.2681	3.11	0.13819	2.19	0.70	0.0666	2.21	834	18	832	26	824	18	−1	0.0020	833	16	0.47
ZR5B*	204.7461	1.1310	3.03	0.12373	2.18	0.72	0.0663	2.10	752	16	768	23	816	17	8	0.0011	758	15	0.64
ZR6N	141.3908	1.1981	4.17	0.13138	2.17	0.52	0.0661	3.57	796	17	800	33	811	29	2	0.0030	796	16	0.44
ZR6B	153.2474	1.1127	4.74	0.12615	2.56	0.54	0.0640	3.99	766	20	759	36	741	30	−3	0.0039	765	18	0.37
ZR7	252.3385	0.9956	4.66	0.10802	3.81	0.82	0.0668	2.68	661	25	702	33	833	22	21	0.0022	681	46	0.89
ZR8N	176.4941	1.1734	3.96	0.12298	2.85	0.72	0.0692	2.75	748	21	788	31	905	25	17	0.0115	761	39	0.62
ZR8B	109.7409	1.2245	3.97	0.13699	2.66	0.67	0.0648	2.95	828	22	812	32	769	23	−8	0.0037	821	19	0.18
ZR9	29.3913	1.3656	9.77	0.14053	6.44	0.66	0.0705	7.35	848	55	874	85	942	69	10	0.0091	856	49	0.51
ZR10N	35.1401	1.3199	9.37	0.14104	5.31	0.57	0.0679	7.73	851	45	854	80	865	67	2	0.0013	851	41	0.57
ZR10B	48.1802	1.3466	6.56	0.14650	4.32	0.66	0.0667	4.94	881	38	866	57	827	41	−7	0.0059	875	33	0.58
ZR11N	75.0474	1.1787	4.10	0.12191	2.52	0.61	0.0701	3.23	742	19	791	32	932	30	20	0.0002	750	35	0.88
ZR11B	78.1162	1.3432	4.27	0.14029	2.88	0.67	0.0694	3.15	846	24	865	37	912	29	7	0.0006	853	22	0.69
ZR12	27.8114	0.9540	8.66	0.10664	4.82	0.56	0.0649	7.19	653	31	680	59	771	55	15	0.0232	656	30	1.25
ZR13	21.3804	1.2684	8.23	0.13839	4.33	0.53	0.0665	7.00	836	36	832	68	821	57	−2	0.0300	835	33	0.83
ZR14N	20.1691	1.2079	10.56	0.12914	6.13	0.58	0.0678	8.60	783	48	804	85	864	74	9	0.0320	787	44	0.73
ZR14B	26.9646	0.7000	12.51	0.08118	10.74	0.86	0.0625	6.41	503	54	539	67	693	44	27	0.0439	517	100	0.13
ZR15	50.7441	1.2670	3.97	0.13645	3.30	0.83	0.0673	2.20	825	27	831	33	848	19	3	0.0052	830	22	1.37
ZR16	45.5011	1.2513	5.47	0.13431	2.77	0.51	0.0676	4.71	812	23	824	45	855	40	5	0.0029	814	21	0.64
ZR17	27.3255	1.5899	11.71	0.13365	7.57	0.65	0.0863	8.93	809	61	966	113	1344	120	40	0.0188	815	100	0.57
ZR18	33.0069	1.1541	7.20	0.11942	4.37	0.61	0.0701	5.72	727	32	779	56	931	53	22	0.0099	735	59	0.58
ZR19N	120.6063	1.2836	4.72	0.13426	2.06	0.44	0.0693	4.24	812	17	838	40	909	39	11	0.0032	815	16	0.59
ZR19B	91.5051	1.1954	3.82	0.13136	1.90	0.50	0.0660	3.31	796	15	798	30	806	27	1	0.0034	796	14	0.35
ZR20N	65.2161	1.2984	4.56	0.13706	3.31	0.73	0.0687	3.13	828	27	845	39	890	28	7	0.0045	836	24	0.68
ZR20B	45.4293	1.1284	7.58	0.12322	4.75	0.63	0.0664	5.91	749	36	767	58	819	48	9	0.0133	753	33	0.06
ZR21N*	65.7096	0.8220	7.34	0.09132	5.88	0.80	0.0653	4.38	563	33	609	45	783	34	28	0.0027	576	62	0.05

(continued on next page)

Table 15 (*continued*)

SM-CMB-148	U ppm	Isotope Ratios						Ages (Ma)				Disc.%	f 206	Age (Ma)	±	$^{232}Th/^{238}U$
		$^{207}Pb^*/^{235}U$	±	$^{206}Pb^*/^{238}U$	±	Rho 1	$^{207}Pb^*/^{206}Pb^*$	±	$^{206}Pb/^{238}U$	±	$^{207}Pb/^{235}U$	±	$^{207}Pb/^{206}Pb$	±				
ZR21B	77.0101	0.9203	5.18	0.10593	3.10	0.60	0.0630	4.15	649	20	663	34	708	29	8	0.0076	651	19	0.04
ZR22	90.8447	1.1323	7.78	0.12456	6.60	0.85	0.0659	4.11	757	50	769	60	804	33	6	0.0024	767	42	0.04
ZR23	192.1723	1.2870	3.48	0.13878	1.06	0.30	0.0673	3.31	838	9	840	29	846	28	1	0.0039	838	8	0.50
ZR24N	251.8186	1.2032	3.34	0.12864	2.51	0.75	0.0678	2.20	780	20	802	27	864	19	10	0.0049	790	17	0.57
ZR24B	175.9142	1.2236	5.65	0.13552	1.47	0.26	0.0655	5.46	819	12	811	46	790	43	−4	0.0039	819	11	0.36
ZR25B	79.1209	1.2531	5.33	0.13668	2.59	0.49	0.0665	4.65	826	21	825	44	822	38	0	0.0089	826	20	0.21
ZR26N	92.4958	1.2731	3.24	0.13878	1.88	0.58	0.0665	2.64	838	16	834	27	823	22	−2	0.0015	837	14	0.55
ZR26B	263.3703	0.9628	5.33	0.10811	4.22	0.79	0.0646	3.26	662	28	685	37	761	25	13	0.0077	672	25	0.16

detectors. The measured Nd and Sr isotope ratios were normalized respectively to the Jnd1 (Tanaka et al., 2000) and to the NBS 987 reference materials. Corrections were applied for instrumental bias and tracer content. Total procedural blanks are below 1 ng for Nd and 0.1 ng for Sm.

The $^{87}Sr/^{86}Sr$ initial ratios were calculated using the $^{87}Sr/^{86}Sr$ ratios measured by TIMS, and Rb and Sr contents from the lithogeochemical analyses, taking into account ^{147}Sm constant decay rate.

7.2. Results

Sixteen representative samples among orthogneisses and amphibolites were selected from the studied area: seven samples from the Serra da Prata Complex, six from the Rio Negro Complex and three amphibolites. The new data are shown in Tables 16 and 17.

Published data from the arc-related granitoids of Ribeira and Brasília belts and basement rocks were added to compare and better base the interpretation (Fig. 15a, b). These data are from the juvenile Goiás Magmatic Arc (Pimentel and Fuck, 1992) and the Rio Negro Arc (Tupinambá et al., 2012), both containing expressive intra-oceanic magmatic arc rocks, and data from Serra da Bolívia Complex (Heilbron et al., 2013). Data from the basement of the São Francisco craton, representing old Paleoproterozoic and Archean basement complexes.

The Nd model ages of mantle extraction (T_{DM}) of the Serra da Prata samples fall between 1.68 and 0.92 Ga. Four samples present model age (T_{DM} = 1.09–0.92 Ga) are similar to the crystallization ages (~850 Ma) whereas three other samples yield Mesoproterozoic model ages between 1.68 and 1.34. Moreover, the Rio Negro complex samples provided similar ages model (T_{DM} = 1.93–1.33 Ga) suggesting mixing with the older source.

The T_{DM} from amphibolites are between zero and 0.87 Ga. The T_{DM} from the amphibolite with MORB affinity (SM-CB-87 – intercalated with the marbles) is close to the crystallization age, geochemical indications of low degrees of differentiation.

The age model of 0.87 Ga for the amphibolite from Macuco Unit enclave (SM-CM-153) is consistent with the inferred age of Serra da Prata arc activity. Moreover, T_{DM} of 0.67 Ga for one amphibolite from Rio Negro Complex enclave (SMM-CMM-184B), agrees with the age of Rio Negro arc activity.

The εNd values for the Rio Negro complex range between −8.4 and −2.5 (calculated for 630 Ma), for the Serra da Prata Complex is $\varepsilon Nd T_{DM}$ = −3.7 to +5.2 (calculated for 850 Ma) and for the amphibolites is εNd = +6.0 to +7.1.

Initial $^{87}Sr/^{86}Sr$ ratios between 0.7032 and 0.7046 for the amphibolites, 0.7062–0.7113 for the Serra da Prata Complex and 0.7098–0.7211 for the Rio Negro Complex.

These results reflect the evolution of the plate convergence and arc environments. In Fig. 16a, the lines of isotopic evolution do not show a relation with basement rocks but are coincident with juvenile arcs data plotted (Goiás Magmatic Arc and medium K Rio Negro arc).

Moreover, these data corroborate the juvenile contribution to the Serra da Prata arc with values more juvenile than the data obtained for the Rio Negro arc. In Fig. 16b, the low εNd values and high initial $^{87}Sr/^{86}Sr$ ratios suggest the increase of crustal contamination from amphibolite to the Serra da Prata arc and finally to Rio Negro arc stage.

In an early stage, the MORB to IAT geochemistry of the most juvenile mafic rocks (Serra da Prata arc) indicate an intra-oceanic island arc. The subsequent development of Rio Negro arc would represent a more mature arc stage, previously reported by Tupinambá et al. (2012) as changing from a more primitive or either intra-oceanic setting to a Cordilleran environment.

These results contrast with the data for the more radiogenic, Serra da Bolívia arc (Heilbron et al., 2013). Compared to less contaminated magmatic arcs (Fig.16a), the Serra da Bolívia magmatic protoliths probably began and evolved in a Cordilleran tectonic setting.

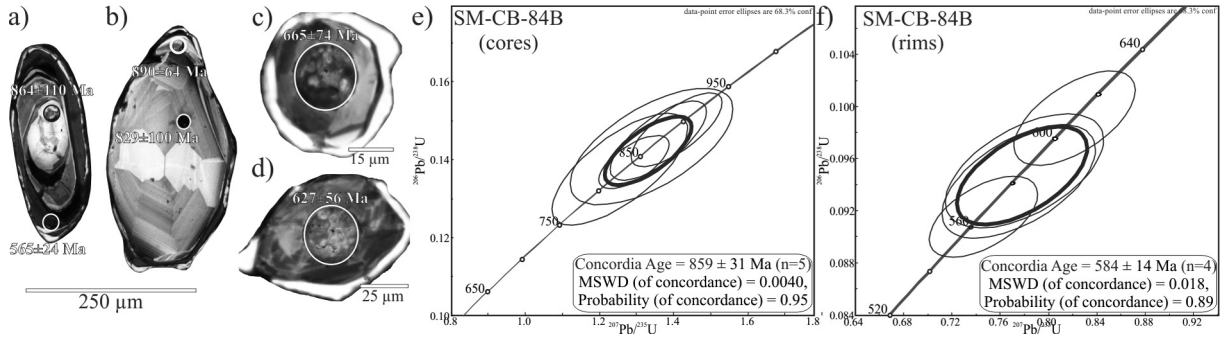

Fig. 11. Cathodoluminescence images and Concordia diagram from amphibolite of Italva Domain. (2 s, decay-const. errors included).

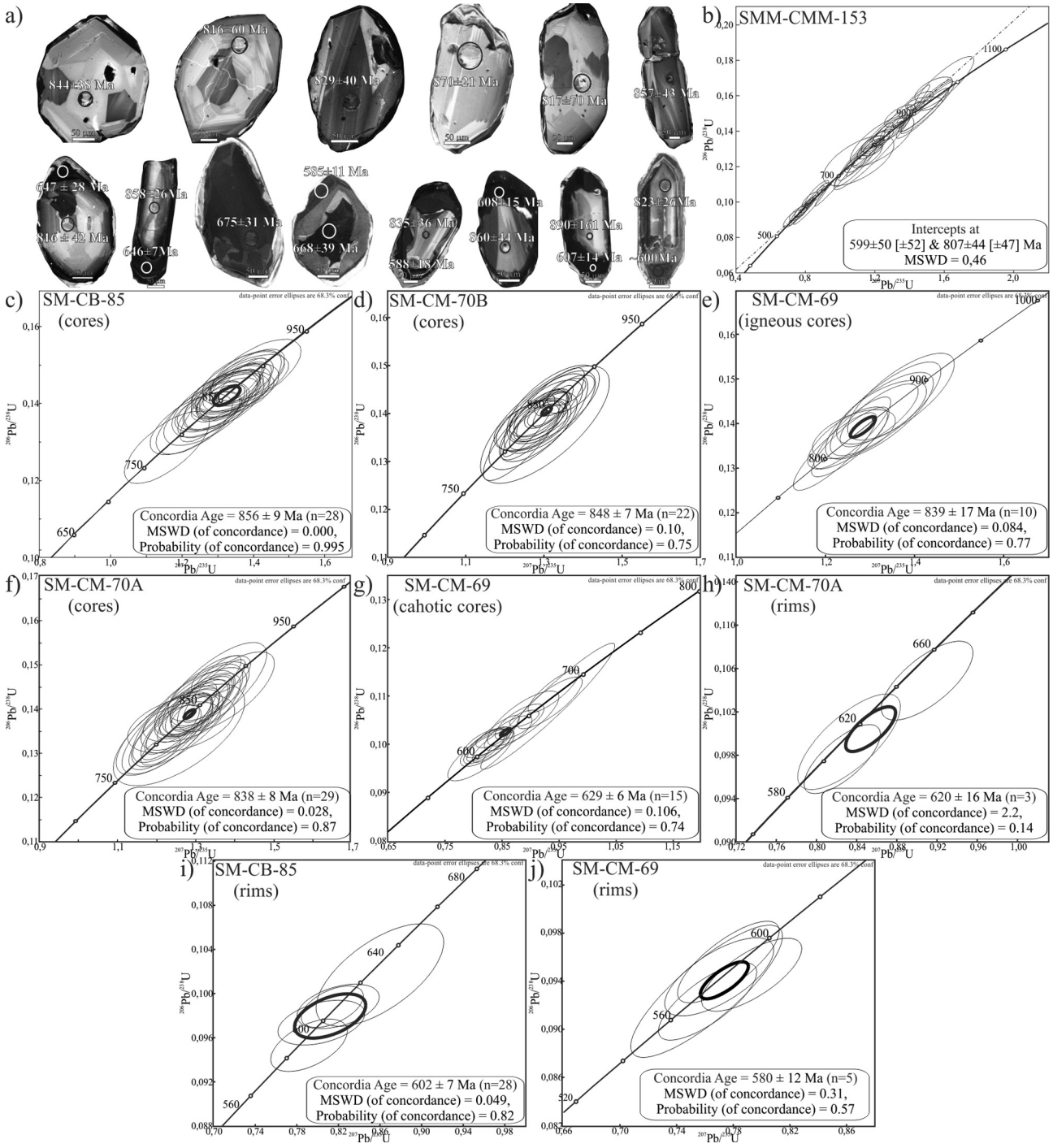

Fig. 12. Cathodoluminescence images and Concordia diagram from Serra da Prata Complex of Italva Domain. (2 s, decay-const. errors included).

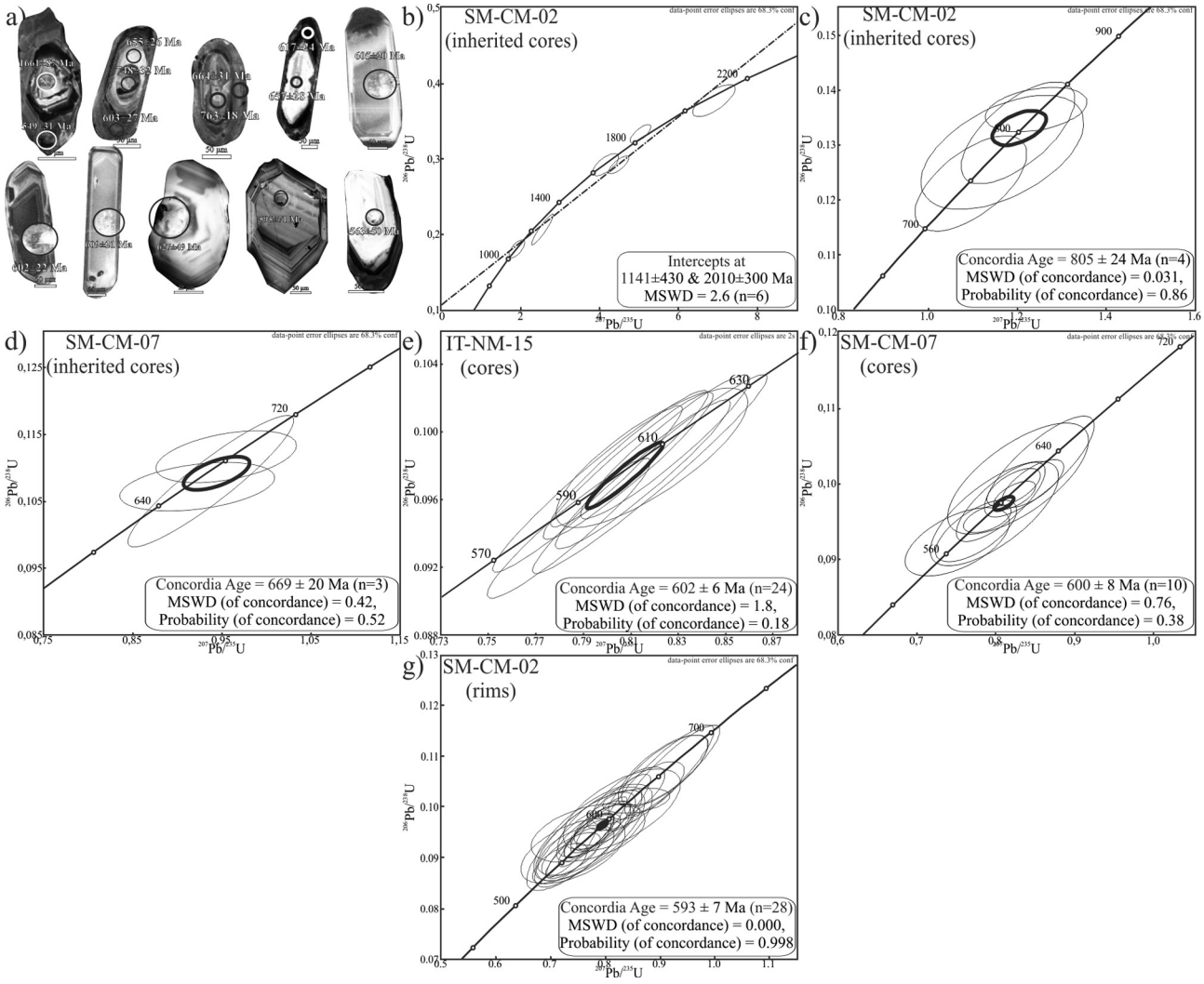

Fig. 13. Cathodoluminescence images and Concordia diagram from Morro do Escoteiro Suite of Italva Domain. (2 s, decay-const. errors included).

8. Discussions

The U-Pb results indicate that the orthogneisses of the Serra da Prata complex and the volcano-metasedimentary units of the Italva group are coeval, with development in the ca. 859–838 Ma interval. This time interval is older than the previous magmatic arc episodes described for the Ribeira Belt, such as the Rio Negro (ca.790–620 Ma) and the Serra da Bolívia-Rio Doce arcs (ca. 640–585 Ma), (e.g. Cordani et al., 1967; Tupinambá et al., 2000, 2011; Heilbron and Machado, 2003; Tedeschi et al., 2016). A similar time interval between ca. 850 and 630 Ma was described in Brazil only for the magmatic arcs of the Northern Brasília Belt (Pimentel and Fuck, 1992; Pimentel et al., 2000) and for the São Gabriel Orogeny (Hartmann et al., 2011), indicating a regional onset of the convergence around São Francisco and minor cratonic blocks. The geochemical and isotopic data of the (arc related) orthogneisses and (IAT to MORB) amphibolites suggest a juvenile arc setting (Ragatky et al., 2007; Sad and Dutra, 1988; Heilbron et al., 2008 and this work), corroborated by juvenile ε_{Nd} values and young T_{DM} model ages between 1.68 and 0.92 Ga.

The association of arc-related rocks of the Serra da Prata complex, with MORB to IAT basic rocks and shallow platform carbonates, is consistent with an active intra-oceanic arc with small islands surrounded by carbonate fringes, similar to the modern island arcs of the Pacific and Caribbean Oceans. The marbles and amphibolites could have been deposited in intra-arc or back-arc basins, where a roll-back in the subducted slab imply an extensional stress field behind the arc. The Tonian development of the Serra da Prata stage is envisaged in the tectonic model of Fig. 17a, d.

Younger arc granitoids with crystallization ages of ca. 635–620 Ma are coeval with the main development of the Rio Negro Arc, pointing to an Ediacaran age of arc development. Changes in composition and isotopic signature suggest the evolution from juvenile to more mature stages of the arc (Rio Negro stage, Fig. 17b, e). The location of the younger Ediacaran arc rocks, together with the development of a subhorizontal metamorphic foliation with in situ anatexis suggests that the extensional regime of the subduction zone has changed to compressive regimes. During this stage, a more mature arc, such as the modern Japan magmatic arc could be a possible scenario.

Finally, the collision of the arc terrane (Oriental terrane) against the Ribeira belt is indicated by ca. 601–580 Ma metamorphic rims around magmatic zircons from the Serra da Prata arc rocks, as well as by the occurrence of foliated Morro do Escoteiro Suite granitoid rocks dating ca. 602–567 Ma (Fig. 17c, f).

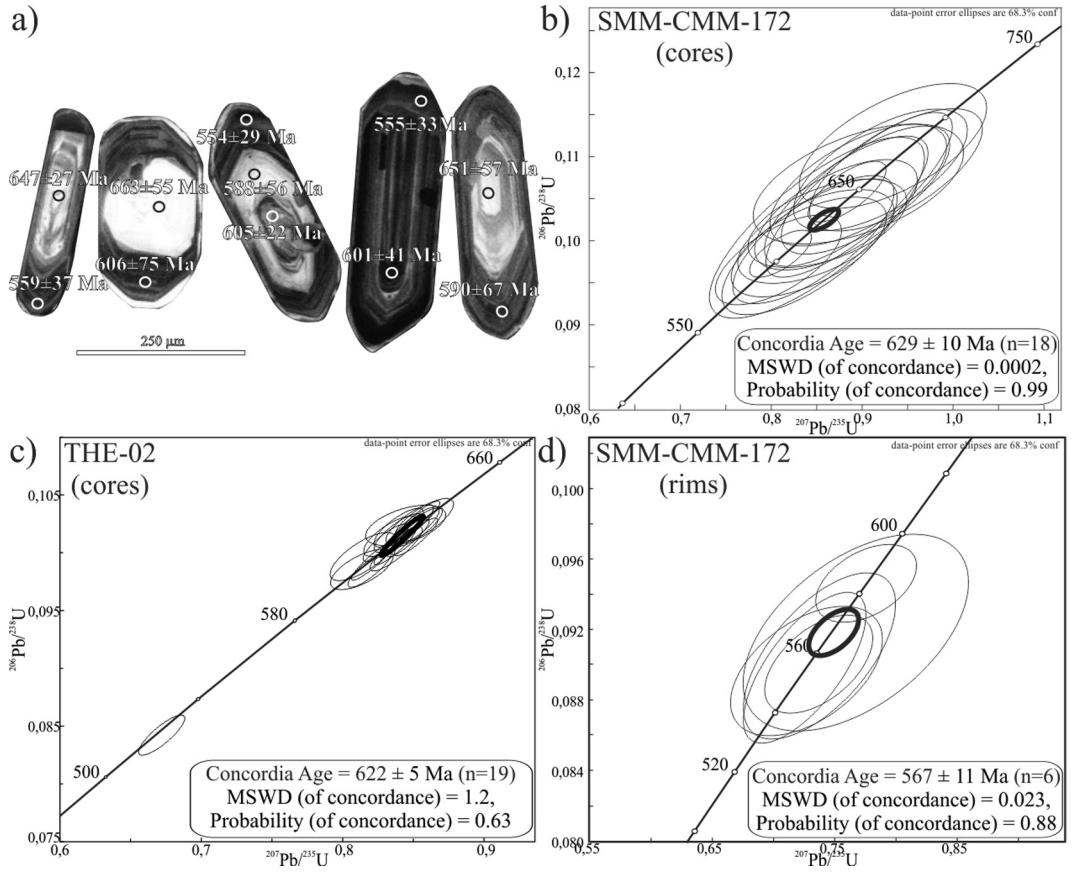

Fig. 14. Cathodoluminescence images and Concordia diagram from Rio Negro Complex of Costeiro Domain. (2 s, decay-const. errors included).

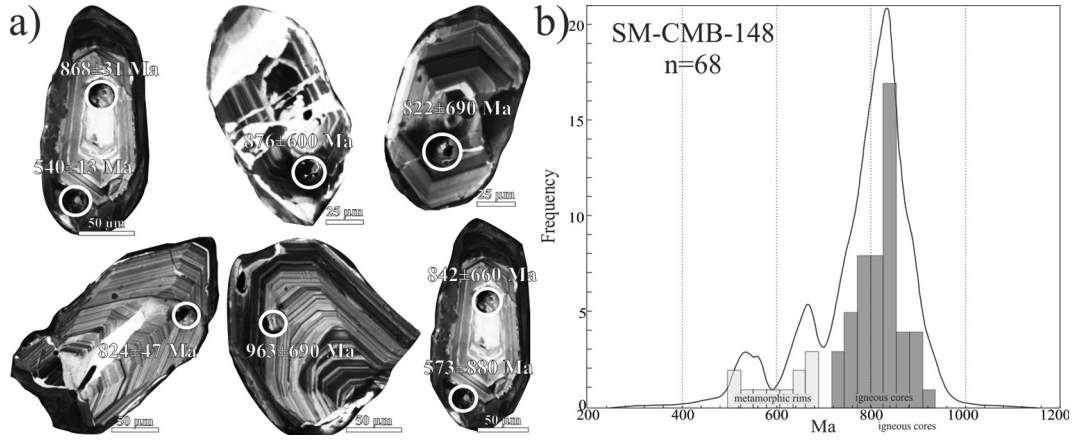

Fig. 15. Cathodoluminescence images and Concordia diagram from Euclidelândia Unit of Italva Domain. (2 s, decay-const. errors included).

Table 16
Sm-Nd whole rock analytical data of the amphibolites, Serra da Prata and Rio Negro Complex.

Samples	Unit	Sm ppm	Nd ppm	f Sm/Nd	$^{143}Nd/^{144}Nd$ (m)	Erro (2s)	$^{147}Sm/^{144}Nd$ (m)	time (t) Ma	$^{143}Nd/^{144}Nd$ (t)	$eNd_{(t)}$	$eNd_{(0)}$	$T_{(CHUR)}$	$T_{(DM)}$
CAM-CMM-184B	AMP	3.4	12.2	−0.14	0.512860	0.000006	0.16920	630	0.512161	6.6	4.3	−1.24	0.67
SAP-CMM-159		4.1	14.5	−0.12	0.512809	0.000008	0.17250	850	0.511847	6.0	3.3	−1.09	0.87
SMM-CB-87		3.0	8.5	0.09	0.513102	0.000005	0.21470	850	0.511905	7.1	9.1	3.87	−0.03
SM-CM-69	SPC	3.6	20.1	−0.45	0.512083	0.000005	0.10816	850	0.511480	−1.2	−10.8	0.96	1.34
SM-CM-70A		2.5	12.0	-0.35	0.512518	0.000009	0.12757	850	0.511807	5.2	−2.3	0.26	0.92
SM-CM-70B		0.8	5.7	−0.55	0.512255	0.000006	0.08886	850	0.511760	4.3	−7.5	0.54	0.95
CM-CB-85		2.2	8.6	−0.21	0.512629	0.000007	0.15557	856	0.511755	4.3	−0.2	0.03	1.05
CR-R-04SP		3.7	16.3	−0.31	0.512471	0.000005	0.13570	850	0.511714	3.4	−3.3	0.42	1.09
SMM-CM-35		4.3	19.8	−0.33	0.512089	0.000006	0.13210	850	0.511352	−3.7	−10.7	1.30	1.68
SMM-CMM-153		5.4	23.2	−0.29	0.512376	0.000008	0.14040	850	0.511593	1.0	−5.1	0.71	1.32
CT-CMM-177A	RNC	1.0	4.4	−0.27	0.512223	0.000005	0.14270	630	0.511655	−3.3	−8.1	1.07	1.55
CT-CMM-177B		2.3	11.7	−0.39	0.512199	0.000007	0.12090	630	0.511700	−2.5	−8.6	0.88	1.33
SAP-SMM-179A		6.1	27.6	−0.32	0.511949	0.000007	0.13320	630	0.511399	−8.3	−13.4	1.65	1.93
SAP-SMM-179B		8.4	51.0	−0.49	0.511836	0.000008	0.09990	630	0.511423	−7.9	−15.6	1.26	1.55
SAP-SMM-179C		7.2	37.3	−0.41	0.511909	0.000004	0.11610	630	0.511429	−7.7	−14.2	1.38	1.68
SMM-CMM-172		9.3	43.2	−0.34	0.511931	0.000007	0.12980	630	0.511395	−8.4	−13.8	1.61	1.89

9. Final remarks: the magmatic arcs of the Ribeira belt in West Gondwana

Based on the data presented here in both the orthogneisses of the Serra da Prata Complex and the marbles with amphibolite intercalations of the Italva group corroborate the characterization of this older and juvenile Tonian magmatic arc stage with related basins within the Ribeira belt. The new U-Pb data indicate that the development of magmatic arc rocks started earlier than previously reported (the Rio Negro and Serra da Bolívia) magmatic arc associations within the Ribeira belt. Nd and Sr isotopic data point to a primitive and probably intra-oceanic setting for this older, Tonian arc stage at the present Oriental terrane.

The geodynamic evaluation of the Serra da Prata and Rio Negro arcs in the Western Gondwana is in table 18 and Fig. 18, a compilation of Tonian and Cryogenian/Ediacaran magmatic arcs. This figure represents older Tonian magmatic arcs, most with juvenile character, and younger Cryogenian/Ediacaran arcs, which display both juvenile and crustal-derived isotopic signatures.

Many coeval magmatic arc episodes include the Goiás arc in the Brasília Belt (ca. 862–630 Ma) and the São Gabriel arc (ca.840–690 Ma), located respectively along the western side of the São Francisco and Rio de La Plata cratons. In the African side, several magmatic arcs of the Arabian-Nubian Shield (ca. 870–690 Ma) and minor occurrences at the Hoggar-Dahomey (ca. 860–740 Ma) are documented.

Altogether, these Tonian juvenile magmatic arc rocks bring out additional evidence that subduction zones occurred around Western Gondwana continental blocks since ca. 860 Ma. In the Western Gondwana scenario, the common juvenile signature suggests an intra-oceanic tectonic settings. The combination of the older Tonian magmatic arcs with the previously reported more evolved Cryogenian to Ediacaran magmatic arcs within the Neoproterozoic belts suggests more than 200 m.y. of subduction around the older cratonic blocks of Western Gondwana, which in turn is indicative of consumption of wide oceanic lithosphere.

Acknowledgements

We thank the CNPq, FAPERJ and FINEP brasilian agencies for funding of the project and two anonymous reviewers for comments and suggestions that brought improvements the original manuscript. We also would like to thank all the laboratories involved in this research, LGPA, and LAGIR at Rio de Janeiro State University; Centro de Pesquisas Geocronológicas at USP, Laboratório de Geocronologia at UNG, and the Geochronology Labs of the Alberta University at Edmonton and ANU at Canberra Australia. This is a contribution to the 648 IGCP project.

Table 17
Sr whole rock analytical data of the amphibolites, Serra da Prata and Rio Negro Complex.

Samples	Unit	Rb ppm	Sr ppm	$^{87}Sr/^{86}Sr$ (m)	Erro(2 s)	$Time_{(t)}$ Ma	$^{87}Sr/^{86}Sr_{(t)}$	$^{87}Sr/^{86}Sr_{(t,CHUR)}$
CAM-CMM-184B	AMP	5.0	474.0	0.70322	0.000008	630	0.70320	0.70442
SAP-CMM-159		4.0	235.0	0.70464	0.000006	850	0.70458	0.70440
SMM-CB-87		5.0	91.0	0.70423	0.000007	850	0.70404	0.70440
SM-CM-69	SPC	26.0	486.0	0.70882	0.000008	850	0.70864	0.70440
SM-CM-70[a]		53.0	298.0	0.70957	0.000005	850	0.70895	0.70440
SM-CM-70B		55.0	339.0	0.70905	0.000005	850	0.70848	0.70440
CM-CB-85		26.0	486.0	0.70523	0.000010	850	0.70504	0.70440
CR-R-04SP		38.0	416.0	0.70647	0.000007	850	0.70615	0.70440
SMM-CM-35		45.0	330.0	0.71178	0.000009	850	0.71130	0.70440
SMM-CMM-153		69.0	422.0	0.70852	0.000009	850	0.70795	0.70440
CT-CMM-177[a]	RNC	70.0	362.0	0.71076	0.000008	630	0.71026	0.70442
CT-CMM-177B		68.0	448.0	0.71016	0.000009	630	0.70977	0.70442
SAP-SMM-179[a]		101.0	289.0	0.71940	0.000009	630	0.71850	0.70442
SAP-SMM-179B		123.0	308.0	0.72017	0.000008	630	0.71914	0.70442
SAP-SMM-179C		113.0	316.0	0.71933	0.000008	630	0.71841	0.70442
SMM-CMM-172		128.0	287.0	0.72225	0.000006	630	0.72110	0.70442

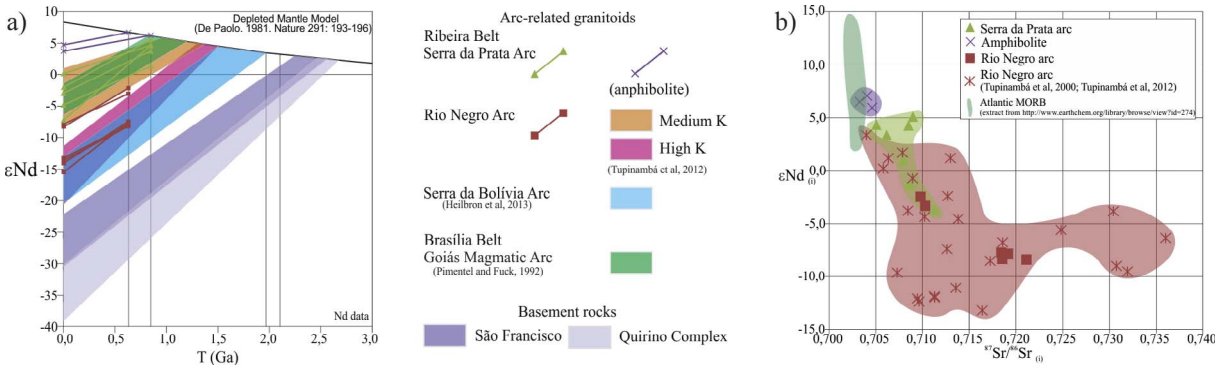

Fig. 16. a) Juvenile Nd isotopic signature of the orthogneisses of the Serra da Prata and Rio Negro Complexes compared to other magmatic arc successions of the Ribeira and Brasília belts. Basement Paleoproterozoic rocks from São Francisco craton, Quirino Complex, and Atlantic MORB are presented for comparison; b) Strontium–neodymium isotope correlation of the amphibolites and orthogneisses of the Serra da Prata and Rio Negro Complexes. The compilation is based on Heilbron et al. (2011), Machado et al. (2010), Pimentel et al. (2000), Tupinambá et al. (2000, 2012) and Sato and Siga Junior (2000).

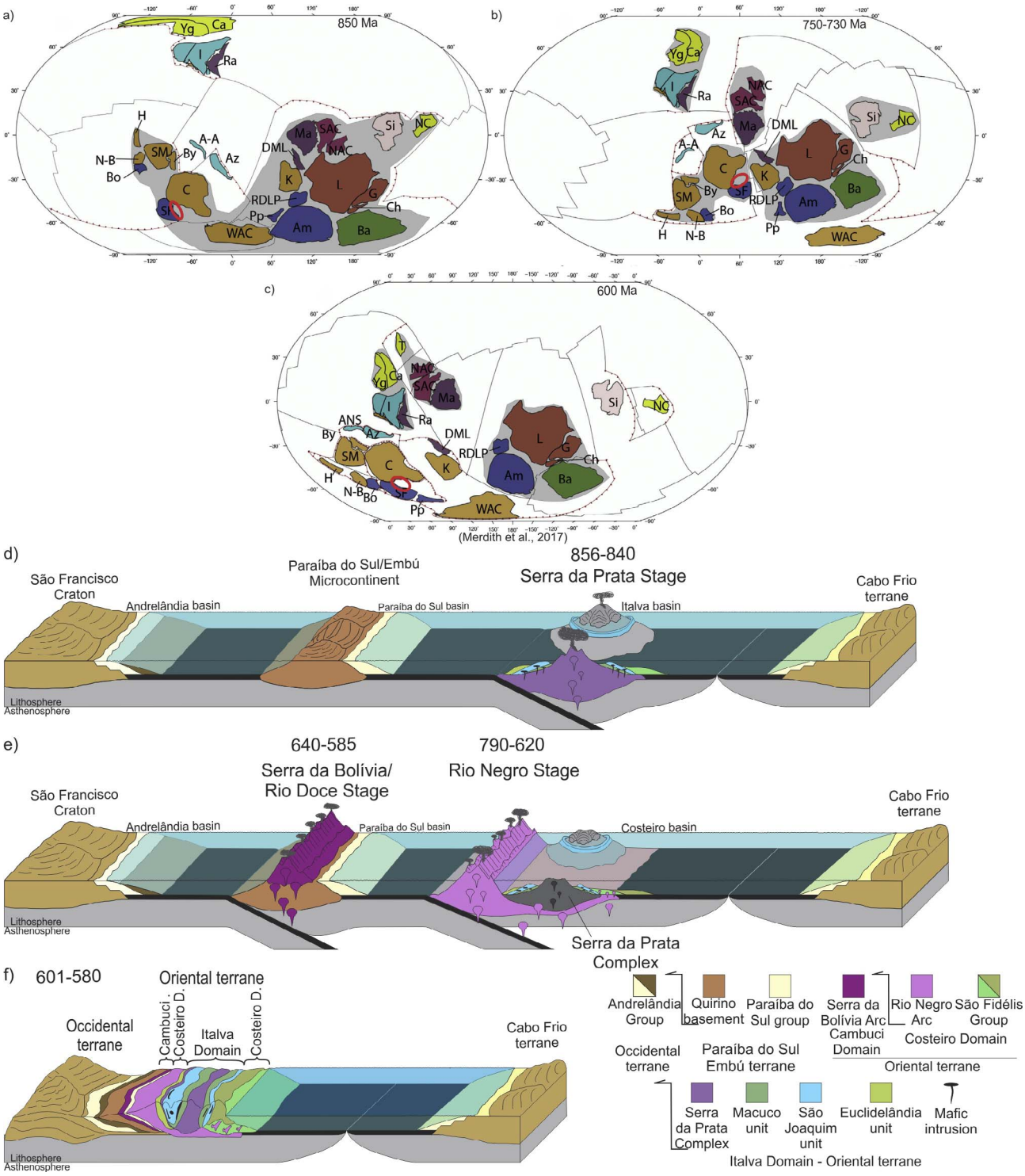

Fig. 17. (a–c) reconstructing models of palecontinents of continental crust fragments in the Neoproterozoic (Merdith et al., 2017). Envisaged tectonic model for the evolution of Serra da Prata ((d)-Tonian) and Rio Negro ((e)-Cryogenian) magmatic arcs of the Ribeira belt, before the main collision episode (f).

Table 18
Summary of the Neoproterozoic reported magmatic arcs of Western Gondwana. Classified according age and isotopic signature.

	Belt	Terranes/Unit	Juvenile Arcs	Evolved Arcs	Selected References
1	Ribeira	Oriental terrane: Rio Negro and Serra da Prata Arcs	860–790 760–620	640–620	This work. Tupinambá et al. (2000), 2011; Peixoto (2010), Heilbron and Machado (2003), Heilbron et al. (2009)
2	Araçuaí-Ribeira	Internal Domain / Paraíba do Sul terrane: Rio Doce and Serra da Bolívia arcs	650–585	635–595	Pedrosa-Soares et al. (2008, 2009), Heilbron et al. (2013), Corrales (2015), Tedeschi et al. (2016)
3	Southern Ribeira	Socorro Arc and magmatic rocks of the Embú terrane		760–620	Hackspacher et al. (2003), Janasi et al. (2001), Janasi and Ulbrich (1991)
4	Kaoko	Coastal terrane		625	Goscombe et al. (2005), Goscombe and Gray (2008), Gray et al. (2009)
5	Dom Feliciano	Pelotas Batolith		670–620	Hartmann et al. (2011), Saalmann et al. (2005) Basei et al. (2009)
6	São Gabriel	Passinho and Vila Nova arcs	900–850 800–700		Babinski et al. (1997), Chemale (2000), Hartmann et al. (2011)
7	Southern Brasília	Guaxupé and Anápolis Itauçu		690–625	Valeriano et al. (2009), Laux et al. (2004, 2005), Janasi et al. (2001)
8	Northern Brasília	Mara Rosa	900–760	660–600	Pimentel and Fuck (1992), Pimentel et al. (1997, 2000) Cordani et al. (2013)
9	Sergipano			640–620	Finnoto et al. (2009)
10	NE system	Martinópole and Santa Quitéria	870–850	640–620	Brito Neves et al. (2002), Santos et al. (2009), Granade de Araujo et al. (2014)
11	Central Africa	Granitoids and Diorites		660–580	Toteu et al. (2004)
12	Eastern African System	Arabian-Nubian shield intra-oceanic arcs	890–710 760–650 680–640	640–580	Fritz et al. (2013) Johnson and Kattan (2007), Johnson et al. (2011), Küster et al. (2008) Ali et al. (2009), Whitehouse et al. (1998)
13	EAS/Madagascar			804–776	Handke et al. (1999), Kröner and Stern (2004)
14	Transaharan (Hoogar Dahomey)	Iskel. Ouguda and Iforas. Tilemsi- amalaoulaou.	868–740 690–650	650–620	Caby (1998, 2003), Berger et al. (2011)
15	West African orogens Rockelides. Bassarides and Mauritanide belts			620–580	Klein and Moura (2008), Feybesse and Milési (1994)

Fig. 18. Location of the Magmatic Arcs of the Western Gondwana, based on Gondwana map of Meet and Liebermam (2008). Numbers and related with the references are presented in Table 18. Legend: Cratonic blocks in gray color; Neoproterozoic belts in magenta; Late Neoproterozoic to Cambrian belts in green; Phanerozoic belts in yellow. Tonian arcs in red stars and Cryogenian arcs in purple stars.

References

Ali, B.H., Wilde, S.A., Gabr, M.M.A., 2009. Granitoid evolution in Sinai, Egypt, based on precise SHRIMP U-Pb zircon geochronology. Gondwana Res. 15, 38–48.

Almeida, F.F.M., 1977. O Cráton do São Francisco. Revista Brasileira de Geociências 7, 349–364.

Almeida, F.F.M., Hasui, Y., Brito-Neves, B.B., Fuck, R.A., 1981. Brazilian structural provinces: an introduction. Earth-Sci. Rev. 17, 1–29.

Babinski, M., Chemale Jr., F., Hartmann, L.A., Van Schmus, W.R., Silva, L.C., 1997. U-Pb and Sm-Nd geochronology of the Neoproterozoic Granitic-Gneissic Don Feliciano Belt, Southern Brazil. J. S. Am. Earth Sci. 10, 263–274.

Basei, M.A.S., Nutman, A., Júnior, O.S., Passarelli, C.R., Drukas, C.O., 2009. The evolution and tectonic setting of the Luis Alves microplate of Southeastern Brazil: an exotic terrane during the assembly of Western Gondwana. Developments in Precambrian Geology 16, 273–291.

Berger, J., Caby, R., Lie 'gois, J.P., Mercier, J.C., Demaiffe, D., 2011. Deep inside a Neoproterozoic intra-oceanic arc: growth, differentiation and exhumation of the Amalaoulaou complex (Gourma, Mali). Contrib. Mineral. Petrol. 162, 773–796.

Boynton, W.V., 1984. Geochemistry of the rare earth elements: meteorite studies. In: Henderson, P. (Ed.), Rare Earth Element Geochemistry. Elsevier, pp. 63–114.

Neves, B.B., Schmus, W.R.V., Fetter, A., 2002. North-western Africa–North-eastern Brazil. Major tectonic links and correlation problems. J. Afr. Earth Sci. 34 (3), 275–278.

Brito Neves, 2003. A saga dos descendentes de Rodínia na construção de Gondwana. Revista Brasileira de Geociências. 33, 1.

Bühn, B., Pimentel, M.M., Matteini, M., Dantas, E.L., 2009. High spatial resolution analyses of Pb and U isotopes for geochronology by laser ablation multi-collector inductively coupled plasma mass spectrometry (LA-MC-ICP-MS). Anais da Academia Brasileira de Ciências 81 (1), 99–114.

Caby, R. 1998. Tectonic history and geodynamic evolution of northern Africa during the Neoproterozoic. In: 14 International Conference on Basement Tectonics, Ouro Preto, Abstracts, 72–75.

Caby, R., 2003. Terrane assembly and geodynamic evolution of central-western Hoggar: a synthesis. J. Afr. Earth Sci. 37, 133–159.

Campos Neto, M.C., 2000. Orogenic Systems from Southwestern Gondwana, an approach to Brasiliano-Pan African cycle and orogenic collage in SoutheasternBrazil. In: Cordani, U.G., Milani, E.J., Thomaz Filho, A., Campos, D.A. (Eds.), Tectonic Evolution of South America, 31st International Geological Congress. Rio deJaneiro, pp. 335–365.

Chemale Jr., F., 2000. Evolução geológica do Escudo Sul-rio-grandense. Geologia do Rio Grande do Sul. CIGO-UFRGS 13–52.

Cordani, U.G., Melcher, G.C., Almeida, F.F.M., 1967. Outline of precambrian geochronology of South America. Can. J. Earth Sci. 5, 629–632.

Cordani, U.G., Sato, K., Teixeira, W., Tassinari, C.C.G., Basei, M. 2000. Crustal evolution of the South American Platform. In: Cordani, U.G., Milani, E.J., Thomaz Filho, A., Campos, D.A. (Eds). Tectonic Evolution of South America. Tectonic Evolution of South America, 31st International Geological Congress; Rio de Janeiro; 2000, pp. 19–40.

Cordani, U.G., Pimentel, M.M., Araújo, C.E.G., Fuck, R.A., 2013. The significance of the transbrasiliano-Kandi tectonic corridor for the amalgamation of West Gondwana. Braz. J. Geol. 43 (3), 583–597.
Corfu, F., Hanchar, J.M., Hoskin, P.W.O., Kinny, P., 2003. Atlas of zircon textures. Rev. Mineral. Geochem. 53, 469–500.
Corrales, F.F.P., 2015. Geologia e Geocronologia do Complexo Marceleza: Vestígios de um arco magmático cordilherano no Terreno Paraíba do Sul, no limite entre os Estados do Rio de Janeiro e Minas Gerais. Dissertação de Mestrado. Faculdade de Geologia, Universidade do Estado do Rio de Janeiro.
D'Agrella-Filho, M.S., Bispo-Santos, F., Trindade, R.I.F., Antonio, P.Y.J., 2016. Paleomagnetism of the Amazonian Craton and its role inpaleocontinents. Braz. J. Geol. 46 (2), 275–299.
Degler, R., Pedrosa-Soares, A., Dussin, I., Queiroga, G., Schulz, B., 2017. Contrasting provenance and timing of metamorphism from paragneisses of the Araçuaí-Ribeira orogenic system, Brazil: Hints for Western Gondwana assembly. Gondwana Res. 51 (2017), 30–50.
Feybesse, J.L., Milési, J.P., 1994. The Archean/Proterozoic contact zone in West Africa: a mountain belt of décollement thrusting and folding on a continent margin related to 2.1 Ga convergence of Archean craton? Precambr. Res. 69, 199–227.
Finnoto, J., Oliveira, E.P., Neal, J., McNaughton, N.J., Laux, J., 2009. U-Pb dating granites in the Neoproterozoic Sergipano Belt, NE-Brazil: implications for the timing and duration of continental collision and extrusion tectonics in the Borborema Province. Gondwana Res. 15 (1), 86–97.
Fritz, H., Abdelsalam, M., Ali, K.A., Bingen, B., Collins, A.S., Fowler, A.R., Ghebreab, W., Hauzenberger, C.A., Johnson, P.R., Kusky, T.M., Macey, P., Muhongo, S., Stern, R.J., Viola, G., 2013. Orogen styles in the East African Orogen: a review of the Neoproterozoic to Cambrian tectonic evolution. J. Afr. Earth Sc. 86, 65–106. http://dx.doi.org/10.1016/j.jafrearsci.2013.06.004.
Goscombe, B., Armstrong, D.G.R., Foster, D.A., Vogl, J., 2005. Event geochronology of the Pan-African Kaoko Belt, Namibia. Precambr. Res. 140 (3), 103 e1–103. e41.
Goscombe, B., Gray, D.R., 2008. Structure and strain variation at mid-crustal levels in a transpressional orogen: a review of Kaoko Belt structure and the character of West Gondwana amalgamation and dispersal. Gondwana Res. 13, 45–85.
Granade de Araujo, C.E., Rubatto, D., Hermann, J., Cordani, U., Caby, R., Basei, M.A.S., 2014. Eduacaran 2,500-km-long synchronous deep continental subduction in the West Gondwana Orogen. Nat. Commun. 5, 1–7.
Gray, D.R., Foster, A., Meert, J.G., Goscombe, D., Armstrong, R., Trouw, R.J.A., Passchier, C.W., 2009. A Damara orogen perspective on the assembly of southwestern Gondwana. Geological Society, London, Special Publications 294 (1), 257–278.
Hackspacher, P.C., Fetter, A.H., Ebert, H.D., Janasi, V.A., Dantas, E.L., Oliveira, M.A.F., Braga, I.F., Negri, F.A., 2003. Magmatismo há ca. 660–640 Ma no Domínio Socorro: registros de convergência pré-colisional na aglutinação do Gondwana Ocidental. Geologia USP. Série Científica 3, 85–96.
Handke, M.J., Tucker, R.D., Ashwal, L.D., 1999. Neoproterozoic continental arc magmatism in West-Central Madagascar. Geology 27 (4), 351–354.
Hartmann, L.A., Philipp, R., Santos, J.O.S., McNaughton, N.J., 2011. Time frame of 753–680 Ma juvenile accretion during the São Gabriel orogeny, southern Brazilian Shield. Gondwana Res. 19 (1), 84–99.
Heilbron, M., Machado, N., 2003. Timing of terrane accretion in the Neoproterozoic-Eopaleozoic Ribeira Orogen (SE Brazil). Precambr. Res. 125, 87–112.
Heilbron, M., Mohriak, W.V., Valeriano, C.M., Milani, E.J., Almeida, J., Tupinambá, M., 2000. From collision to extension: the roots of the southeastern continental margin of Brazil. In: Talwani, M.; Mohriak, W.U. (Org.). Atlantic Rifts and Continental Margins. Washington DC, EUA: American Geophysical Union, Geophysical Monograph Series, 2000, vol. 115, pp. 1–34.
Heilbron, M., Soares, A.C.P., Campos, N., Silva, L.C., Trouw, R., Janasi, V., 2004. Província Mantiqueira. In: Virgino Mantesso-Neto; Andrea Bartorelli; Celso Dal Ré Carneiro; Benjamin Bley de Brito Neves. (Org.). Geologia do Continente Sul Americano: Evolução da Obra de Fernando Flávio Marques de Almeida. 1ª ed. São Paulo: Beca Produções Culturais Ltda., 2004, vol. I, pp. 203–234.
Heilbron, M., Valeriano, C., Tupinambá, M., Almeida, J.C.H., Duarte, B.P., Valladares, C., Schmitt, R., Geraldes, M., Ragatky, D., Palermo, N., Gontijo, A., 2004. Tectonic Episodes related to West Gondwana Amalgamation in the Ribeira orogen. In: 1 Symposium on Neoproterozoic-Early Paleozoic Events in SW-Gondwana, IGCP-Project 478. Extended Abstracts: São Paulo; 2004. vol. 1. pp. 36–38.
Heilbron, M., Valeriano, C., Tassinari, C.C.G., Almeida, J.C.H., Tupinambá, M., Siga, O., Trouw, R., 2008. Correlation of Neoproterozoic terranes between the Ribeira Belt, SE Brazil and its African counterpart: comparative tectonic evolution and open questions. Geol. Soc., London, Spec. Publ. 2008 (294), 211–237.
Heilbron, M., Tupinambá, M., Duarte, B.P., Nogueira, J.R., Valladares, C., Almeida, J.C.H., Silva, L.G.E., Ragatki, C.D., Valeriano, C., Geraldes, M., Schmitt, R., 2009. Faixa Ribeira Central e suas Conexões com as Faixas Araçuaí e Ribeira Sul. In: XI simpósio de geologia do sudeste, São Pedro (SP). XI Simpósio de Geologia do Sudeste, 2009. vol. 1.
Heilbron, M., Almeida, J.C.H., Silva, L.G.E., Tupinambá, M., Valente, S., Duarte, B. P., Corval, A., Guedes, E., Valeriano, C., Schmitt, R., Valladares, C., Ragatky, D., Geraldes, M., Peixoto, C.A. Arcabouço Regional. In Heilbron, M. Geologia e Recursos Minerais da Folha santo Antônio de Pádua. In: Monica Heilbron. (Org.). Geologia e Recursos Minerais da Folha Santo Antônio de Pádua-SF.26-X-D-VI, escala de 1:100, 000. first ed. Belo Horizonte: CPRM, 2012, vol. 1, pp. 22–36.
Heilbron, M., Tupinambá, M., Valeriano, C., Armstrong, R., Silva, L.G.E., Melo, R.S., Simonetti, A., Pedrosa Soares, A.C., Machado, N., 2013. The Serra da Bolívia complex: the record of a new Neoproterozoic arc-related unit at Ribeira belt. Precambr. Res. 238 (2013), 158–175.
Hoskin, P.W.O., Black, L.P., 2000. Metamorphic zircon formation by solid-state recrystallization of protolith igneous zircon. J. Metamorphic Geol. 2000 (18), 423–439.
Hoskin Paul, W.O., Schaltegger, UR.S., 2003. The composition of Zircon and igneous and metamorphic petrogenesis. Rev. Mineral. Geochem. 53, 27–62.
Irvine, T.N., Baragar, W.R.A., 1971. A guide to the chemical classification of the common volcanic rocks. Can. J. Earth Sci. 8, 523–548.
Jackson, S.E., Pearson, N.J., Griffina, W.L., Belousova, E.A., 2004. The application of laser ablation inductively coupled plasma-mass spectrometry to in situ U-Pb zircon geochronology. Chem. Geol. 211, 47–69.
Janasi, V.A., Ulbrich, H.H.G.J., 1991. Late Proterozoic granitoid magmatism in the state of São Paulo, southeastern Brazil. Precambr. Res. 51 (1), 351–374.
Janasi, V.A., Leite, R.J., Van Schmus, W.R., 2001. U-Pb chronostratigraphy of the granitic magmatism in the Agudos Grandes Batholith (west of Sao Paulo, Brazil)—implications for the evolution of the Ribeira Belt. J. S. Am. Earth Sci. 14 (4), 363–376.
Johnson, P.R., Andresen, A., Collins, A.S., Fowler, A.R., Fritz, H., Ghebreab, W., Kusky, T., Stern, R.J., 2011. Late Cryogenian-Ediacaran history of the Arabian-Nubian Shield: a review of depositional, plutonic, structural, and tectonic events in the closing stages of the northern East African Orogen. J. Afr. Earth Sci. 61 (3), 167–232.
Johnson, P.R. & Kattan, F.H. 2007 Geochronologic dataset for Precambrian Rocks in the Arabian Peninsula. A catalog of U-Pb, Rb-Sr, Ar-Ar, and Sm-Nd ages. Open-File report SGS-OF-2007-3, the Saudi Geological Survey, Jeddah, Kingdom of Saudi Arabia.
Klein, E.L. & Moura, C.A.V., 2008. São Luís Craton and Gurupi Belt (Brazil): possible links with the West African Craton and surrounding Pan-African belts. West Gondwana: Pre-Cenozoic Correlations Across the South Atlantic Region. In: Pankhurst, R.J., Trouw, R.A.J., Brito Neves, B.B., De Wit, M.J. (eds). Geological Society, London, Special Publications, vol. 294, pp. 137–151.
Kröner, A., Cordani, U.G., 2003. African and South American 8_53 cratons were not part of the Rodinia supercontinent: evidence from field relationships and geochronology. Tectonophysics 375, 325–352.
Kröner, A., Wan, Y., Liu, X., Liu, D., 2014. Dating of zircon from high-grade rocks: which is the most reliable method? Geosci. Front. 5, 515–523.
Kröner, A., Stern, R.J., 2004. Africa/Pan-African Orogeny Encyclopedia of Geology, vol. 1 Elsevier, Amsterdam.
Küster, D., Liégeois, J.-P., Matukov, D., Sergeev, S., Lucassen, F., 2008. Zircon geochronology and Sr, Nd, Pb isotope geochemistry of granitoids from Bayuda Desert and Sabaloka (Sudan): evidence for a Bayudian event (920–900 Ma) preceding the Pan-African orogenic cycle (860–590 Ma) at the eastern boundary of the Saharan metacraton. Precambr. Res. 164, 16–39. http://dx.doi.org/10.1016/j.precamres.2008.03.003.
Laux, J.H., Pimentel, M.M., Dantas, E.L., Armstrong, R., Armele, A., 2004. Mafic magmatism associated with the Goiás Magmatic Arc in the Anicuns-Itaberaí region, Goiás, Brazil: Sm-Nd isotopes and new ID-TIMS and SHRIMP U-Pb data. J. S. Am. Earth Sci. 16 (7), 599–614.
Laux, J.H., Pimentel, M.M., Dantas, E.L., Armstrong, R.A., Junges, S.L., 2005. Two Neoproterozoic crustal accretion events in the Brasília Belt, central Brazil. J. S. Am. Earth Sci. 18, 183–198.
Ludwig K.R., 2003. Isoplot/Ex 3.00: a geochronological toolkit for Microsoft Excel. Berkeley: Berkeley Geochronology Center. Disponível em: http://www.bgc.org/klprogrammenu.html > .
Machado, N., Gauthier, G., 1996. Determination of $^{207}Pb/^{206}Pb$ ages on zircon and monazite by laser ablation ICP-MS and application to a study of sedimentary provenance and metamorphism in southeastern Brazil. Geochim. Cosmochim. Acta 60, 5063–5073.
Machado Filho, L., Ribeiro, M.W., Gonzalez, S.R., Schemini, C.A., Santos Neto, A.S., Palmeira, R.C.B., Pires, I.L., Teixeira, W., Castro, H.F. Folhas SF 23/24 Rio de Janeiro e Vitória. 1983; Geologia. RADAMBRASIL, vol. 32.
Machado, N., Valladares, C., Heilbron, M., Valeriano, C., 1996. U-Pb Geochronology of the central Ribeira belt (Brazil) and implication for the evolution of the Brazilian Orogeny. Precambr. Res. 1996 (79), 347–361.
Machado, H.T., Valladares C., Valeriano, C., Medeiros, S., Duarte, B., 2010. Orthogneisses of the Quirino Complex, Central Ribeira belt, Se Brazil: Sr and Nd isotopic data. 2010. In: VII South American Symposium on Isotope Geology, Brasília, 25th–28th July 2010.
Meert, J.G., Torsvik, T.H., 2003. The making and unmaking of a supercontinent: Rodinia revisited. Tectonophysics 375, 261–288.
Meet, J.G., Liebermam, B.S., 2008. The Neoproterozoic assembly of Gondwana and its relationship to the Ediacaran-Cambrian radiation. Gondwana Res. 14, 5–21.
Menezes, S.O., 1973. Contribuição a geologia de Cantagalo. Dissertação de mestrado. Instituto de Geociências, Universidade Federal do Rio de Janeiro, Rio de Janeiro, pp. 45.
Merdith, A.S., Collins, A., Williams, S.E., Pisarevsky, S., Foden, J.D., Archibald, D.B., Blades, M.L., Alessio, B.L., Armistead, S., Plavsa, D., Clark, C., Müller, R.D., 2017. A full-plate global reconstruction of the Neoproterozoic. Gondwana Res.
Miyashiro, A., 1974. Volcanic rock series in island arcs and active continental margins. Am. J. Sci. 274, 321–355.
Moraes, J.M., 2006. Caracterização geoquímica dos ortoanfibolitos de Grupo Italva, Setor Central da Faixa Ribeira. Uerj; Monografia Final de Graduação, Rio de Janeiro.
Nalini-Junior, H.A., Bilal, E., Paquette, J.L., Pin, C., Machado, R., 2000. Geochronolo-gie U-Pb et géochimie isotopique Sr–Nd des granitoides neoproterozoiques dessuites Galiléia et Urucum, vallée du Rio Doce, Sud-Est du Brésil. C. R. Acad. Sci., Paris 331, 459–466.
Nalini-Junior, H.A., Machado, R.M., Bilal, E., 2005. Geoquímica e petrogênese da SuíteGaliléia: exemplo de magmatismo tipo-I, metaluminoso, pré-colisional, neoproterozóico da região do Médio Vale do Rio Doce. Revista Brasileira de Geociências 35 (4), 23–34.
Oliveira, J.A. D., Machado Filho, L., Ribeiro, M.W., Liu, C.C., Meneses, P.R. 1978. Mapa Geológico do Estado do Rio de Janeiro Baseado em Imagens MSS do Satélite Landsat-

1 (Texto Explicativo, DRM - Niterói).
Pearce, J.A., 1982. Trace element characteristics of lavas from destructive plate boundaries. In: Thorpe, R.S. (Ed.), Andesites. Wiley, Chichester, pp. 525–548.
Pearce, J.A., Gale, G.H., 1977. Identification of ore-deposition environment from trace element geochemistry of associated igneous host rocks. Geol. Soc. Spec. Publ. 7, 14–24.
Pedrosa-Soares, A.C., Alkmim, F.F., Tack, L., Noce, C.M., Babinski, M., Silva, L.C., Martins-Neto, M.A., 2008. Similarities and differences between the Brazilian and African counterparts of the Neoproterozoic Araçuaí-West Congo Orogen. In: Pankhurst R.J., Trouw R.A.J., Brito Neves B.B. & de Wit M.J. (eds), West Gondwana: Pre-Cenozoic Correlations Across the South Atlantic Region. Geological Society London, Special Special Publications, vol. 294: pp. 153–172.
Pedrosa-Soares, A.C., Chaves, M., Scholz, R. 2009. Eastern Brazilian pegmatite province. In: 4th International Symposium on Granitic pegmatites, field trip guide, p28.
Peixoto, C. & Heilbron, M., 2010. Geologia da Klippe Italva na região entre Cantagalo e Itaocara, Nordeste do Estado do Rio de Janeiro. São Paulo, UNESP, Geociências, vol. 29, n. 3, pp. 277–289.
Peixoto, C.A., 2010. Geologia e geocronologia U-PB (LA-ICP-MS) do Domínio Italva na região entre Cantagalo e Itaocara. Dissertação de mestrado. Faculdade de Geologia, Universidade de Estado do Rio de Janeiro, pp. 133.
Peixoto, C.A., 2008. Mapeamento Geológico da Klippe Italva na Região entre Cantagalo e Itaocara, Estado do Rio de Janeiro. Universidade do Estado do Rio de Janeiro, Rio de Janeiro p. 45.
Pimentel, M.M., Fuck, R.A., 1992. Neoproterozoic crustal accretion in central Brazil. Geology 20, 375–379.
Pimentel, M.M., Whitehouse, M.J., Viana, M.G., Fuck, R.A., Nuno, M., 1997. The Mara Rosa Arch in the Tocantins Province: further evidence for Neoproterozoic crustal accretion in Central Brazil. Precambr. Res. 81 (3), 299–310.
Pimentel, M.M., Fuck, R.A., Gioia, S.M.C.L., 2000. The Neoproterozoic Goiás Magmatic Arc, Central Brazil: a review and New Sm-Nd isotopic data. Revista Brasileira de Geociências (1), 035–039.
Pisarevsky, S.A., Wingate, M.T.D., MCA Powell, C., Johnson, S., Evans, D.A.D., 2003. Models of Rodinia assembly and fragmentation. In: Yoshida, M., Windley, B.F., Dasgupta, S. (Eds.), Proterozoic East Gondwana: Supercontinent Assembly and Breakup. Geological Society, London, Special Publications, vol. 206, pp. 35–55.
Pisarevsky, S.A., Murphy, J.B., Cawood, P.A., Collins, A.S., 2008. Late Neoproterozoic and Early Cambrian paleogeography: models and problems. In: Pankhurst, R.J., Trouw, R. A.J., Brito Neves, B. B., De Wit, M.J. (eds.) West Gondwana: Pre-Cenozoic Correlations Across the South Atlantic Region. Geological Society, London, Special Publications, vol. 294, pp. 9–31.
Ragatky, D., Maceira, J., Duarte, B.P., Valente, S., Parisotto, M. 2007. Geoquímica preliminar dos ortoanfibolitos da Bacia Italva, setor central da Faixa Ribeira. In: XI Congresso Brasileiro de Geoquímica: Atibaia.
Rosier, G.F, 1957. A Geologia da Serra do Mar, entre os Picos de Maria Comprida e do Desengano (Estado do Rio de Janeiro). D.R.M., Bol. 166. Rio de Janeiro.
Rubatto D., Williams I. S., Günther D. Trace-Element Characterization of Metamorphic Zircons. Ninth Annual V. M. Goldschmidt Conference, August 22–27, 1999, Cambridge, Massachusetts, abstract no. 7111.
Saalmann, K., Hartmann, L.A., Remus, M., 2005. Tectonic evolution of two contrasting Schist belts in Southernmost Brazil: a plate tectonic model for the Brasiliano Orogeny. Int. Geol. Rev. 47, 1234–1259.
Sad, J.H.G. & Donadello, M.M., 1978. Geologia e Recursos minerais da Folha Santa Maria Madalena, Estado do Rio de Janeiro, Brasil. Texto Explicativo. GEOSOL LTDA. DRM, RJ. 1978; p. 295.
Sad, J.H.G., Donadello, M.M., Figueiras, RR, Arantes, D. Projeto Carta Geológica do Estado do Rio de Janeiro. Escala 1:50.000. Folha Santa Maria Madalena (SF-23-X-D-VI-4): Texto Explicativo. 1980. GEOSOL LTDA. DRM-RJ.
Sad, J.H.G., Dutra, C., 1988. Chemical composition of supracrustal rocks from Paraíba do Sul Group, Rio de Janeiro State, Brazil. Geochim. Brasil 7 (2), 143–174.
Santos, T.J.S., Fetter, A.H., Neto, J.A.N. 2009. Comparisons between the northwestern Borborema Province, NE Brazil, and the southwestern Pharusian Dahomey Belt, SW Central Africa. IN: Pankhurst et al., 2009 eds, West Gondwana: Pre-Cenozoic Correlations across the South Atlantic Region. Geological Society of London, Special Publications, vol. 294: pp. 101–119.
Sato, K. & Siga Junior, O. 2000. Superproduction Evidence of the Continental Crust During Paleoproterozoic in South American Platform. Implications Regarding the Interpretative Value of the Sm-Nd Model Ages. Revista Brasileira de Geociências, Rio de Janeiro-Brazil, vol. 30, n. 1, pp. 147–160, 2000.
Schmitt, R.S., Trouw, R.A.J., Van Schmus, W.R., Pimentel, M.M., 2004. Late amalgamation in the central part of Western Gondwana: new geochronological data and the characterization of a Cambrian collisional orogeny in the Ribeira belt (SE Brazil). Precambr. Res. 2004 (133), 29–61.
Shervais, J.W., 1982. Ti–V plots and the petrogenesis of modern and ophiolitic lavas. Earth Planet. Sci. Lett. 59, 101–118.
Simonetti, A., Heaman, L.M., Chacko, T., Banerjee, N.R., 2006. In situ petrographic thin section U-Pb dating of zircon, monazite, and titanite using laser ablation–MC–ICP-MS. Int. J. Mass Spectrom. 253, 87–97.
Tanaka, T., Togashib, S., Kamiokab, H., Amakawac, H., Kagamid, H., Hamamotod, T., Yuharad, M., Orihashie, Y., Yonedaf, S., Shimizug, H., Kunimarug, T., Takahashih, K., Yanagii, T., Nakanoj, T., Fujimakik, H., Shinjol, R., Asaharaa, Y., Tanimizua, M., Dragusanua, C., 2000. JNdi-1: a neodymium isotopic reference in consistency with LaJolla neodymium. Chem. Geol. 168 (3–4), 279–281.
Tedeschi, M., Novo, T., Pedrosa-Soares, A.C., Dussin, I., Tassinari, C., Silva, L.C., Gonçalves, L., Alkmim, F.F., Lana, C., Figueiredo, C., Dantas, E., Medeiros, S., De Campos, C., Corrales, F., Heilbron, M., 2016. The Ediacaran Rio Doce magmatic arc revisited (Araçuaí-Ribeira orogenic system, SE Brazil). J. S. Am. Earth Sci.
Toteu, S.F., Penaye, J., Djomani, Y.P., 2004. Geodynamic evolution of the Pan-African Belt in Central Africa with special reference to Cameroon. Can. J. Earth Sci. 41, 73–85.
Trouw, R.A., Heilbron, M., Ribeiro, A., Paciullo, F., Valeriano, C., Almeida, J.H., Tupinambá, M., Andreis, R. 2000. The central segment of the Ribeira belt. In: Cordani et al. (Eds.), Geotectonics of South America. Special Publication for the 31 IGC/2000. pp. 297–310.
Tupinambá, M., Heilbron, M., Valeriano, C.M., Porto Jr., R., Eirado, L.G., Almeida, J.C.H., 2012. Juvenile contribution of the Neoproterozoic Rio Negro Magmatic Arc (Ribeira Belt, Brazil): Implications for Western Gondwana amalgamation. Gondwana Res. 1, 12–20.
Tupinambá M. & Heilbron M. 2002. Reconstituição da Fase Pré-colisional Neoproterozóica da Faixa Ribeira: o Arco Magmático e as Bacias de Ante-Arco e Retro-arco do Terreno Oriental. In: 31 Congresso Brasileiro de Geologia, João Pessoa. Anais, vol. 1. p. 345.
Tupinambá, M., Teixeira, W., Heilbron, M., 2000. Neoproterozoic Western Gondwana assembly and subduction-related plutonism: the role of the Rio Negro Complex in the Ribeira Belt, South-eastern Brazil. Revista Brasileira de Geociências 30, 7–11.
Valeriano, C.M., Silva, V., Medeiros, S.R., Aguiar Neto, C.C., Ragakty, C.D., Geraldes, M. C., 2008. The Neodymium isotope composition of the Jndi-1 oxide reference material: results from the Lagir Laboratory, Rio de Janeiro. In: VI South American Symposium on Isotope Geology, 2008, San Carlos de Bariloche. Proceedings of the VI South American Symposium on Isotope Geology. vol. 1. pp. 1–2.
Valeriano, C. M., Medeiros, S. R., Vaz, G. S., Neto, C.C.A. 2009. Sm-Nd isotope dilution TIMS analyses of BCR-1, AGV-1 and G-2 USGS rock reference materials: first results from the LAGIR Laboratory at UERJ, Rio de Janeiro. In: Simpósio 45 Anos de Geocronologia no Brasil, São Paulo – USP- IGC. Boletim de Resumos Expandidos, vol. 1, pp. 146–148.
Whitehouse, M.J., Windley, B.F., Mahfood, A.O., Ba-Bttat, C., Fanning, M., Rex, D.C., 1998. Crustal evolution and terrane correlation in the eastern Arabian Shield, Yemen: geochronological constraints. J. Geol. Soc., London 155 (1998), 281–295.